A Study on Two-Phase Flow Characteristics in Cross-Linked Microchannel Heat Sinks

Minh Nhat Dang

A Thesis

in

The Department

of

Mechanical and Industrial Engineering

Presented in Partial Fulfillment of the Requirements

for the Degree of Master of Applied Science (Mechanical Engineering) at

Concordia University

Montreal, Quebec, Canada

August 2007

Your file Votre référence
ISBN: 978-0-494-34741-6
Our file Notre référence
ISBN: 978-0-494-34741-6

Abstract

A Study on Two-Phase Flow Characteristics in Cross-Linked Microchannel Heat Sinks

Minh Nhat Dang

Thermal management for high performance of miniaturized electronic devices using microchannel heat sinks has recently become of interest to researchers and industry. Obtaining heat sink designs with uniform flow distribution is strongly desired. Mal-distribution in a standard straight microchannel heat sink has become a problematic issue in this research area. A cross-linking scheme, introduced in the channel core promises an appropriate solution to this problem due to flow sharing through the cross-links. In the present thesis, a number of experimental and numerical studies have been conducted to seek appropriate designs for microchannel heat sinks. The effects of cross links, introduced in the channel core of an array of parallel scaled microchannels, are investigated, by comparing the flow distribution and pressure drop in six different multi-channel configurations. A standard straight channel test section and five cross-linked test sections are experimentally investigated. All test sections have 45 parallel rectangular channels, with a hydraulic diameter of 1.59 mm. The flow distribution is monitored at four selected channels. The working mixture is air and water with superficial velocities ranging from 0.03 to 9.93 m/s, and 0.04 to 0.83 m/s, respectively. The results show that the cross-linked designs improve the flow distribution between channels compared to the standard straight channel configuration. Flow patterns obtained from flow visualization

are presented in terms of fractional time function and a flow pattern map was developed. Compared with a single channel flow regime map, the expected intermittent flow regime is observed 84% to 90 % of the time for the cross-linked designs, but only 65% to 80% of that for the straight channel design. A new cross-linked microchannel heat sink is proposed with the support of numerical investigations. The new design shows a significant improvement, up to 55%, on flow distribution when compared to the standard straight channel configuration without a penalty in pressure drop.

Acknowledgements

I want to thank my supervisor, Dr. Ibrahim Hassan, for his support and guidance and for his faith in me throughout my graduate studies.

I also want to thank all my colleagues in the microscale heat transfer research group for sharing their knowledge and experience during the last two years. I would like to thank, in particular, Dr. R. Muwanga and Dr. S.I. Kim, for their help and guidance during my research program.

Special thanks to Dr. G. S. Newsham, R.C. Bowden, and T. Ahmad for their time and patience in helping me edit my thesis.

Last but not least, I am deeply grateful to my parents, my sister, my girlfriend, and my friends for supporting, understanding, and encouraging me to go this far in my academic studies.

Table of Contents

List of Figures

List of Tables

Nomenclature

A	Cross section area, (m^2)
C	Constant Value, ($5 \leq C \leq 20$)
D	Diameter, (m)
f	Fractional time function, $f = \frac{Ni}{T}$
F	Body force, (N)
G	Mass flux, (kg/m^2)
j_G	Superficial gas velocity, (m/s)
j_L	Superficial liquid velocity, (m/s)
K	Martinelli parameter, $K^2 = \frac{\left(\frac{\Delta P}{\Delta L}\right)_L}{\left(\frac{\Delta P}{\Delta L}\right)_G}$
L	Channel length, (m)
$\dot{M}$	Mass transfer due to cavitation, (kg/s)
$\dot{m}$	Mass flow rate, (kg/ s)
N_i	Number of observations of a flow configuration
N	Number of value x
n	Number of phases
O	Mass flow rate percentage of the four selected channels
P	Channel wetted perimeter, (m)

Q	Volume flow rate, (m^3/s)
R	Deviation percentage
S	Slip ratio, $S = \frac{j_G}{j_L}$
T	Total number of observations
U	Velocity, (m/s)
U	Uncertainty estimate
V	Velocity along the Y-direction, (m/s)
$\vec{v}_{dr,k}$	Drift velocity for phase k, $\vec{v}_{dk,k} = \vec{v}_k - \vec{v}_m$ (m/s)
$\vec{v}_m$	Mass average velocity of the mixture, $\vec{v}_m = \frac{\sum_{k=1}^{n} \beta_k \rho_k \vec{v}_k}{\rho_m}$ (m/s)
W	Total deviation percentage
x	Flow quality, $x = \frac{\dot{m}_G}{\dot{m}_G + \dot{m}_L}$
x	One value in a set of data
$\bar{x}$	The mean of all values x
X	X-coordinate, (m)
Y	Y-coordinate, (m)
Z	Z-coordinate, (m)
$\Delta P \left(or \frac{dp}{dz} \right)$	Pressure drop, (Pa)
Re	Reynolds number, $Re = \frac{\rho v d}{\mu}$

Φ^2	Two-phase multiplier
We	Weber number, $We = \frac{G^2 D_h}{\rho_{TP}\sigma}$
Fr	Froude number, $Fr = \frac{G}{gD\rho_{TP}^2}$

Greek Letters

f	Friction factor
μ	Dynamic viscosity, ($N.s/m^2$)
ρ	Density, (kg/m^3)
β	Volume fraction
σ	Surface tension, (N/m)

Subscripts

dr, k	The drift velocity for secondary phase k
f	Frictional
FM	Flow meter
G	Gas
GC	Graduated cylinder
GO	All gas flow only
h	Hydraulic
k	Phase k
L	Liquid

LL	Laminar-laminar
LO	All liquid flow only
LT	Laminar-turbulent
m	Mixture
T	Timer
TL	Turbulent-laminar
TT	Turbulent-turbulent
TP	Two-phase

Superscripts

T	Transpose

Abbreviations

CCD	Charged-coupled device
CFD	Computational fluid dynamics
CR-2	Two cross-linked channel
CR-2A	Two-times larger cross-linked channel
CR-2B	Three-times larger cross-linked channel
CR-4	Four cross-linked channel
CR-6	Six cross-linked channel
STR	Standard straight channel
STDEV	Standard deviation,

Chapter 1

Introduction

1.1 Motivation

In recent years, the electronics industry has been producing micro-chips with increased circuitry and decreased size in order to meet the demands of high performance miniaturized electronic devices. However, such electronic circuits typically generate high heat fluxes which can cause damage to their components if not appropriately dissipated. A prime contender for thermal management of these electronic devices is the two-phase microchannel heat sinks. In the early 1980s, the first microchannel heat sink was introduced by Tuckerman and Pease (1981). This heat sink consisted of long micro-channels that ran in one direction and parallel to the heat sink base. They succeeded in dissipating a heat flux of 790 W/cm^2, and maintained the chip's surface temperature under 120°C. Since their pioneering work, many studies have been conducted to investigate heat transfer characteristics of microchannel heat sinks. These studies included investigations of flow distribution, two-phase adiabatic flow pattern and flow boiling, involving microchannel heat sinks. The goal has been to develop reliable and predictive tools for pressure drop and heat transfer evaluation in microchannel heat sinks. Such studies resulted in a significant number of two-phase flow patterns maps and two-phase pressure drop models for a single channel with a large scale channel size. However, there is a lack of studies dealing with multiple channels. Moreover, mal-distributed flow in an array of parallel channels has required further investigation. Currently, designs of

microchannel heat sinks are ever evolving as new technologies develop. One of the promising solutions to mal-distribution is introducing cross-links to the channel core. This allows flow communication between channels improving the flow distribution.

1.2 Objectives and Organization

The objectives of this work are:

- To provide new experimental data for channel array configurations
- To investigate the effects of cross-links on:
  - Two-phase flow distribution
  - Two-phase flow patterns
  - Two-phase pressure drop
- To develop a multi-channel flow pattern map
- To propose and evaluate an appropriate design for a two-phase cross-linked microchannel heat sinks, with improved flow distribution.

A comprehensive review of the literature is presented in Chapter 2. Chapter 3 introduces a description of the experimental investigation. Chapter 4 presents the experimental results of cross-linked scaled-up microchannel heat sinks, under adiabatic two-phase flow conditions. A numerical investigation, in continuation of this work, is discussed in Chapter 5. Finally, Chapters 6 and 7 summarize the results generated in this work, and give suggestions for future research.

Chapter 2

Literature Review

2.1 Flow Distribution

Unequal flow distribution among channels in microchannel heat sinks will cause non-uniform temperature distribution. This leads to a poor cooling performance of the microchannel heat sink. Improving flow distribution is necessary, in an array of parallel channels, since mal-distribution among channels will lead to poor cooling performance. This is particularly true for non-uniform temperature distributions on the surfaces of heat sinks. A number of studies have been conducted to investigate flow distribution in parallel multi-channel configurations. Some studies focused on the modification of header designs, whereas some introduced cross-links into the channel core.

2.1.1 Effects of Header Design

One of the studies done to improve flow distribution through header modifications for conventional two-phase heat exchangers was that of Samson et al. (1987). The aim of this study was to examine the flow distribution in three different header designs which were: the inlet header with four outlet tubes, the spreader header with five outlet tubes, and the symmetrical headers with six outlet tubes. An air/water mixture was used for adiabatic two-phase flow into the headers. The flow distribution was found to be unequal in the in-line header design. However the flow distribution was better than that in the spreader header but only for flow qualities below 50%. The symmetrical header was much better

than the previous two headers. However, this type of header is difficult to build in a compact design because the exit tubes radiate in all directions. For this reason, the half-symmetrical header was recommended by the authors. However, the flow distribution was not satisfactory with flow qualities exceeding 50%.

Osakabe et al. (1999) conducted an experiment to examine the distribution behavior of water, with or without a gas-phase, in a horizontal header. The cross-section and the diameter of the header and four vertical branch pipes were 40mm X 40 mm, and 10 mm, respectively. Their results showed that flow distribution was approximately equal when the Reynolds number (Re) was larger than 1500, and it was unequal with a lower Re for single-phase flow. This result was considered to be due to the flow instability in the distribution system. For two-phase flow, the contamination of a small amount of bubbles significantly affected the flow distribution behavior in the header. It was concluded that a larger pipe length could ensure a uniform distribution in a single phase flow. However, for two-phase flow, a non-uniform flow distribution would be promoted in a header contaminated with a small amount of bubbles.

Kim et al. (2003) listed the geometrical factors that affected flow distribution. The factors they listed were the cross-sectional area of the branch as a fraction of the tank/header/distributor cross sectional area, the tube spacing, and the orientation of the branch. The other factors included the total mass flow rate, the vapor quality in the tank, and the heating load on the branch. Since there are currently no tools available to

determine the flow distribution in headers, both single and two-phase flow studies need to be conducted in a variety of header designs

Hrnjak (2004) presented an overview of the issue. This showed the basic options for uniformly distributing single phase as well as two-phase flow in a horizontal header. The paper included a description of a method to determine mal-distribution. It was stated that the reason for the mal-distribution was the differences in pressure drop along the channels for both single-phase and multi-phase flow. One approach to overcome this, specifically for single phase flows, was the use of a branching network. In this case, a single header branches into a number of channels sequentially by first passing through a lesser number of channels. The main disadvantage of this approach is the space requirement for the branching network. According to Hrnjak, flow distribution is more complex for two phases due to the differences in the thermo-physical properties of each phase, for example, density, viscosity, and surface tension. These affect the intensity of inertia, gravitation, shear, and capillary forces on each of the phases. In the paper, three approaches were designed to improve two-phase flow distribution. They were the homogenous zone, separation of the phases with separate distribution, and mist generation. These types of headers are difficult to manufacture and also have large space requirements. For mini and microchannels, fabrication of these designs may not be feasible.

2.1.2 Effects of Channel Core Geometry

Flow distribution can also be improved through modification of the channel core. Some recent studies have considered modification of the channel core through introduction of cross-linked channels.

Jiang et al. (2002) compared two configurations of microchannel heat sinks of 18 stream-wise channels with a cross-section of 700μm wide and 300 μm deep. One differs from the other by 5 cross-linked channels of 100 μm and 300 μm deep. The comparison was made by applying hotspots, which is defined as a partially non-uniform heat flux, on the microchannel heat sink surface. They found that the cross-linked microchannel improved in distribution uniformity at a low flow rate of 1 ml/min. They suggested that the result was due to lateral fluid transport through the cross-link channels. However, the effect of cross-linked channels was reduced with increasing temperature of the heater, since only one cross-linked channel was within the hotspot region in their experiment. They therefore recommended that more cross-linked channels should be incorporated in the hotspot region. In addition, the cross-linked dimensions should be optimized to improve their effectiveness.

Following the same trend as Jiang et al. (2002) in improving flow distribution, Cho et al. (2003) compared the performance of two cross-linked microchannel heat sinks and regular parallel microchannel heat sinks. They examined two different hotspot configurations, called 1D and 2D, which were classified by their thermal boundary condition of heat flux. With a 20 ml/min water flow rate, the result was that a cross-

linked microchannel heat sink had better cooling performance for the 1D hotspot when compared to regular microchannel heat sinks. They recommended microchannel heat sink configurations should be optimized in order to be applied for different cooling demands, targeting heat flux, flow rate, and hotspot configuration.

2.2 Two-Phase Flow Visualization

Flow patterns play an important role in microchannel heat sinks due to their direct effect on the pressure drop and heat transfer characteristics. Thus, knowledge of flow pattern and flow pattern transitions is essential to develop a reliable predictive tool for pressure drop and heat transfer in two phase microchannel heat sinks.

2.2.1 Flow Visualization in Single Channel

Flow patterns have been investigated through adiabatic two-phase flow experiments. Much single channel research has been conducted for different shapes, sizes, and working fluids. From these studies, different flow patterns have been observed and generally defined as bubbly flow, stratified flow, plug flow, slug flow, churn flow, and annular flow. A significant number of single channel flow pattern maps have been constructed for a large range of channel sizes.

Xu et al. (1999) conducted an experimental investigation for adiabatic vertical two-phase flow of air and water in rectangular channels (12 mm wide X 260 mm long) with narrow gaps of 0.3, 0.6-1.0 mm. The cross sections of channels in three test models were 12mm x 0.3mm, 12mm x 0.6mm, 12mm x 1mm respectively. Flow regimes were observed by

using a CCD (Charge Coupled Device) camera, and were identified by examining the video images. They found that the flow regimes for gaps of 1.0 and 0.6 mm were similar to those in the existing literature. They were classified into bubbly flow, slug flow, churn - turbulent flow and annular flow. With the decrease of the channel gap, the transition from one flow regime to another occurs at smaller gas flow rates. However, the flow regimes for micro-gaps of 0.3 mm or less were quite different from the previous studies since bubbly flow was never observed, even at very low gas flow rates. They found that the liquid droplets adhered to the wall surface and were pushed by the gas phase due to the increased influence of the surface tension force and the frictional shear stress in channels with a micro-gap. Flow regimes as observed in these micro-gaps were classified into cap bubbly flow, slug droplet flow, churn flow and annular droplet flow.

Triplett et al. (1999) conducted a study on two-phase flow of air and water in circular microchannels with 1.1 and 1.45 mm inner diameters, and in microchannels with semi-triangular (triangular with one corner smoothed) cross- sections with hydraulic diameters 1.09 and 1.49 mm. The gas and liquid superficial velocity ranges were 0.02-80 and 0.02-8 m/s, respectively. Five major flow patterns such as bubbly, slug, churn, slug-annualr and annular were observed for all test sections in this work. However, neither of the test sections supported stratified flow. Overall, the experimental results showed that the flow regime maps obtained for semi-trianglular and the circular test sections were similar to one another and were mostly covered by the slug and slug-annular flow patterns. Therefore, it was concluded that the effect of geometry was not very significant under the tested flow conditions.

Coleman et al. (1999) conducted experiments on two-phase flow patterns with different test section configurations ranging from 5.5 to 1.3 mm in hydraulic diameter. Circular and rectangular shapes were examined in their work. A mixture of water and air was used as a two-phase working fluid. Bubble, dispersed, elongated bubble, slug, stratified, wavy, annular-wavy, and annular flow patterns were observed. The results of their experiments showed that the effect of diameter and surface tension might be negligible, as in previous studies, in terms of determining flow regimes for pipe diameters in the order of 10mm or larger. However, they play a vital role in determining flow patterns and transition in smaller tube diameters. The authors found that the transition to the dispersed flow regime at a higher liquid superficial velocity, and the stratified flow regime occurred at a lower gas superficial velocity in a rectangular tube. However, they stated that more investigations of the effect of tube shapes on flow patterns were needed.

Hibiki and Mishima (2001) conducted an experiment for air–water flows in narrow rectangular channels with gaps of 0.3–17 mm. The data in this experiment showed satisfactory agreement with the data in the experiment done by Xu et al. (1999). The flow regime was classified by four basic patterns: bubbly, slug, churn, and annular flows. The authors stated that present flow regime transition criteria could be applied over wide ranges of parameters, as well as to boiling flow. However, in order to apply these criteria to gaps narrower than 1 mm, they suggested that a new model may be needed for the prediction of the distribution parameter for very narrow rectangular channels.

Chung et al. (2004a) conducted an experiment on the effect of channel diameter on adiabatic two-phase flow characteristics in microchannels. The experiment was

performed with a mixture of nitrogen gas and water in circular channels of 530, 250, 100, and 50μm diameters. The flow patterns were observed in the channels of D_h =250 and 530 μm consistent with those appearing in minichannels of D_h ~1 mm, namely: bubbly, slug, churn, slug–annular and annular flow. The flow patterns in channels of D_h = 50 and 100 μm, were only slug flow under the flow conditions investigated. The absence of bubbly, churn, slug–annular and annular flow in channels of $D_h \leq 100$ μm was attributed to the greater viscous and surface tension effects on the liquid flow. The experimental results clearly revealed a channel diameter effect on two-phase flow. However, according to them, the applicability of the present findings should be limited to similar gas–liquid flow, since little is yet known about the effects of surface tension and liquid property on adiabatic two-phase flow in microchannels.

Chung et al. (2004b) also conducted an experiment to investigate the effect of channel geometry on two-phase flow characteristics in horizontal square microchannels. Adiabatic two-phase flow of a water-nitrogen mixture was pumped through a 96 μm square microchannel and the resulting flow pattern, void fraction, and frictional pressure drop data were compared with those previously reported by the authors for a 100 μm circular microchannel. The results showed that the pressure drop data were best estimated using a separated-flow model and the void fraction increased non-linearly with volumetric quality, regardless of the channel shape. However, the flow maps exhibited transition boundaries that were shifted depending on the channel shape. Only slug flow was identified in both of the microchannels. Bubbly, churn, and annular flow were not observed for the testing flow conditions. They concluded that the absence of the bubbly

and churn flow patterns were attributed to the laminar nature of liquid flow in the microchannels. An inspection of the liquid film structure in the slug flow pattern revealed a gas core flow with a smooth or ring-shaped liquid film and a serpentine-like gas core flow surrounded by a deformed liquid film. They also defined four new flow patterns on the probability of the interfacial structure appearing, namely, slug-ring flow, ring-slug flow, semi-annular flow and multiple flows. They based definitions of these new flow patterns in the slug flow region to develop the flow pattern maps for both channels, and to compare them with each other.

Qu et al. (2004) performed a study involving rectangular microchannels having a 0.406mm x 2.032 mm cross-section, and superficial velocities of nitrogen and water ranging from 0.08 to 81.92 m/s and 0.04 to 10.24 m/s, respectively. Compared to the results in macrochannels from previous studies, the flow patterns in microchannels deviate significantly. Slug and annular flow constitute dominant flow patterns in microchannels, and transition to annular flow occurs at lower values of superficial gas velocity than in macrochannels. Bubbly flow occurred only occasionally, stratified and churn flow were never observed in this experiment. The authors employed the experimental data of this study to validate an annular two-phase flow boiling model that was previously developed by the present authors to describe pressure drop and heat transfer characteristics. The previous model was modified based on the new findings from the adiabatic two-phase flow study which predicted the transition between annular flow and other flow patterns. Good agreement was achieved between the modified annular flow boiling model predictions and the experimental data for both pressure drop

and the saturated flow boiling heat transfer coefficient in water-cooled two-phase microchannel heat sinks.

Hassan et al. (2005) extended the range of the existing flow regime data by experimenting with three different circular test sections with hydraulic diameters of 3mm, 1mm, and 0.8 mm. Each test section was made of borosilicate glass tubing 200mm in length. Pressure differences were applied over the range 0-500kpa, and the range of superficial velocities of water and air were 0.02-1m/s and 10-100m/s, respectively. Bubbly, dispersed, stratified, slug, annular, and churn flows were observed in a horizontal channel with large hydraulic diameters. However, stratified flow has not been seen in any microchannel experiment. This was explained by the suppression of buoyancy in a microchannel. Surface tension effects were much more significant than in macrochannels. Surface tension and the effects of inertia have to be taken into account when classifying the flow regimes observed in microchannels. The effects of surface tension resulted in flow regimes characterized by large and elongated gas bubbles such as the bubbly, plug, and slug flows, whereas the effect of inertia resulted in the annular and dispersed flows. Four general flow regimes were defined to create a simplified flow map. Bubbly, intermittent, churn, and annular were separated into surface-tension-dominated and inertia-dominated regimes. In summary, they found that the universal transition line gave a good approximation of the regime transitions for all studies made so far. However, there is a lack of data pertaining to two-phase flow inside microchannels, particularly in microchannels with hydraulic diameters of less than 0.5mm.

2.2.2 Flow Visualization in Multiple Channels

There have been limited studies to investigate the features in channel array configurations. Recent studies have shown that many flow configurations can occur in multi-channels, under fixed flow conditions and with a common entrance or manifold. Thus, universal flow maps for a single channel may not be appropriate for two-phase multi-port microchannel heat sinks.

Nino et al. (2003) conducted two-phase flow visualization experiments using R134A in a 6 port rectangular micro-channel with 1.59 mm hydraulic diameter tubes. They defined the fractional time function, or the probability, that a flow pattern may exist in a particular flow condition. They used this to construct a qualitative flow map for an array of parallel microchannel heat sinks. The fractional time function values were defined as the number of observations of a flow configuration divided by the total number of observations under a particular flow condition. The stratified flow regime, dispersed flow regime, and the annular mist flow patterns of annular flow regime were not observed. In this work, the results showed that the refrigerant flow was distributed evenly throughout the ports for high mass flux, and quality conditions where annular flow was a dominant flow regime. The authors recommended that different working fluids should be investigated in order to analyze the variation of fractional time function.

In addition, there are some studies investigating flow visualization on flow boiling in parallel microchannels. Steinke and Kandlikar (2004) conducted experiments on flow boiling characteristics of water in six parallel horizontal microchannels with a hydraulic

diameter of 207 μm. Nucleate boiling, bubbly flow, slug flow, annular flow, annular flow with nucleation in the thin film, churn flow, and dry out were observed. They found that the bubbly flow was very intermittent. The most observed flows were the annular-slug flow and slug flow. They also encountered the phenomenon of flow reversal as observed in some previous studies. They stated that such a phenomenon is caused by the presence of the parallel channels, which allow a path of lower resistance during explosive growth of nucleating bubbles. The local dry-out phenomenon was also observed in the experiment.

Recently, Kandlikar (2006) found that flow patterns strongly influence heat transfer during flow boiling in minichannels and microchannels. One of the most influential flow patterns in this regard is the expanding bubble flow pattern which is identified as a nucleating bubble growing rapidly and occupying the entire channel. This flow pattern traps a liquid film which evaporates into the core and dries out until the slug comes to re-wet the channel walls. The rapid expansion of the bubbles is considered a cause of flow reversal during flow boiling in minichannels and microchannels.

2.3 Pressure Drop in Two-Phase Flow

Two-phase pressure drop experiments have been increasingly studied to seek appropriate models. A number of studies have been conducted to investigate two-phase pressure drop in mini- and microchannels. The results of two-phase pressure drop experiments were compared with some widely used models, namely, the homogeneous model, the Chisholm (1967) model, and the Friedel (1979) model.

The homogenous model is one of the simplest models defined for two-phase pressure drop calculations. This model considers the two phases as a single phase, and assumes that the two phases form a homogeneous mixture.

$$\Delta P_f = f_{TP} \frac{L}{D} \frac{\rho_{TP} U^2}{2} \qquad 2.1$$

where f_{TP} and ρ_{TP} are given by:

$$f_{TP} = 57 / \mathrm{Re}_{TP} \text{ (Laminar)} \qquad 2.1.1$$

$$f_{TP} = 0.3164\, \mathrm{Re}_{TP}^{-0.25} \text{ (Turbulent)} \qquad 2.1.2$$

$$\mathrm{Re}_{TP} = \frac{\rho_{TP} U D}{\mu_{TP}} \qquad 2.1.3$$

$$\rho_{TP} = \left(\frac{x}{\rho_G} + \left(\frac{1-x}{\rho_L} \right) \right)^{-1} \qquad 2.1.4$$

$$\mu_{TP} = \left(\frac{x}{\mu_G} + \left(\frac{1-x}{\mu_L} \right) \right)^{-1} \qquad 2.1.5$$

A separated flow model is found from the work of Chisholm (1967), whose correlation can be expressed as:

$$\left(-\frac{dp}{dz} \right)_{f,TP} = \Phi_L^2 \left(-\frac{dP}{dz} \right)_{f,L} \qquad 2.2$$

where:

$$\Phi_L^2 = 1 + \left(\frac{C}{K}\right) + \left(\frac{1}{K}\right)^2 \qquad 2.2.1$$

$$K^2 = \frac{\left(\frac{\Delta P}{\Delta L}\right)_L}{\left(\frac{\Delta P}{\Delta L}\right)_G} \quad \text{, Lockhart et al. (1949)} \qquad 2.2.2$$

The $\left(-\frac{dp}{dz}\right)_{f,L}$ represents the single phase frictional drop in pure liquid, where a mass flux of G (1-x) flows in the channel and X represents the Martinelli factor, where C may have values in a range of 5 to 20. Based on the Reynolds number of gas and liquid (Re_L and Re_G), the given constant values of C are: C = 20 for turbulent-turbulent, C = 12 for laminar-turbulent, C = 10 for turbulent-laminar, while C = 5 for laminar-laminar. In these cases, the Reynolds number was calculated as:

$$Re_L = \frac{G(1-x)D}{\mu_L} \qquad 2.2.3$$

$$Re_G = \frac{G(x)D}{\mu_G} \qquad 2.2.4$$

$$Re_{GO} = \frac{GD}{\mu_G} \qquad 2.2.5$$

$$Re_{LO} = \frac{GD}{\mu_L} \qquad 2.2.6$$

Whalley (1987) suggested that the Chisholm (1967) correlations should be mostly used for $\mu_L / \mu_G > 1000$ and $G > 100\ kg/m^2s$.

Another separated flow model can be found from the work of Friedel (1979) who proposed a correlation, based on a wide range of experimental data. This model is suggested to be used for $\mu_l / \mu_g << 1000$ (Whalley, 1987). The correlation can be expressed in terms of multiplier as following:

$$\left(-\frac{dp}{dz}\right)_{f,TP} = \Phi_{LO}^2 \left(-\frac{dp}{dz}\right)_{f,LO} \qquad 2.3$$

where:

$$\left(-\frac{dp}{dz}\right)_{f,LO} = \frac{2f_{LO}}{D}\frac{G^2}{2\rho_L} \qquad 2.3.1$$

For horizontal and vertical upward flow configurations, Friedel (1979) suggested the following,

$$\Phi_{LO}^2 = A + 3.24x^{0.78}(1-x)^{0.24}\left(\frac{\rho_L}{\rho_G}\right)^{0.91}\left(\frac{\mu_G}{\mu_L}\right)^{0.19}\left(1-\frac{\mu_G}{\mu_L}\right)^{0.7} Fr^{-0.0454} We_{TP}^{-0.035} \qquad 2.3.2$$

where;

$$A = (1-x)^2 + x^2\rho_L f_{GO}(\rho_G f_{LO})^{-1} \qquad 2.3.3$$

$$Fr_{TP} = \frac{G}{gD\rho_{TP}^2} \qquad 2.3.4$$

$$We_{TP} = \frac{G^2 D}{\rho_{TP}\sigma} \qquad 2.3.5$$

Some studies showed that these models could fairly predict their results, as seen in the work of Triplett et al. (2004), and Pehlivan et al. (2006) whose results agreed with those from the homogenous model and the Chisholm (1967) model. However, some other studies showed that these models failed to predict the pressure drop for channels with a smaller hydraulic diameter, as shown in the work of Chen et al. (2001), when they investigated the pressure drop for two-phase flow in the round copper channel having an inner diameter of 1.02, 3.17, 5.05, and 7.02mm. Furthermore, Chung et al. (2004) showed that the homogeneous model cannot effectively predict their results of pressure drop in channels with hydraulic diameters of 96 μm and 100 μm.

2.4 Numerical Literature Review

With the advantage of both hardware and software today, CFD (computational fluid dynamics) software can be used to simulate two-phase flow in multi-channel system. Compared to experimental data of two-phase flow investigations, numerical studies are found to be lacking in the literature. A number of studies have been carried out for two-phase flow in single channels, tubes, tube bends, and T-junctions., by using different methods such as VOF (Volume of Fluid), Mixture, and Eulerian.

Qian and Lawal (2006) studied slug Taylor flow at a T-junction in a single microchannel, using Fluent's VOF method. They compared the slug length to those in other experiments and the results showed good agreement. Correlations were also made to predict the gas and liquid slug lengths. Yang et al. (2001) studied bubbly two-phase flow in a narrow channel, using the Lattice-Boltzamann method. Their results showed that the average

film thickness of the liquid fluid between the Taylor bubble and the channel wall agreed well with classical analytical correlation developed by Bretherton (1960).

Other studies used two fluids other than gas and liquid to study the blocking length in the pipe when fluid and solid were incorporated into the two-phase pipe flow (Conde et al., 2004). Shepel and Smith (2006) used a new level set method for modeling two-phase incompressible flows with moving boundaries, and the method was implemented in the code CFX-4. Amornkul et al. (2005) used the Eulerian method to study three dimensional two-phase flow in pipe bends. The results showed that modeling can well predict the experimental pressure drop for single phase. However, it did not predict well the experimental data for two-phase pressure drop in their studied range.

Numerical investigation of two-phase flow in multiple parallel channels is rare in the literature. Some can be found in single phase flow to optimize the geometrical design of parallel multi-channel configurations of heat sinks (Jayanti and Deshpande, 2005; Tonomura et al., 2003; Lu and Wang, 2006). Unlike single phase flow, two-phase flow behavior in an array of parallel channels is very complex. Thus, simulation of two-phase flow in multiple channels should be expected to cause some issues because of time consumption for convergence, or insufficient memory of available computer resources. Due to such possible problems, computational domains as well as simulation methods are being carefully considered. Moreover, since a universal two phase model is not yet available, various two phase models are still being developed.

2.5 Overview of Current Study

In developing cross-linked microchannel heat sinks, a number of unknown parameters exist. These include the cross-link width and the number of cross-link paths. The role of these parameters plays on two-phase flow characteristics and heat transfer is not yet clear. Ideally, heat transfer investigations could be carried out to scale on each of the possible configurations. This, however, is an expensive endeavor. The present work investigates scaled microchannel heat sinks under adiabatic conditions. The aim is to provide an initial iteration on the influence of cross-links under two-phase flow conditions. This is part of a larger research program whereby the knowledge gained will be helpful in identifying promising designs to be investigated under to-scale conditions with heat transfer.

Experimental data is collected under adiabatic two-phase flow conditions to investigate the effects of cross-links in six different channel core configurations for an array of parallel scaled microchannels. One configuration is a standard straight parallel system, whereas the other five have cross-links incorporated into the channel core. Six test sections were designed to enable liquid flow rate measurements in select channels. The fractional time function is used in this paper to plot flow patterns versus flow conditions, so as to understand more about the mechanism of flow as well as flow distribution in multichannel micro-heat sinks.

An extended study was conducted numerically to gain further insight into the effects of cross-links, because continual experimental investigations are expensive. A 3D mixture

model was used to simulate different cross-linked configurations using Fluent 6.3. The results were compared to the experimental results, and a new cross-linked configuration is proposed.

Chapter 3

Experimental Investigation

3.1 Overview

To conduct experimentally two-phase flow in multiple channels requires a large amount of effort to develop a test facility as well as to design test sections. Recently, Pehlivan (2003) built an experimental test facility for his work on two-phase flow in single mini- and micro-channels. The frame and the mixer from the Pehlivan (2003) design were used in the present work, but with a significant number of modifications. The modifications were in the major components, components such as flow meters, pump, test section support, etc. A large range of flow meters was established for both water and air. A gear pump replaced the recharged water tank used for two-phase flow in single channel. These components were carefully selected, consideration given to the requirements of this and further experiments.

Test section design is the most challenging part of this study. The challenge is that four channels are selected for flow measurement, while keeping the same pressure drop over all parallel channels as well as the same channel lengths. Methods of flow measurements, flow visualization, and pressure drop measurements were also challenging.

3.2 Experimental Test Facility

Figure 3.1 shows a schematic drawing of the main components used in the closed loop test facility. The adiabatic experiments are performed using air and water as the two-phase working fluid. A 40L tank contains distilled water. The water is driven through a gear pump with an output of 2.8 l/min and a maximum pressure of 689.5 kPa (100 psi). A ball valve and water filter are located on the suction line of the pump. Water is then pumped to the delivery line, where two needle valves are installed. Initially, these two valves are kept fully open. The first one is used to drain the water to the tank, whereas the second is used to lead water to the test section. A pressure gauge is also installed on the pressure line behind the second valve to observe the pressure of the liquid before it enters the test section. The flow rate for the water is controlled by slowly closing the first valve. Water is then led to the mixer through the flow meters which have a full-scale range of 0.0242 to 7.57 l/min. Air is supplied with a constant pressure of 724 kPa (105 psi), and is controlled by a pressure transducer and a flow meter, having a range of 0.012 to 87.95 l/min. The air passes through a check valve before entering the mixer, which is installed vertically to assure the two-phase flow is well mixed prior to entering the test section. The mixer (Figure 3.2) is made of a cylindrically shaped acrylic shell with two circular aluminum plates fastened to both ends. The bottom plate is designed for the entrance of two-phase working fluids. There is a small circular bar located in the middle of this plate with a hole drilled through its core to guide the air flow before it exits from an array of small holes in a spray form. A second hole is located on the bottom plate to introduce the liquid flow, whereas the top aluminum plate has only one hole in the middle, where the two-phase flow exits the mixer. Each flow meter for water and air is also controlled by a

needle valve which remains fully open. After passing through the test section, the liquid is drained back into the tank to complete the closed loop liquid circuit. A Sony DXC-9000 3- CCD camera is mounted on top of the test section to capture images of the flow inside the channels. Images are captured at a rate of 30 frames per second, with the shutter speed set to 1/10000. The lighting system consists of four halogen bulbs to evenly light the region of interest. Image acquisition is performed using LabVIEW™. A pressure transducer (PX01), ranging from 0-75 psi, is also established between a line connecting the mixer and the test section for pressure measurements. The output of pressure drop measurements then is monitored through an automatic data acquisition system using LabVIEW™. These main components are listed in the Table 1.

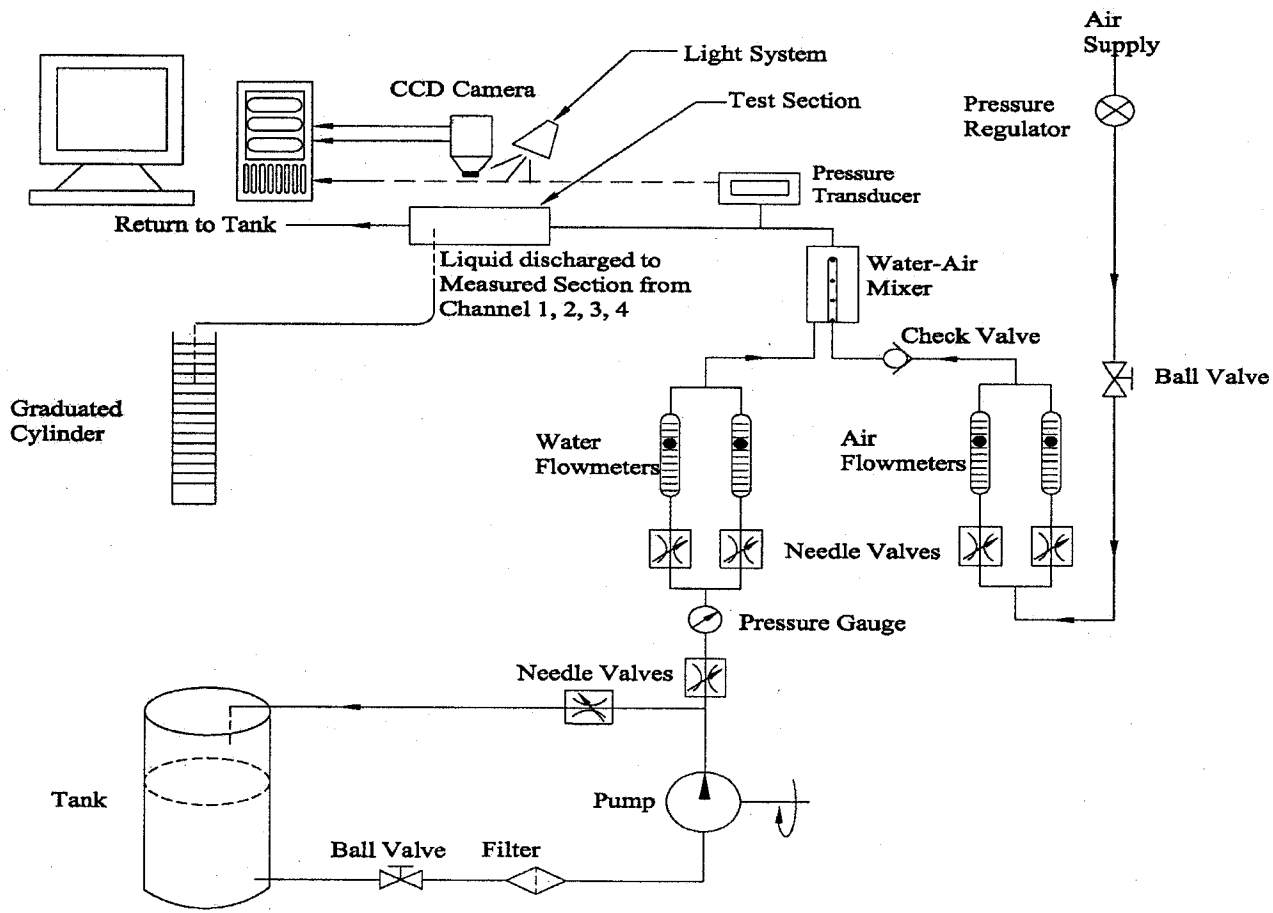

Figure 3.1. Schematic drawing of the experimental setup.

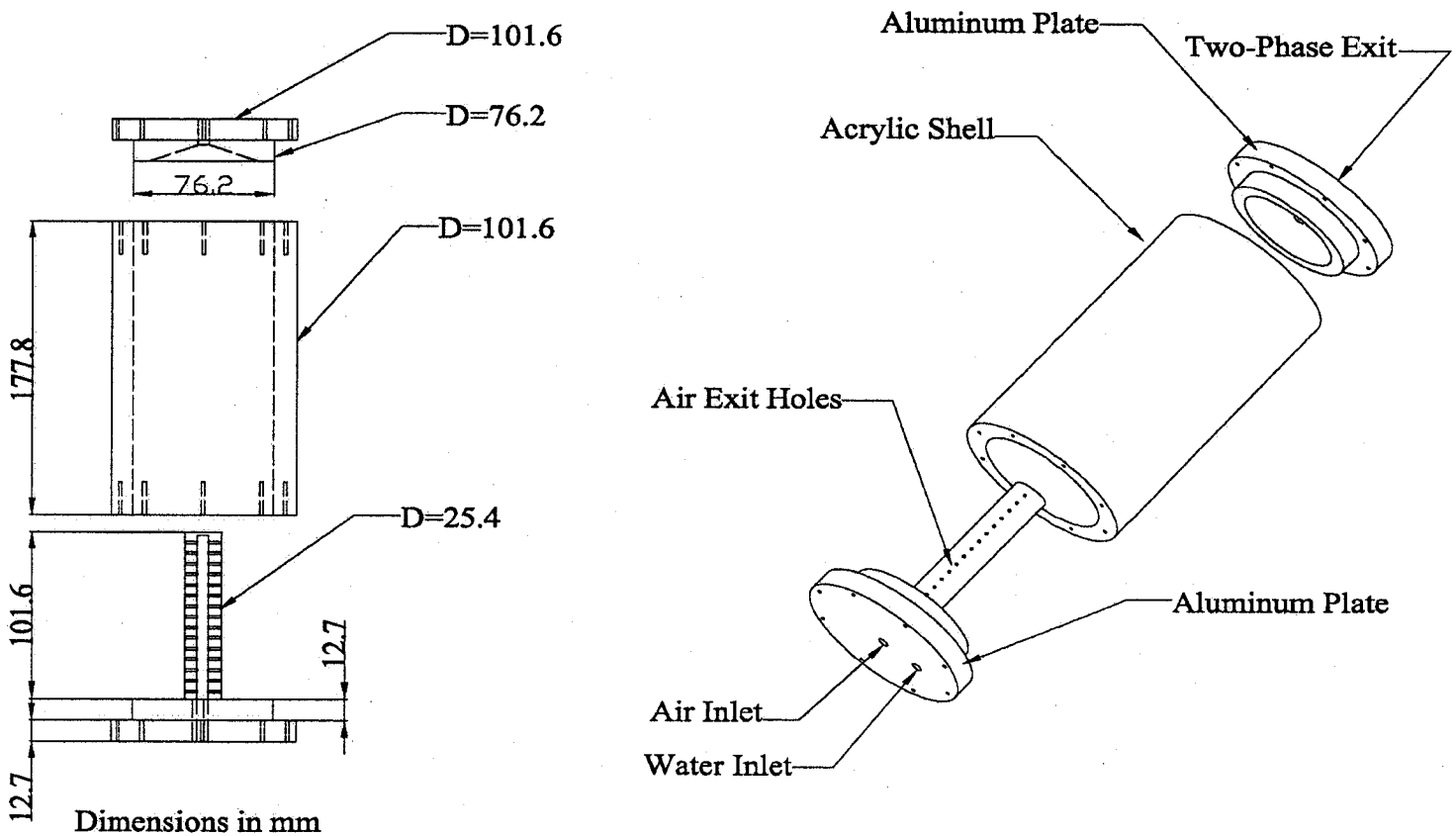

Figure 3.2. Mixer assembly.

Table 3.1. Main components for test facility.

No	Description	Quantity	Manufacture	Part Number	Range
1	Pressure Regulator	1	Parker	06E12A13A*SB	0-160 psi (0-1103 kPa)
2	Needle Valve	4	Swagelok	B-4JN	
3	Air Flow Meter	2	Omega	FL-113, FL-115	0.0242 - 7.57 l/m
4	Water Flow Meter	2	Omega	FL-113, FL-115	0.012 - 87.95 l/m
5	Needle Valve (Gate Valve)	2	Parker	N200S/N400S	
6	Cylindrical Tank	1	Cole Parmer	C-06317-61	10 Gal.
7	Pressure Gauge	1	Omega	PGS-25L-160	0-160 psi (0-1103 kPa)
8	Test Section	6			
9	Filter	1	Cole Parmer	EW-2959-17, 55, 73 and 89	80 micron
10	Differential Pressure Transducer	1	Omega	PX821-075DV	0-75 psi (0-517 kPa)
11	Check Valve	1	Parker		
12	Mixer	1	Home-made		
13	Pressure Gauge	1	Omega		0-100 psi (0-689 kPa)
14	3- CCD	1	Sony	DXC-9000	
15	Computer	1	Dell		

3.3 Test Section

The test sections consist of four parts which are assembled (see Figure 3.3), and the geometry of each part is provided in Appendix B. The parts are a cover plate, a channel plate, a metering plate and a metering container in which six different designs of the channel plate are investigated (Figure 3.4 and Table 3.2).

Each channel plate was glued with the cover plate to form a minichannel heat sink test section. The test sections are a scale up of approximately 9 times the heat sinks used in the work of Muwanga and Hassan (2006), so as to provide rapid and cost effective flow visualization experiments. They are all made from transparent acrylic to facilitate visual access of the flow characteristics. The channel plate consists of a horizontal header with a cross sectional area of 9 mm by 1.59 mm, connected to 45 parallel channels whose cross sections are 1.59 mm by 1.59 mm. Four channels, the 1^{st}, the 15^{th}, the 30^{th}, and the 45^{th} having the same length of 131.3 mm to other 41 channels, are selected for flow distribution tracking, as shown in Figure 3.4. At the exit of these four channels, the fluid is diverted to metering containers through slots which are open to the atmosphere.

A metering plate is used to collect the liquid coming from the remaining channels, whose exits are also open to the atmosphere, and drains the flow into the reservoir. The inlet hole is located in the middle of the cover plate (Figure 3.3), guiding the two-phase flow into the header of the channel plate.

The difference between the six heat sink designs (Table 3.2) is that the cross-links were introduced to the channel core of the standard straight channel test section. The CR-2, CR-2A and CR 2B test sections consist of two cross-links that were located at 1/3 and 2/3 of the channel length, and their width varied by one, two and three times the channel width, respectively. The CR-4 and CR-6 test sections consist of four and six cross-links divided along the channel length into five and seven equal sections, respectively, and their width and height are the same as the channel width.

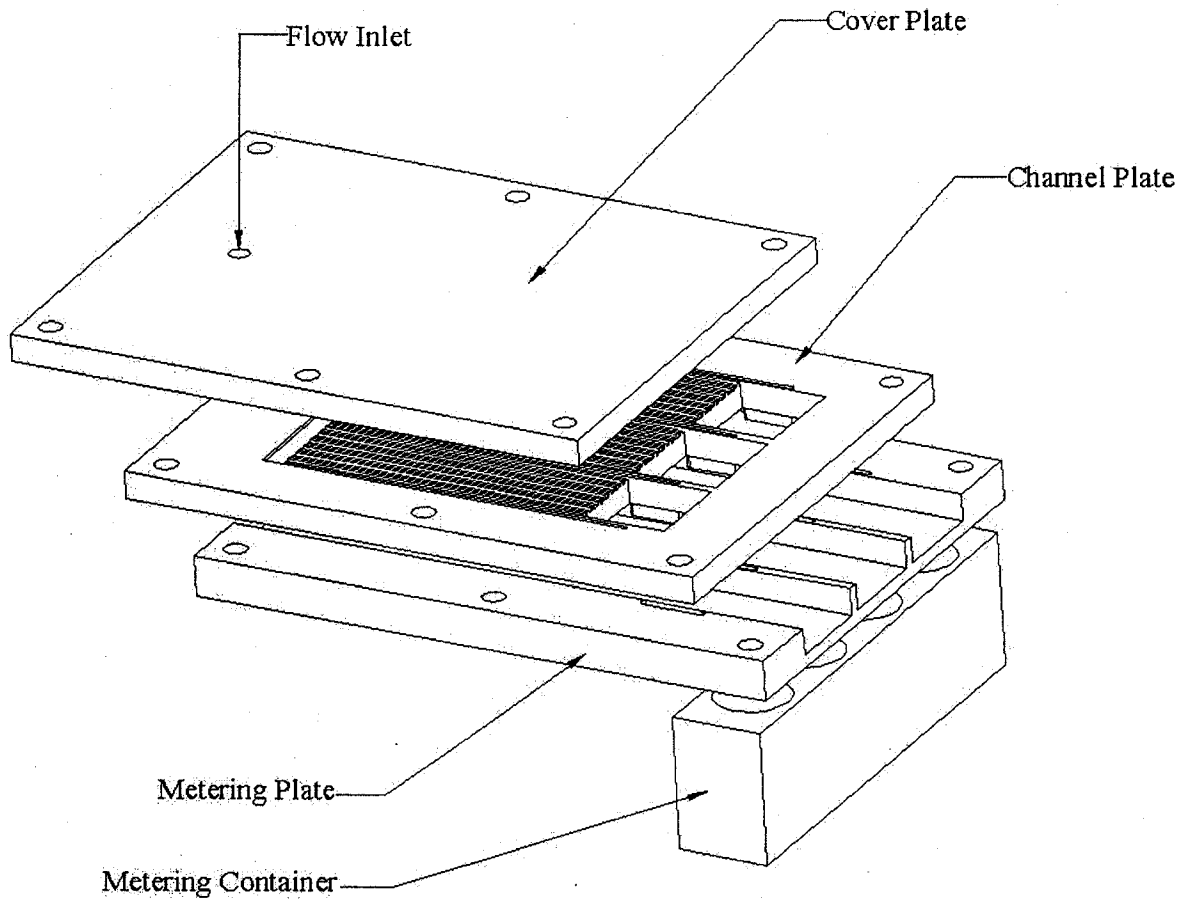

Figure 3.3. Test section assembly.

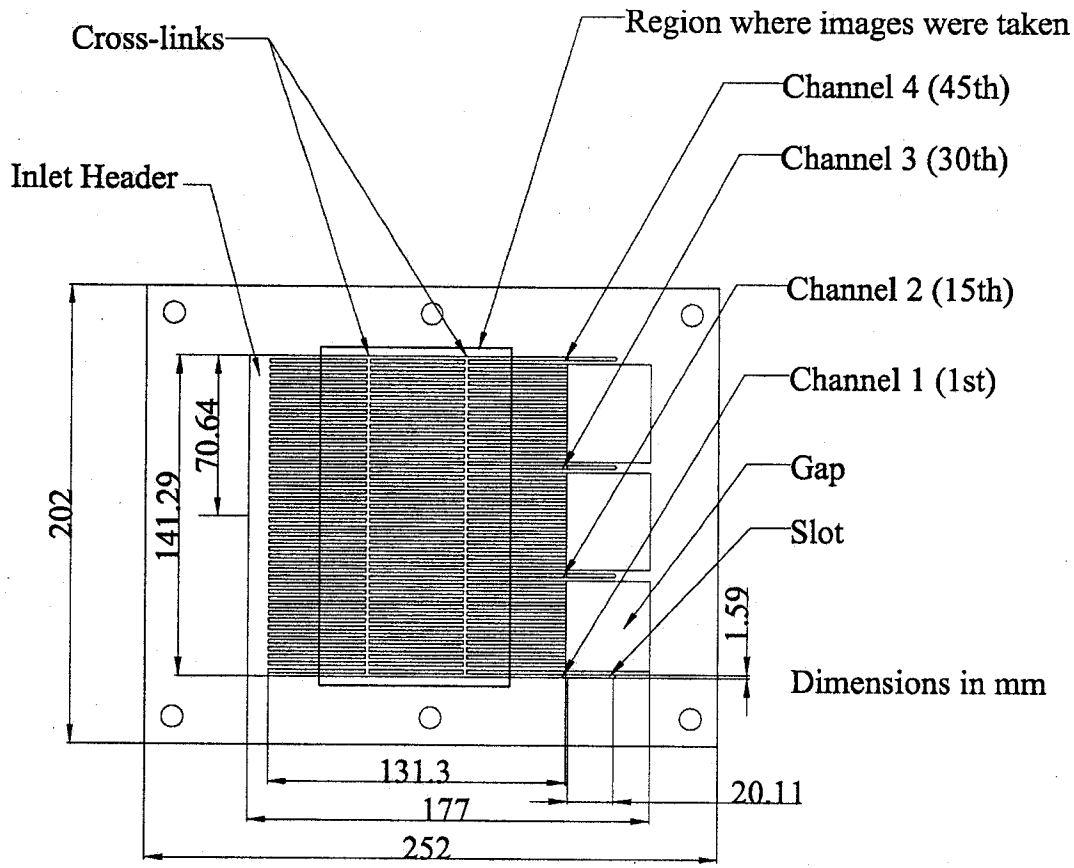

Figure 3.4. Cross-linked channel plate.

Table 3.2. Summary of test section geometries.

Test Sections	Number of Channels	Channel width (mm)	Channel Length (mm)	Number of Cross-links	Width of Cross-Links (mm)	Positions of Cross-Links respected to channel length
STR	45	1.5875 (1/16")	131.3	—	—	—
CR-2	45	1.5875 (1/16")	131.3	2	1.5875 (1/16")	1/3 and 2/3s
CR-2A	45	1.5875 (1/16")	131.3	2	3.175 (2/16")	1/3 and 2/3s
CR-2B	45	1.5875 (1/16")	131.3	2	4.7625 (3/16")	1/3 and 2/3s
CR-4	45	1.5875 (1/16")	131.3	4	1.5875 (1/16")	1/5, 2/5s, 3/5s, and 4/5s
CR-6	45	1.5875 (1/16")	131.3	6	1.5875 (1/16")	1/7, 2/7s, 3/7s, 4/7s, 5/7s, and 6/7s

3.4 Experimental Procedure

After installation of all components such as the pump, flow meters, test section support, etc., the test section was mounted on the test rig. A bubble level was used to make sure the test section was horizontal on the set-up. On first operating the gear pump, great care was taken with the installation. The level of water in the tank (Figure 3.1) was set high enough to avoid pump cavitation. Attention was paid to the gears from the suction and the pressure sides of the pump were wet for lubrication before operating. The flow was run through the test section to test for water and air leaks in the system.

After testing for leaks in the system, a desired flow rate was set. The system was put in operation for 5 to 10 minutes in order to achieve an approximate steady flow before any data was taken. A description of the procedure for taking data from flow measurements, flow observation, and pressure drop measurement will be found in the following section on methodology.

3.5 Methodology

As this work was carried out in a scaled-up configuration, under adiabatic conditions with an air-water mixture, the applicability of the results to microscale systems needs some special consideration. A number of non-dimensional groups which are relevant to two-phase flow studies in microchannels are listed in the work of Kandlikar (2004). Relevant to the present system is the Weber number (We), which represents the ratio of inertia to surface tension forces. The Weber number is considered a useful dimensionless

parameter to analyze fluid flows where there is an interface between two different fluids. It may be defined with respect to the hydraulic diameter as in Equation 3.1.

$$We = \frac{G^2 D_h}{\rho_{TP} \sigma} \qquad 3.1$$

Considering the scaling of a system, whereby the two-phase mixture and system temperature remain constant, the density and the surface tension, which are fluid properties, would remain constant. For a fixed Weber number, then, reducing the diameter by nine times in relation to the present work, the mass flux should be increased three times. Given the mass flux range examined in the current work (41 kg/m²s – 834 kg/m²s) and for a fixed Weber number, the results will be applicable in microscale systems of similar two-phase mixture for a mass flux range of 124 kg/m²s to 2503 kg/m²s. It is noted that mass fluxes, over 1000 kg/m^{2}s, have been used in microsystems, as in the work of Steinke and Kandlikar (2004).

3.5.1 Flow Measurement

After flowing through the test section, the liquid is collected in a graduated cylinder (Figure 3.1) from one of the four selected channels, while the elapsed time is recorded. This procedure is repeated for each of the four selected channels.

Before taking measurements, the calibration chart provided for the flow meters from the manufacturers should be verified. To do so, water is used to verify the calibration charts. If it shows good agreement for water, flow meters which are used for the air flow can be

trusted to adequately measure the flow. After performing calibration for all flow meters, the flow measurements in the 4 selected channels were taken. Before a desired flow condition was set to take measurements, flow was run through the test section with a high water flow rate in order to purge the air inside the channels. When the flow condition was set, the system was operated for about 5 minutes prior to taking measurements in order to have the flow as steady as possible.

A graduated cylinder was put under the metering container (Figure 3.1) to collect liquid flow in the four selected channels. Flow measurement was taken separately for each of the four selected channels, while the time was recorded simultaneously with a stop watch. The recording time was from 2- 5 minutes depending on the flow rates. After recording the flow rates for each of the 4 selected channels, the data was input into the computer and a plot was constructed for flow distribution.

3.5.2 Flow Visualization

The images are taken from the central region of the test sections, as shown in Figure 3.4. Since an image of all four selected channels does not provide a high enough resolution of the flow patterns, images of channels 1 and 2 were taken separately from channel 3 and 4. Flow patterns are analyzed for each of the four selected channels from these images. These flow patterns are then plotted for various flow qualities (Eq. 3.2) in terms of a fractional time function (f) which is defined as the number of flow patterns (N_i) divided by the total number of observation (T) at a particular flow condition (Eq. 3.3).

$$x = \frac{\dot{m}_G}{\dot{m}_G + \dot{m}_L} \tag{3.2}$$

$$f = \frac{Ni}{T} \tag{3.3}$$

Before taking images, a trial was carried out in order to optimize image quality by adjusting the light and the height of the camera from the region of interest. As mentioned earlier, to improve the quality of the images, three sets of images were taken separately for channels 1 and 2, channels 2 and 3, and channels 3 and 4. The zoom of the camera was set as close to the region of interest as possible, while uniform lighting in this region was required. Images are captured at a rate of 30 frames per second. Image acquisition was performed using LabVIEW™. The speed was also set to 1/10000 in order to freeze the frame for analyzing flow patterns, as described in the following section. Based on these flow patterns, flow configurations were plotted in terms of fractional time function (Eq. 3.3).

3.5.3 Two-Phase Pressure Drop

Three sets of 400 data points were taken in two seconds to measure pressure drop for a particular flow condition. The mean of these three measured sets was calculated for the pressure drop of the test section, including the pressure loss from the tube connecting to the test section inlet. The same procedure was then repeated for the tube only. The pressure drop for the test section is the differences of the means of the above pressure drop measurements.

The pressure drop measurements for test sections and for the tube were taken separately. The tube should be set up carefully. The end of the tube should be mounted in the same position as it is connected to the test section. The fitting should be connected to the tube end and it should be firmly fixed when flow is run through. This prevents vibration and shifting of the position. Pressure drop data of the six test sections are then taken afterwards, whereas the pressure drop outputs of these two measurements are monitored through an automatic data acquisition system using LabVIEW™.

3.6 Experimental Uncertainty

An uncertainty of less than 5 % is estimated for flow measurements, based on the uncertainties in the measurement instrumentation, including the timer, flow meters, and graduated cylinders. The uncertainty for flow measurement can be calculated by using the Equation 3.4, where it is the sum of the uncertainties in the above instrumentation.

$$U_{FM}^2 = U_{FL}^2 + U_T^2 + U_{GC}^2 \qquad 3.4$$

The uncertainties in the flow meter (U_{FL}) and in the graduated cylinder (U_{GC}) take into account the accuracy and the reading uncertainty. For example, the accuracy of the flow meter provided by the manufacturer is typically about ± 2%. Uncertainty of reading the scale is estimated as the ratio of the half grade value and the maximum value, yielding 0.3 %. The stop watch is used for time recording. Hence, the uncertainty of the timer (U_T) takes into account the uncertainty of time recording and the accuracy of the stop watch.

The uncertainty of the time recording is estimated as the difference between the recorded time and the appearing time when the time is stopped. The difference is considered very small, less than 0.05% of error. The accuracy of the stop watch can be estimated as 1.5 second per day.

Surface roughness is not measured prior to sealing the channels. However, based on The Machinery's Hand Book, Oberg et al. (2000), the surface roughness is expected to be in the range of 6.3 to 1.6 μm. The lower range is expected due to the low feed rates used when machining acrylic material.

Images are taken from the region of the test sections as shown in Figure 3.4. Since the region where images are taken is about 2/3 of the channel length, the observed flow patterns can be considered as dominant flow patterns in a whole length of channels. For the pressure drop measurements, the estimated uncertainty is 0.45 kPa (0.065 psi), based on instrument specifications.

Chapter 4

Experimental Results and Discussion

4.1 Overview

In this chapter, experimental results are presented in terms of flow distribution, flow visualization and two-phase pressure drop for six different configurations. Results of flow distribution are generated by measuring liquid in the four selected channels for six test sections. The results are then plotted and compared between the test sections. The results of flow observation are presented in terms of flow patterns in the four selected channels. The two-phase pressure drops of all test sections are measured and compared with each other as well as with some widely used two-phase pressure drop models. The influence of cross-links and two-phase flow characteristics in the array of parallel channels are then discussed.

4.2 Two-Phase Flow Measurements

Two-phase flow measurements were carried out by monitoring the liquid flow from four channels. Six cases (Table 4.1) were examined in the present work, based on the simplified flow map presented by Hassan et al. (2005) (Figure 4.1), in three different regions, namely bubbly, intermittent, and annular flow regimes. The purpose of choosing these cases is to cover a range of potential flow patterns and to compare flow characteristics within the six test sections presented in this study.

Table 4.1. Liquid and gas superficial velocities and flow qualities of the examined flow range.

Case	J_G (m/s)	J_L (m/s)	x	G (kg/m²s)
1	0.025	0.835	3E-05	834.44
2	0.378	0.273	0.002	273.65
3	0.378	0.142	0.003	141.97
4	4.604	0.142	0.038	146.98
5	4.604	0.036	0.135	41.61
6	9.926	0.036	0.245	47.91

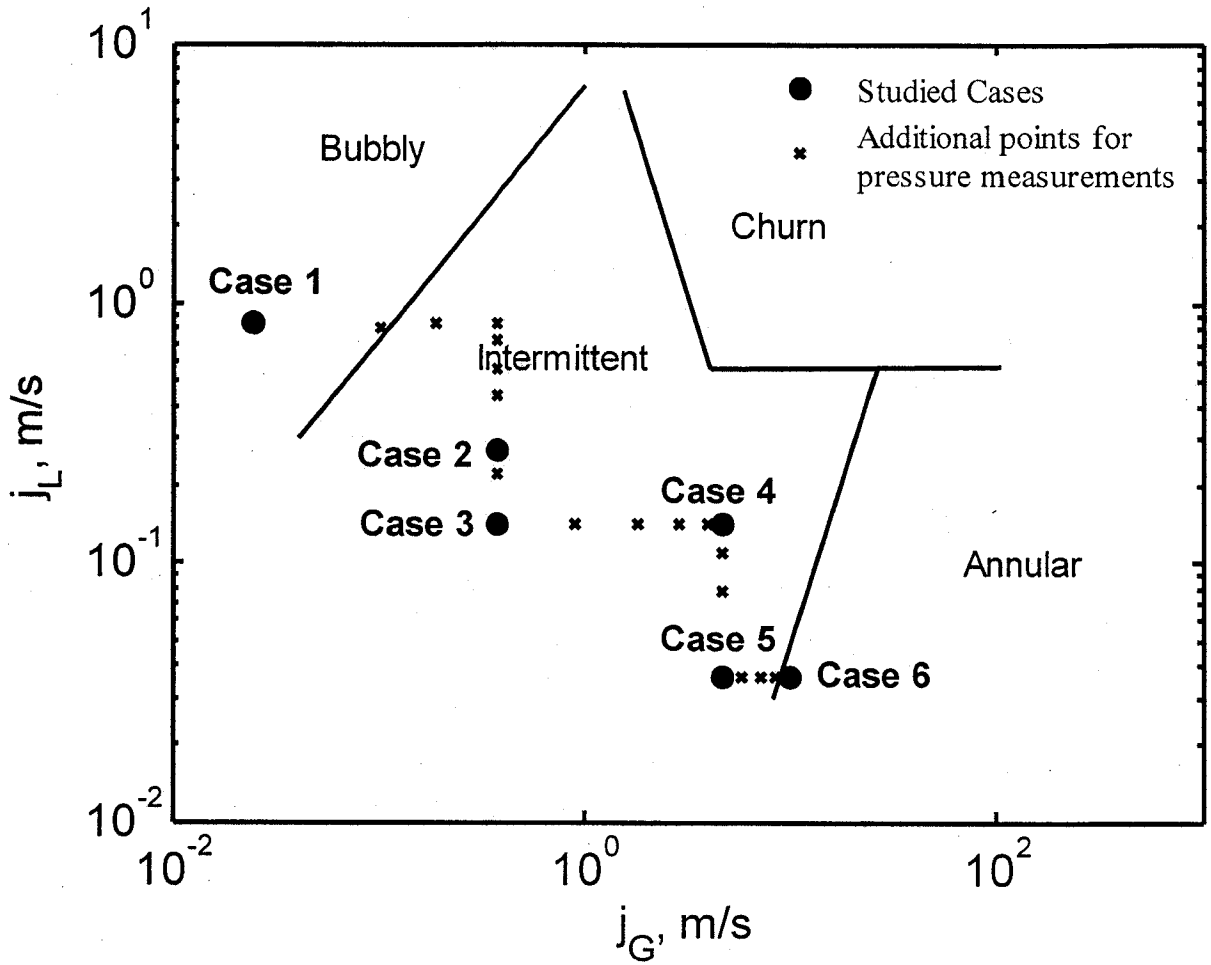

Figure 4.1. A simplified flow map, Hassan et al (2005).

4.2.1 Flow Distribution Comparison

Figure 4.2 presents the mass flow rate percentage of the four selected channels. The mass flow rate percentage (O) is the ratio of the measured flow in the four selected channels to the total liquid flow rate, whereas the ideal mass flow rate percentage is the ratio of ideal flow, assuming equally distributed flow in all channels. The results vary from 5% to 17% of the total flow, compared to the ideal case of 8.8 %. Figures 4.3 and 4.4 present flow distribution in terms of the total deviations percentage (W) in the four selected channels due to the effects of the number of cross-links and the cross links width, respectively. The deviation percentage is defined as the absolute values of the difference in the measured to the ideal flow rate with respect to the ideal flow rate. By definition, the flow distribution would approach a uniform distribution throughout the channels if W moved toward zero. The results show that W is very large and there is no discernible trends between the test sections. The highest deviation that occurred for all test sections is for Case 4 (x= 0.0371), where the gas flow was significantly increased while the liquid flow remained constant from Case 3 (Table 4.1). However, the results show lower deviations for the CR-4, CR-6, CR-2A, and CR-2B test sections for Case 4, in which less than 390% of the deviation for the CR-4, CR-6, CR-2A, and CR-2B test sections compared to over 450% of the deviation in the STR and CR-2 test sections.

4.2.2 The Effects of Cross-Links on Flow Distribution

Figure 4.5 presents flow distribution in terms of deviation percentage (R), which is defined in the previous paragraph, from Case 1 to Case 6. From Cases 1-4, high liquid was observed in channels 1 and 4, which is likely accounted for by the two other

channels, 2 and 3, having an opposing trend. Hence, channels 2 and 3 have lower liquid flow in such cases. However, the results show that liquid flow increases in these channels for the cross-linked test sections, compared to that for the straight test section. It is interesting to note that liquid flow is significantly increased in channels 2 and 3 for the CR-2A, CR-2B, and CR-6 test sections which considerably provide more space for flow sharing along the cross-links. Cases 5 and 6 (Figures 4.5 d and e) show that liquid flow increases in channels 2 and 3, whereas it starts decreasing in channels 1 and 4 for all test sections. It is possibly due to high gas and low liquid flows taken in these two cases (Table 4.1) in which low liquid flow is preferably driven (by air) to channels closed to the inlet. In these cases, the cross-linked test sections overall show better flow distribution compared to the straight test section. These cases, however, contain high gas and low liquid flows. Working under these flow conditions is not recommended if heat is applied to the surface of the heat sinks because hotspots could occur.

Although the cross-link configurations studied in the current work did not significantly improve the mal-distribution caused by the inlet configuration, the influence of cross-links on the results of two-phase flow distribution is helpful in seeking promising designs to overcome the entrance effects. As a result, it is proposed that the more cross-links which are added to the channel core the better the flow communicated between channels. The larger the width of cross-links, the larger the available space in which fluids can communicate between channels. Moreover, the CR-2A test section which has two cross-links whose width is two-times larger the channel width, in overall, shows better flow distribution in the four selected channels.

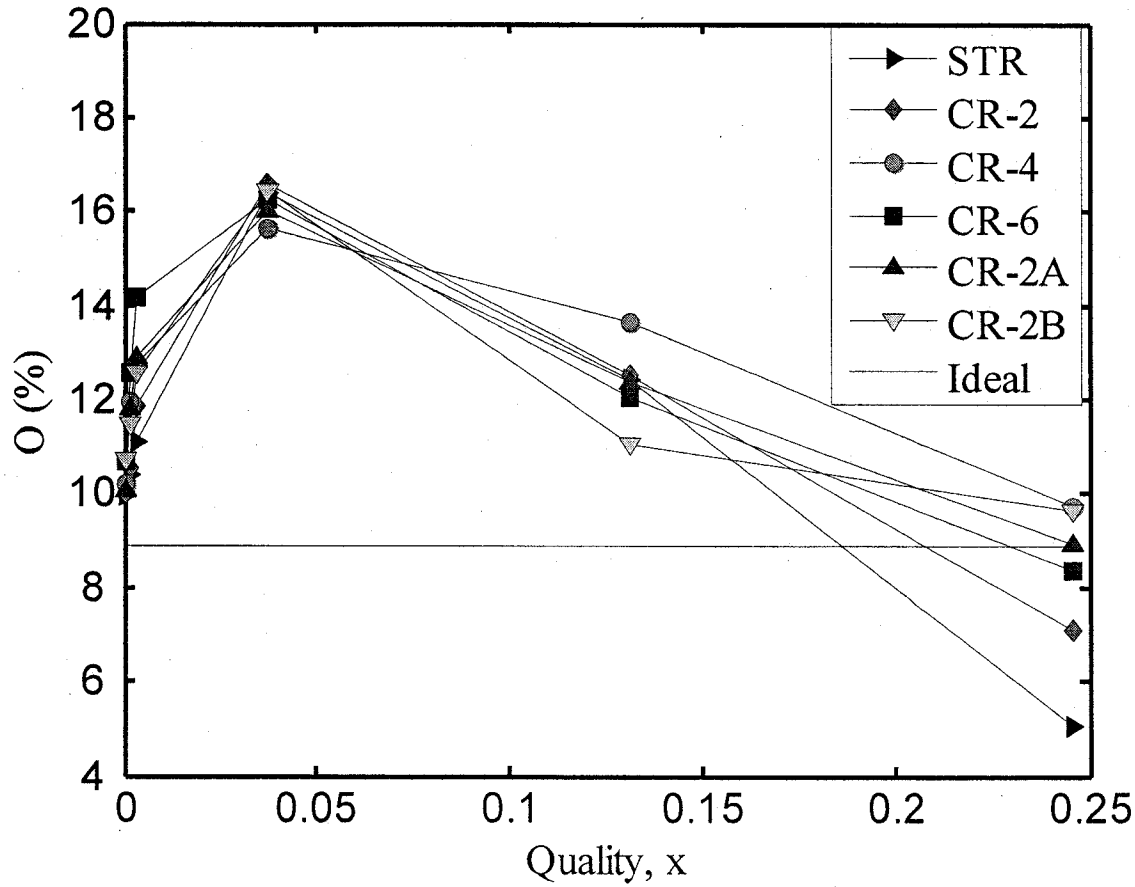

Figure 4.2. Two phase flow percentage in four selected channel.

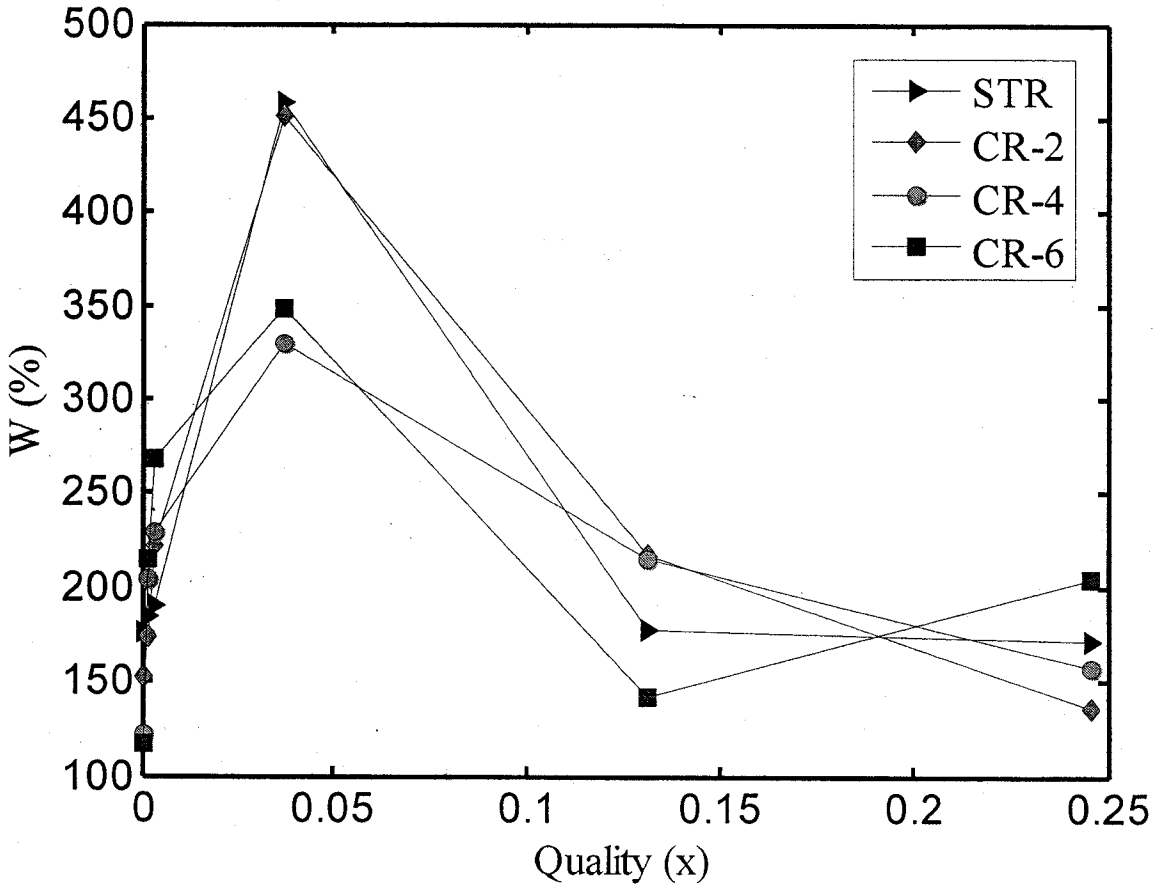

Figure 4.3. Two-phase flow measurements due to the effect of number of cross-links.

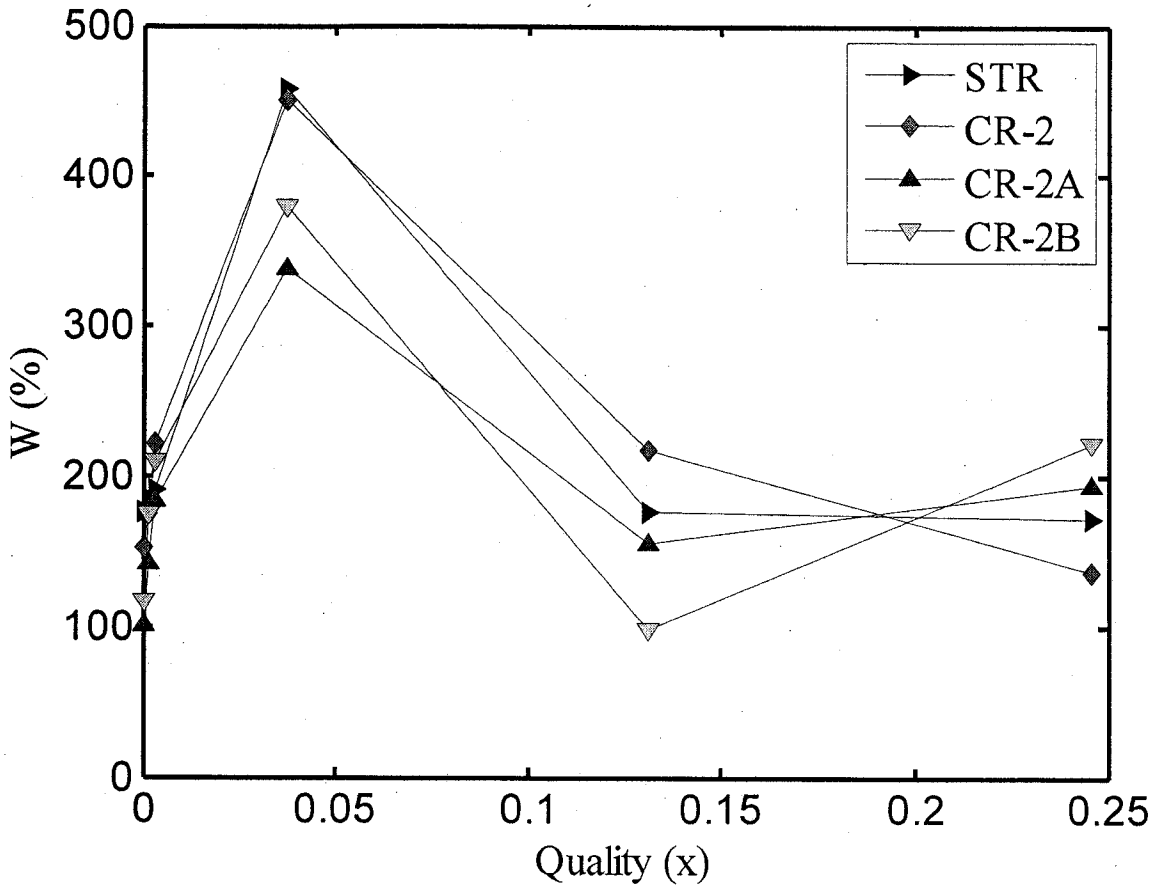

Figure 4.4. Two-phase flow measurements due to the effect of the cross-links width.

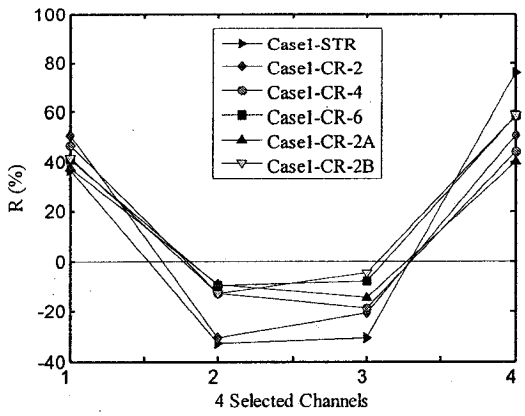

a) Case 1 (x = 0.0000348)

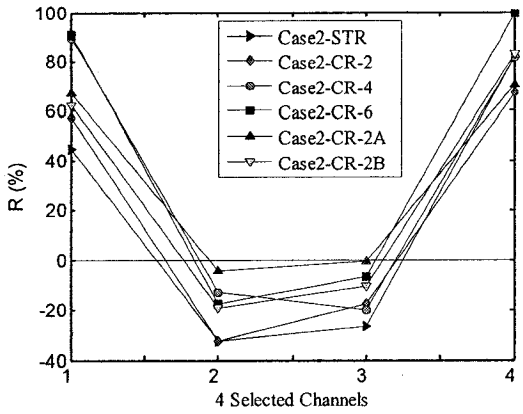

b) Case 2 (x = 0.0016)

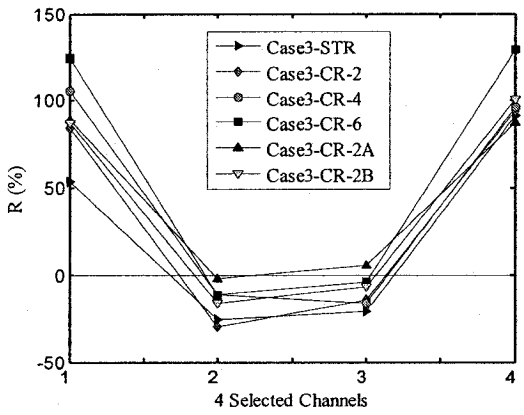

c) Case 3 (x = 0.0032)

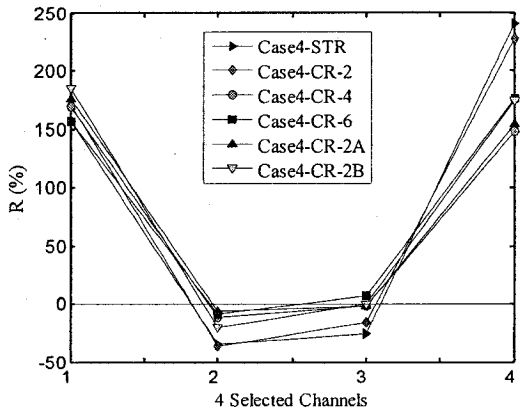

d) Case 4 (x = 0.0371)

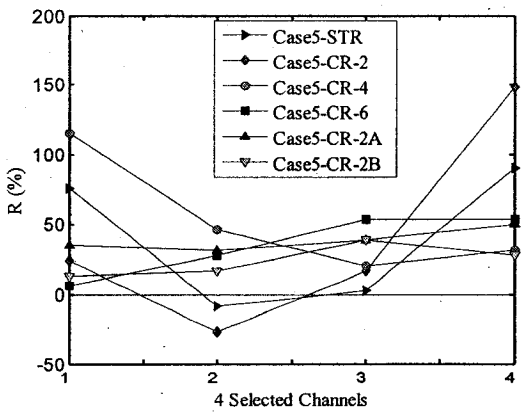

d) Case 5 (x = 0.1311)

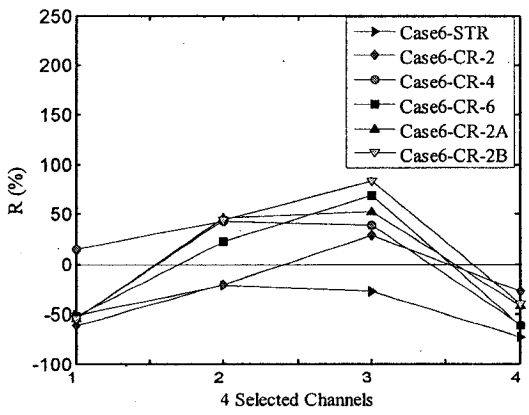

e) Case 6 (x = 0. 2454)

Figure 4.5. Flow Distribution in four selected channels for each studied cases.

4.3 Two-Phase Flow Visualization

Experimental data for two-phase flow patterns in multiple channels in this work will provide new data in this research field. The results also lead to further insight into the effects of cross-links incorporated into the channel core as well as lead to better understanding of two-phase flow distribution in parallel multi-channel systems.

4.3.1 Flow Pattern Determination

Three flow regimes, which are the dispersed flow regime, the intermittent flow regime, and the annular flow regime, are observed in the present work and are discussed in the following paragraphs.

Dispersed Flow Regime

The dispersed flow regime (Figure 4.6a) is defined as a combination of bubbly flow and the dispersed bubble flow. It is seen for a high flow rate of liquid when small bubbles are dispersed in turbulent liquid flow. The bubbly flow pattern is defined as gas phase distributed as small bubbles through the turbulent liquid phase. Dispersed flow pattern is observed when the flow rate of gas is increased. The bubbles start to decrease in size and disperse into the liquid flow.

Intermittent Flow Regime

The intermittent flow regime (Figure 4.6b) is defined as a regime consisting of discontinuous flow in the liquid and gas flows. In this regime, the plug flow, elongated bubble flow, and interspersed bubble within elongated bubble flow are observed. Since

the flow measurement was examined, plug flow can be qualitatively defined as small plugs of bubbles, like bullets, flowing uniformly in the liquid flow. Elongated bubble flow consists of long bubbles and some shorter bubbles interspersed between them, whereas interspersed elongated bubble flow consists of tiny bubbles interspersed within the elongated bubble flow. Both are however considered as the elongated bubble flow.

Annular Flow Regime

The annular flow regime (Figure 4.6c) is defined as the separated flow of liquid and gas, with a gas core flow in the middle of the channels and liquid flow along the walls. In this flow regime, the top and the side annular flow are observed. The top annular flow pattern is the annular flow in which the liquid is observed from the top of the test section, whereas liquid is on the side walls of the channels defines the side annular flow pattern.

4.3.2 Discussion on Flow Visualization

This section will discuss two-phase flow observations in a multi-channel system by comparing flow patterns observed in six test sections. Figure 4.7 shows different flow patterns observed in multiple channels for a particular flow condition. Figures 4.8 and 4.9 show samples of the dominant flow patterns that appeared in the selected channels for some cases.

As discussed earlier, more liquid was collected in channels 2 and 3 for the CR-4, the CR-6, the CR-2A, and the CR-2B test sections, than the STR and the CR-2 test sections. This can be illustrated in Figure 4.8, which shows that the dominant flow pattern in channel 3

is the elongated bubble flow for the STR and the CR-2 test sections, whereby plug flow dominates in the same channel for the remaining test sections. On the other hand for channel 4, elongated bubble and annular flow are observed for the CR-4, the CR-6, the CR-2A, and the CR-2B test sections, while the plug flow was observed in this channel for the STR and the CR-2 test sections (Figure 4.9). Hence, less liquid was collected in channel 4 from the CR-4, the CR-6, the CR-2A, and the CR-2B test sections than that from the STR and the CR-2 test sections. Such results also lead to different flow deviations for all test sections, as discussed in the earlier section (4.2.1), when the cross-links are incorporated in the channel core.

4.3.2 The Effects of Cross-Links on Flow Visualization

The effect of cross-links on flow characteristics can be seen in Figure 4.10, which shows flow communicating between channels through the cross-links. The cross-links can be considered as outlet headers, where the exit flow in channels can be freely expanded. Hence, flow may be shared with neighboring channels. It was observed that bubbles got trapped between two channels which have similar strength of flow field. It was observed that bubbles got trapped between two channels which have similar strength of flow field. They were observed circulating in between channels, especially between two high flow channels.

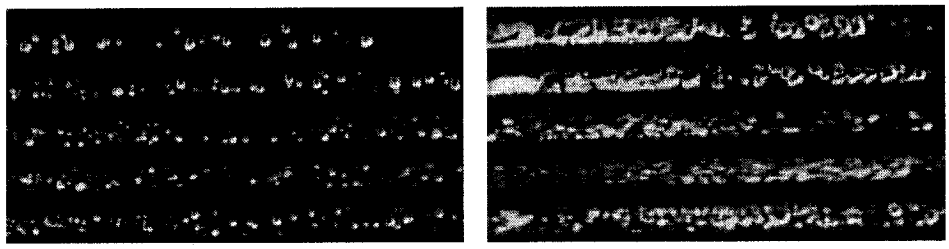

Bubble flow pattern (x=0.0000348) **Dispersed flow pattern (x=0.0016)**

a) Dispersed flow regime.

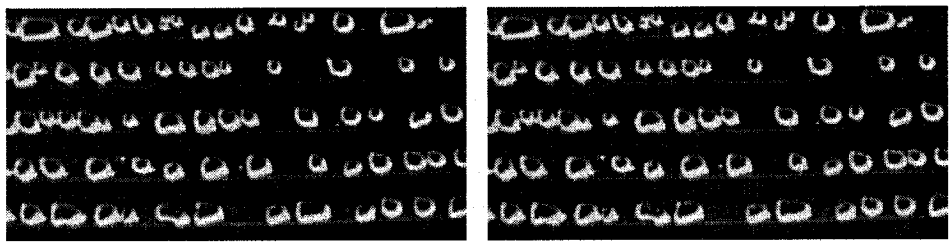

Plug flow pattern (x = 0.0000348)

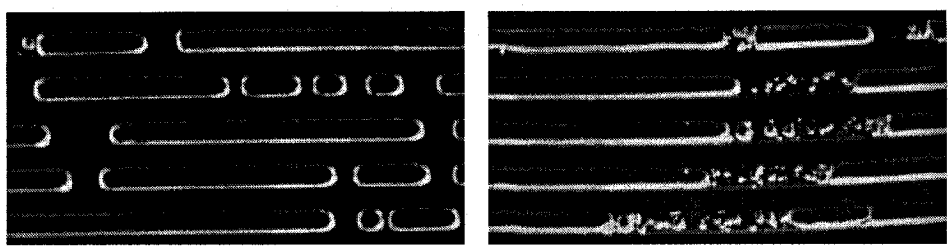

Elongated bubble flow pattern (x = 0.0032) **Interspersed bubbles within elongated bubble flow pattern (x = 0.0032)**

b) Intermittent flow regime.

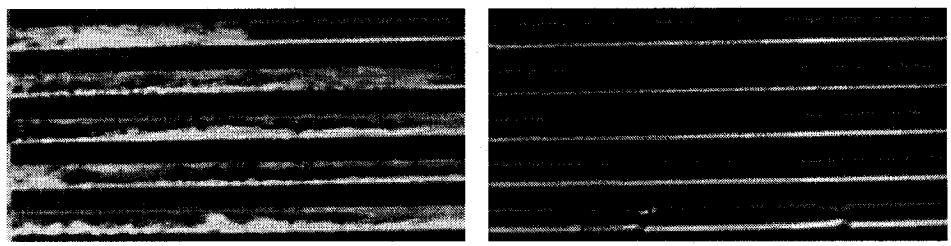

Annular flow pattern (x = 0.0371) (Liquid from the top- wall) **Annular flow pattern (x = 0.1311) (Liquid from the side-walls)**

c) Annular flow regime.

Figure 4.6. Samples of flow patterns

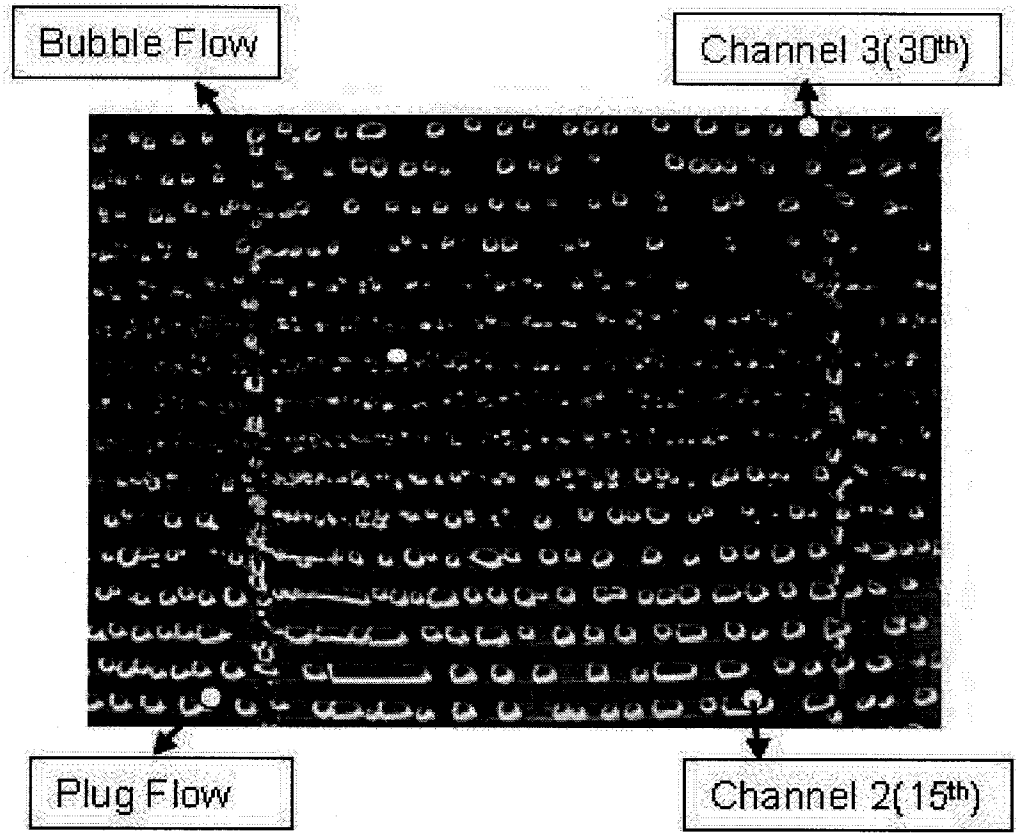

Figure 4.7. Samples of flow patterns observed throughout 45 channels.

(Direction of flow is from the left to right)

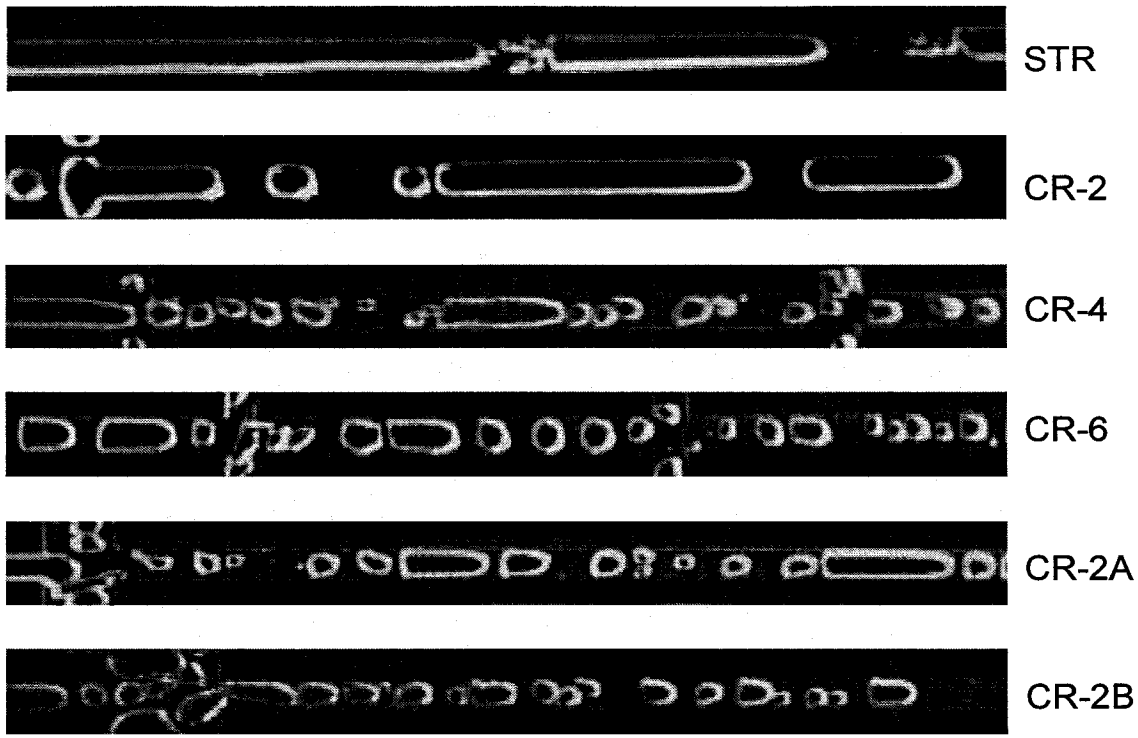

Figure 4.8. Samples of dominant flow patterns comparison in channel 3- Case3.
(Direction of flow is from left to right)

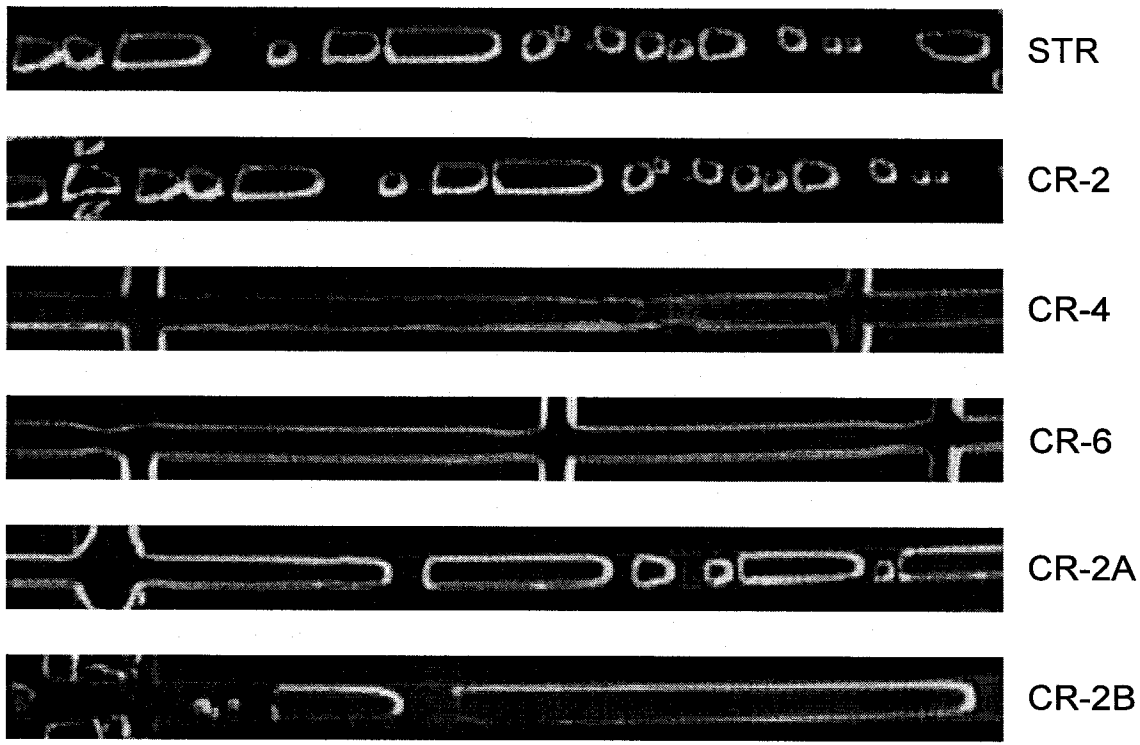

Figure 4.9. Samples of dominant flow patterns comparison in channel 4 - Case3.
(Direction of flow is from left to right)

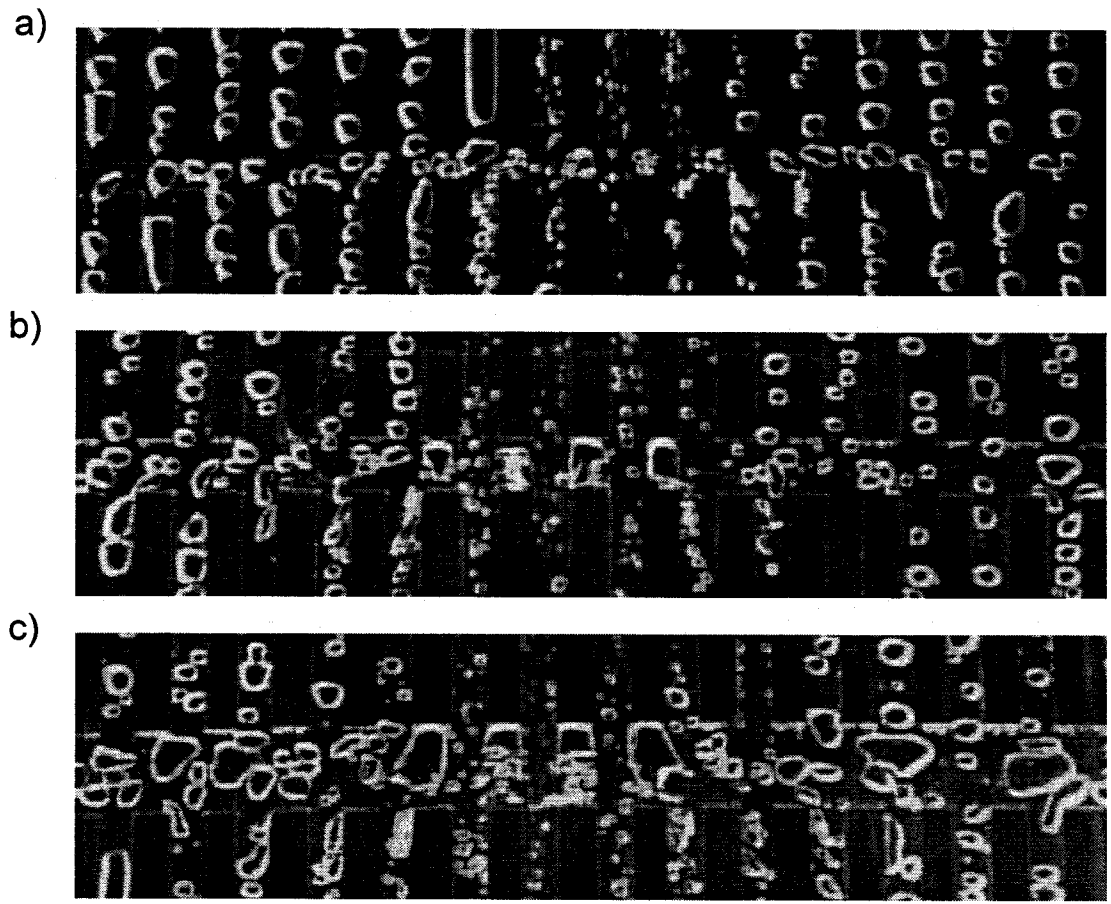

Figure 4.10. Samples of flow interaction- a) CR-2; b) CR-2A; c) CR-2B.
(Direction of flow is from top to bottom)

For the CR-2 test section, these observed bubbles have almost the same size as the size of the cross links (Figure 4.10a), this results in less liquid sharing between channel flow paths. There will be more space for flow communication as the width of cross-links is increased (Figures 4.10b, and 4.10c). As a result, more liquid is transferred to some channels such as channels 2 and 3 from the CR-2A and CR-2B test sections than the remaining test sections (Figure 4.5). However, bigger bubbles were observed to be trapped between channels which have similar high flow, and more of that is observed from the CR-2B test section (Figure 4.10c). This leads to more liquid collected in channels 2 and 3 from the CR-2A than CR-2B test sections in some particular cases. It can be proposed that increasing the width of cross-links would give more benefit to flow sharing than increasing the number of cross-links, which have the same width as the channel width. However, too large a width of the cross-links might not be effective, as in the case of the CR-2B test section.

4.3.3 Flow Pattern Comparison in terms of Fractional Time Function

Flow distribution can be better understood when discussing flow patterns in terms of fractional time function. Based on the observed dominant flow patterns, the fractional time functions were constructed for Cases 1-4 as shown in Figure 4.11. Cases 5-6 are not presented because of the difficulty in distinguishing the gas flow and the annular flow patterns at these high flow qualities. High liquid flow, which was measured in channels 1 and 4, can be explained based on observed flow patterns. Figures 4.11c and 4.11d show that no annular flow regime was observed in channels 1 and 4 at Case 3 (x = 0.0032), and no intermittent flow patterns were observed in channels 2 and 3 at Case 4 (x = 0.0371),

the highest deviation case. It was noted that there was no bubbly flow observed in four selected channels for these cases. Intermittent flows are lower quality flow patterns than annular flow, and hence more liquid passes when they are present compared to when there is annular flow. It is also seen that more intermittent and less annular flows are observed in channels 2 and 3 from the cross-linked test sections compared to those in the straight test section. As a result, more liquid was collected in these channels from the cross-linked test sections.

4.3.4 Flow Pattern Analysis

Two-phase flow patterns can also be analyzed based on the effects of surface tension and inertia (Hassan et al. 2005). Based on this, the results in channels 1 and 4 for Case 2, 3, and 4 are then due to the effects of surface tension in which the plug and elongated bubbles dominate. Whereas, the results in channels 2 and 3 are due to effects of both inertia and surface tension for the same cases, in which elongated and annular flow dominate. Moreover, the results in channels 1 and 4 are due to the effects of inertia for Case 1, whereas the results in channels 2 and 3 are due to the effects of surface tension. Combining the results from flow distribution and flow visualization, the air superficial velocity at the inlet of the four selected channels can be estimated based on the flow patterns and the ratio of gas inertia to liquid inertia (slip ratio, see Eq. 4.2).

$$S = \frac{j_G}{j_L} \tag{4.2}$$

Neglecting the viscosity along the channel walls, the superficial velocity of the water can be calculated from flow distribution, whereas the superficial velocity of the gas can be estimated based on flow patterns appearing in the channels. For example, annular or dispersed flow patterns are due to the effects of inertia, hence the slip ratio can be estimated to be greater than or less than one, respectively. On the other hand, plug or elongated bubble flow patterns will have a slip ratio of approximately one, due to the effects of surface tension. However, how close the slip ratio is to one depends on the specific characteristics of the intermittent flow patterns; for example, the elongated bubble flow pattern will have a slip ratio closer to one than the plug flow pattern. Considering this approach, it is conjectured that liquid and gas flows should be present in Case 1 and Case 4 respectively. Figure 4.12 presents the measured superficial velocity of liquid in the four selected channels and the ideal superficial velocity of gas, assuming equally distributed gas flow in all channels. Considering Case 1 in this figure, the ideal gas superficial velocity is very low compared to the liquid superficial velocity for channels 2 and 3. As plug flow dominates in these channels, which is a surface tension effect, the gas superficial velocity in these channels is expected to approach the liquid superficial velocity. This, in turn, will produce a gas superficial velocity in other channels close to zero, due to mass conservation and consequently should produce instances of all liquid flow. Conversely, the same argument may be used for the existence of all gas flow during Case 4. The all liquid or gas flow patterns were not observed in the selected channels, nor in the other 41 channels over the 30 frames captured at a given time instant. They are therefore expected to occur at different time instances. These occurrences, however, are not expected to influence the dominant flow patterns determined due to the

similarity in characteristics between symmetry channels (e.g. channels 1 and 4) and the similarity between test sections, all of which are taken at different time.

4.3.5 Comparison Flow Patterns to Single Channel Flow Map

Since there are no appropriate flow maps constructed for multi-channel configurations, dominant flow patterns are compared to flow pattern for single channels. Figure 4.13 presents the flow regime in terms of the fractional time function for the six test sections, assuming the four selected channels represent the entire test section. The fractional time from these figures is calculated by dividing the number of observations of flow configurations by 120 (30 images x 4 channels). If the fractional time is equal to 1 at a particular flow condition, it is assumed that the flow is distributed uniformly throughout the channels. Figure 4.13b shows that the intermittent flow regime for all test sections dominates in Case 2 (x = 0.0016) and in Case 3 (x = 0.0032). In these cases, the cross-linked test sections have a higher number of occurrences for this flow regime, from 70% to 90% compared to 65% to 80% of such observations for the straight design. For other flow regimes, there were less than 50% of bubbly flow and over 58% of annular flow observations for all test section at Case 1(x = 0.0000348) and Case 4 (x = 0.0371), respectively (Figure 4.13a and c). Both flow regimes, dispersed and intermittent, are therefore considered as dominant flow regimes in Case 1, whereas intermittent and annular are dominant flow regimes in Case 4.

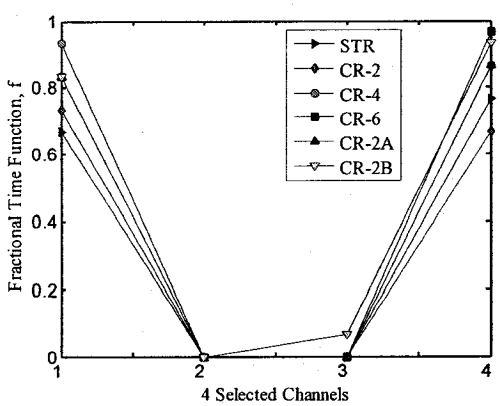

a) Case 1 – Bubbly

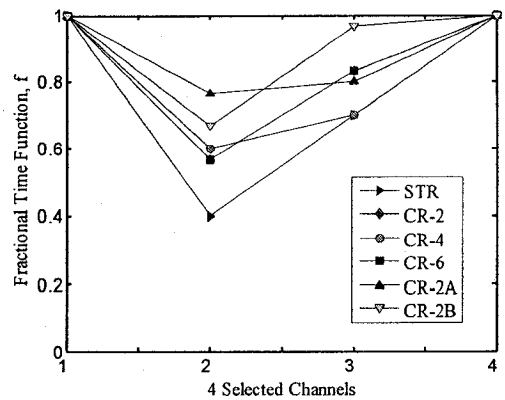

b) Case 2 – Intermittent

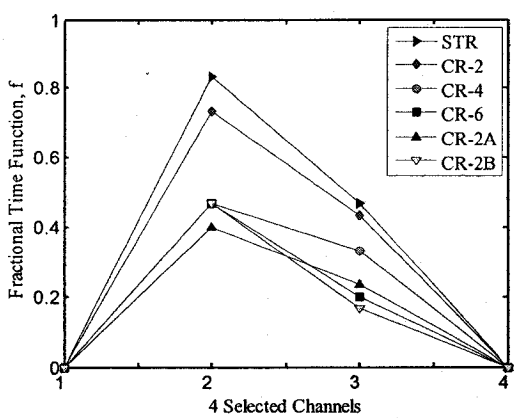

c) Case 3 – Annular

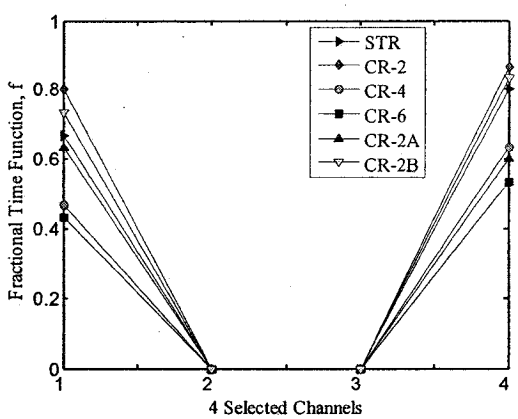

d) Case 4 - Intermittent

Figure 4.11. Flow patterns plotted in terms of fractional time function.

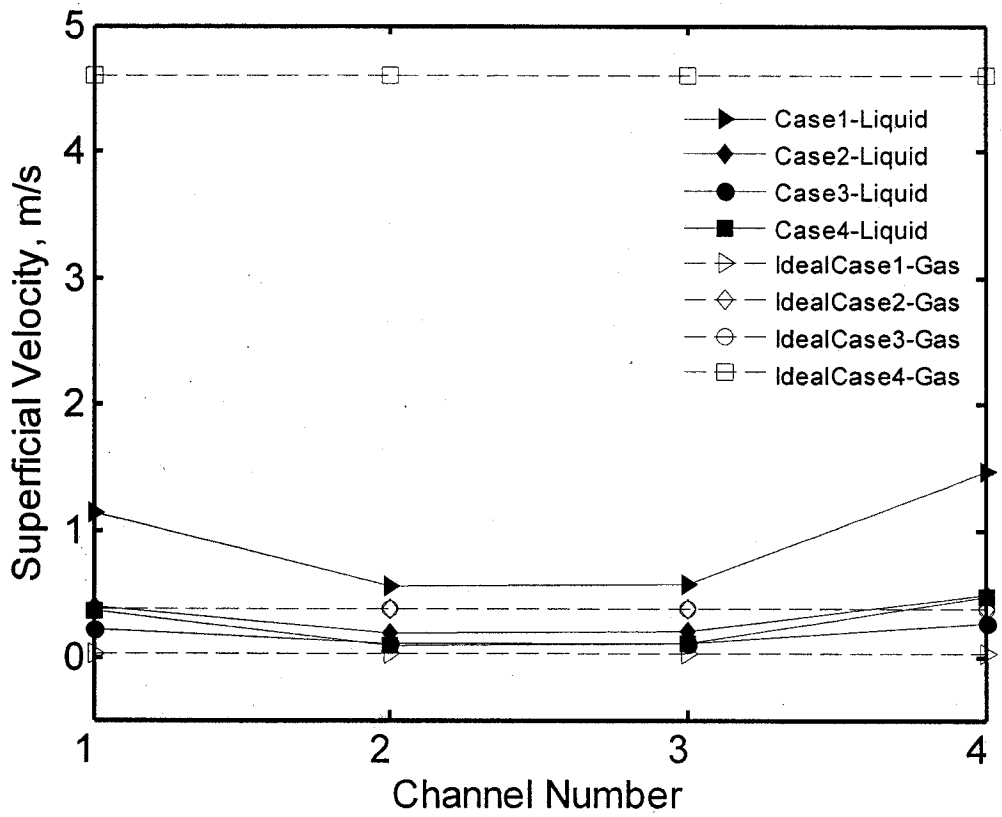

Figure 4.12. An example of comparison between measured superficial velocity of liquid and ideal superficial velocity of gas in 4 selected channels.

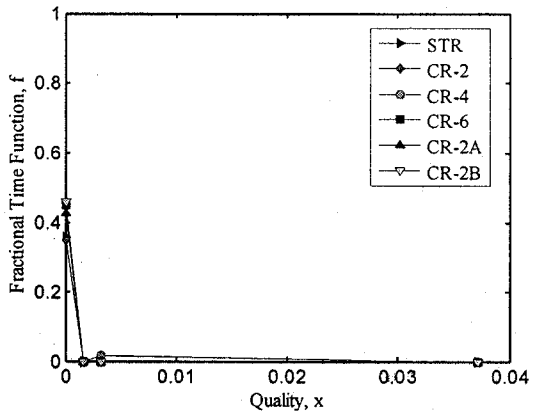

a) Bubbly and dispersed flow.

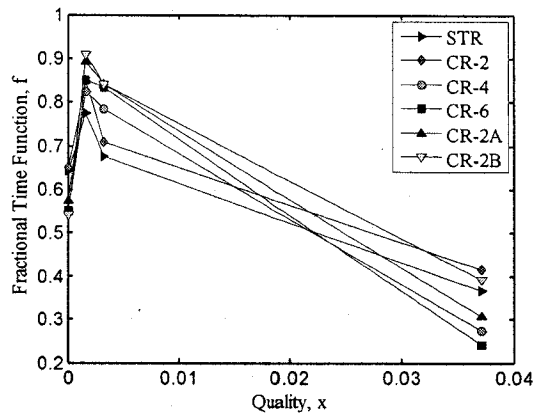

b) Intermittent.

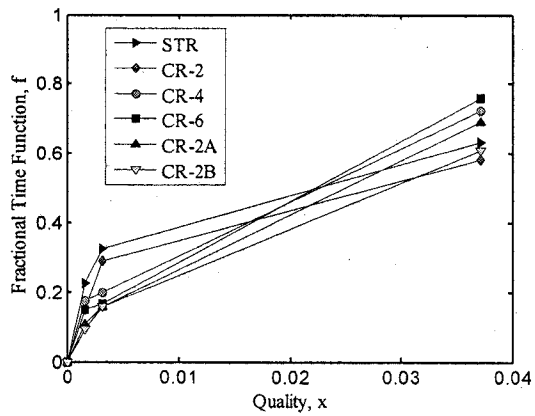

c) Annular flow.

Figure 4.13. Fractional time flow patterns for four channels of six test sections.

Three single flow maps, one of Coleman and Garimella (1999) and two of Triplett et al. (1999) with comparable hydraulic diameters to the present study, are considered as typical single channel flow maps to be compared with dominant flow patterns observed in the above four cases. Figures 4.14a - c show the locations of the examined cases in these single channel flow maps. From these figures, the results show good agreement in Case 2 and 3 with the above three flow maps. Also note that the slug flow pattern, defined in the work of Triplett et al. (1999), are similar to plug and elongated bubble flow patterns defined in the present work. In addition, dominant flow patterns for Case 4 compare favorably with those in the flow maps of Triplett et al. (1999). This implies that a single channel flow pattern map, such as the ones of Triplett et al. (1999), may be a practical guide for multi-channel arrangements at some particular flow conditions, such as in Cases 2, 3, and 4 in this work.

Adapting the single channel flow pattern map of Triplett et al. (1999), a flow pattern map was sketched (Figure 4.15) to predict the dominant flow patterns which would occur for two-phase flow in the present multi-channel systems. It is probable that the four selected channels in the present work might represent the entire test section, and single flow maps such as the ones of Triplett et al. (1999) may be used as a predictive tool for dominant flow patterns when investigating two-phase flow patterns in multiple channels. However, more data should be gathered to determine whether or not this is a proper assumption for other flow regimes and to ascertain where transitions occur.

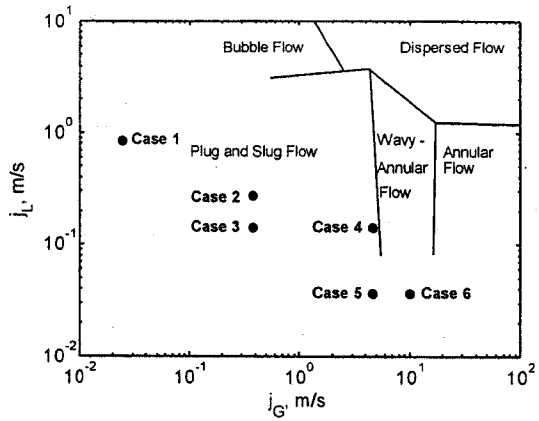

a) Circular tube with $D_h = 1.75$mm.

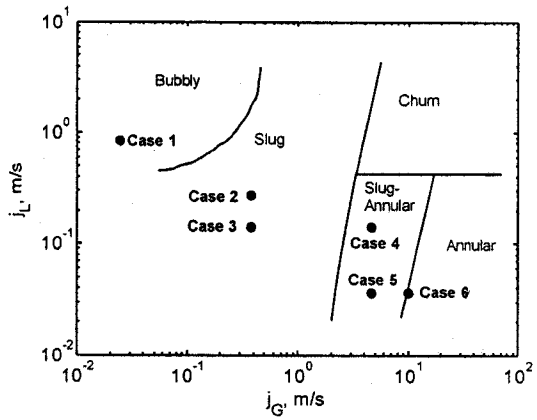

b) Circular tube with $D_h = 1.45$mm.

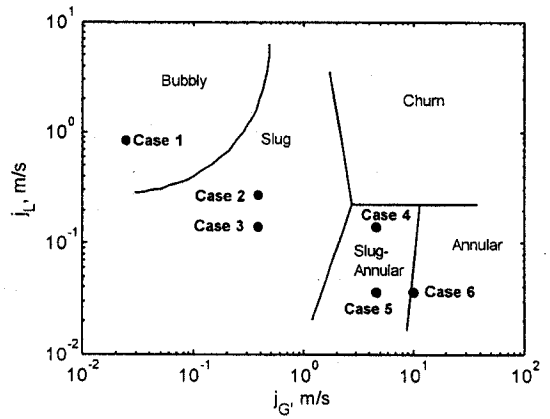

c) Semi-triangular with $D_h = 1.49$mm

Figure 4.14. Horizontal single minichannel flow pattern maps of a) Coleman and Garimella (1999), and b) and c) Triplett et al. (1999).

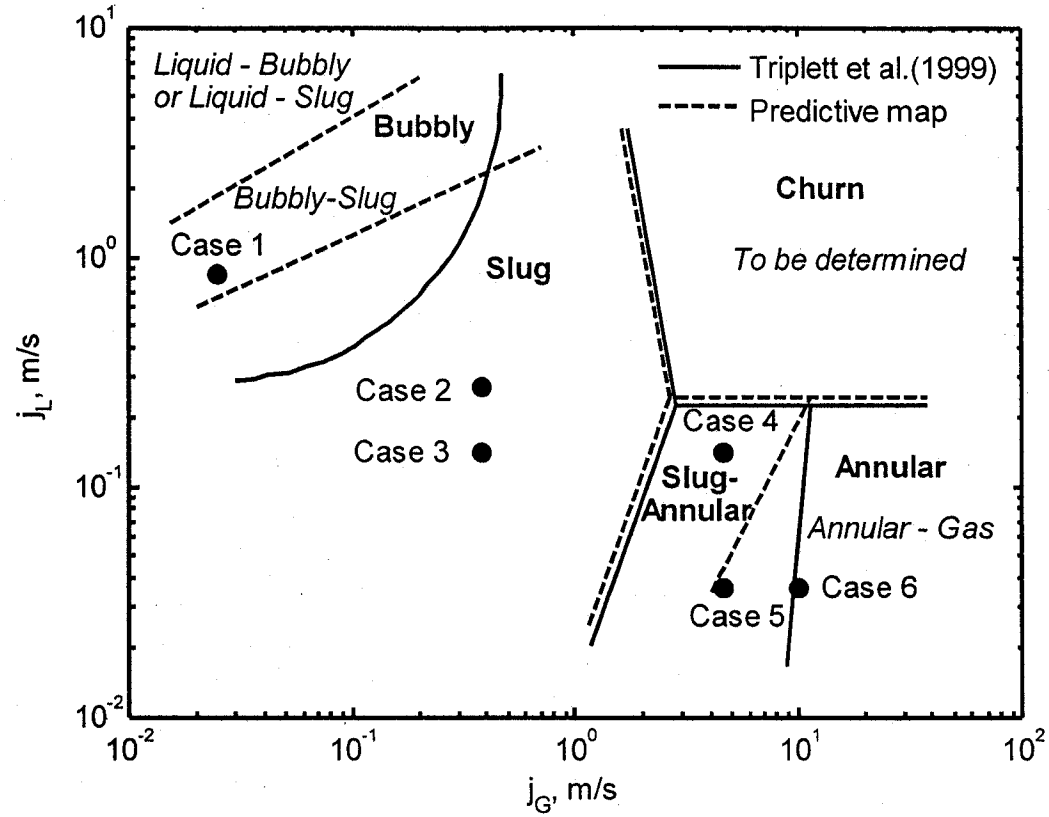

Figure 4.15. A sketch of dominant flow patterns map in multiple channels, using a single channel flow map of Triplett et al. (1999).

4.4 Pressure Drop

4.4.1 Overview

In this study, pressure drop is measured and compared for six test sections in order to acquire further insight into the effects of cross-links. Single-phase frictional pressure drop is also measured to calibrate the system before acquiring data for two-phase pressure drop. The single-phase pressure drop is measured with the same method as the two-phase pressure drop measurements. Figure 4.16 shows the sample of the frictional pressure drop for single phase. From this figure, the results of the pressure drop for the STR test section are compared with the theoretical results (obtained from Eq. 4.1) which conventionally accounts for laminar flow (f = 56.916/Re) and turbulent flow ($f = 0.3164\,\mathrm{Re}^{-0.25}$, Blasisus correlation).

$$\Delta P_f = f \frac{L}{D} \frac{\rho\ U^2}{2} \tag{4.1}$$

The results are satisfactory, whereas the average deviation is 19%. The pressure drop is observed to vary significantly from the cross-linked test section, when the Reynolds number is increased. The pressure drop increases with an increasing number of cross-links as well as with an increasing width of cross-links. As a result, the CR-2B and CR-6 test sections have the highest pressure drop. This result is possibly due to the pressure drop for the re-developing flow in the test sections which incorporate cross-links, whereas fully-developed flow is assumed throughout the straight test section. The results

of single-phase pressure drop therefore verify the method for two-phase pressure measurements.

4.4.2 Two-Phase Pressure Drop Comparison between Test Sections

The two-phase pressure drop, accounting for the pressure loss from the inlet tube which causes fluctuations in two-phase pressure drop measurement (Figure 4.17), is presented in terms of mean values as shown in Figure 4.18. Figure 4.18 presents the effect of the number of the cross-links on the pressure drop, whereas the effect of the cross-links width is presented in Figure 4.19. From these figures, the trend of two-phase pressure drop is not discernible for 22 pressure drop measurements, including the six cases studied (Figure 4.1). The trend varies irregularly, from one test section to the other, within 0 to 3 psi. The two-phase pressure drop was compared between the test sections in terms of the average deviation percentage. The average deviation percentage is defined as the average value of deviations, accounting for all studied cases. The deviation is the difference of values of two-phase pressure drop from two test sections for a particular case. Compared to the straight test section, the average deviations are 41 %, 45%, 65 %, 24%, and 49 % for CR-2, CR-4, CR-6, CR-2A, and CR-2B, respectively. The lowest average deviation is for the CR-2A test section. In addition, the CR-2A test section is considered as a better design in terms of flow distribution due to the effectiveness of flow sharing from high flow channels to low flow channels, as discussed earlier. Hence, this design can be considered as an approach design for further investigation into the effects of cross-links. For example, it would be possible to change the position of the cross-links or to incline

the cross-links with respect to the channel core, while maintaining the same width of the cross-links.

4.4.2 Two-Phase Pressure Drop Comparison with Models

Since there is no appropriate experimental work to be compared with, the present data of two-phase pressure drop of the straight test section is compared with those calculated from the homogeneous model, the Friedel (1979) model, and the Chisholm (1967) model, as seen in Figure 4.20. The average deviation percentages of the pressure drop of the straight test section and the models of homogeneous, the Friedel (1979), and the Chisholm (1967) are observed as 436.18%, 100.7%, and 600.36%, respectively. The homogeneous model and the Chisholm model under-predict the present data for the whole studied range in the present work. The Friedel model under-predicts for the quality range from Case 1 to Case 2, which are in a very low range of quality. In these cases, the bubbly and the plug flows are expected to be minor and major flow patterns, respectively. However, the Friedel model fairly predicts the present data in the range from the point located just below Case 2 to the point which is identical to Case 6 (Figure 4.1). This studied range covers flow patterns such as plug, elongated bubble, and annular, as discussed earlier. For this range, the average deviation of the present data is observed as 29.25% compared to the Friedel model, whereas an average deviation of 432.43% and 685.18% is observed, when compared to the homogeneous model and the Chisholm (1967) model, respectively.

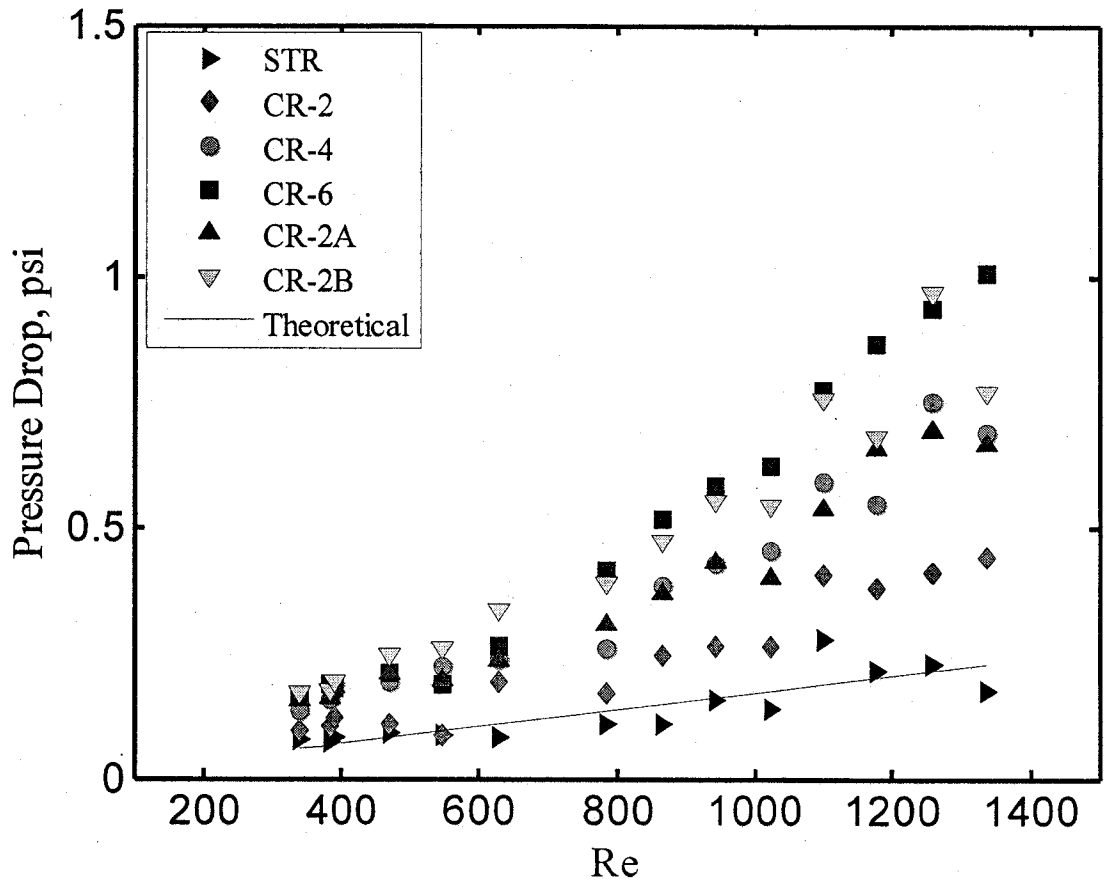

Figure 4.16. Single-phase pressure drop comparison for laminar flow.

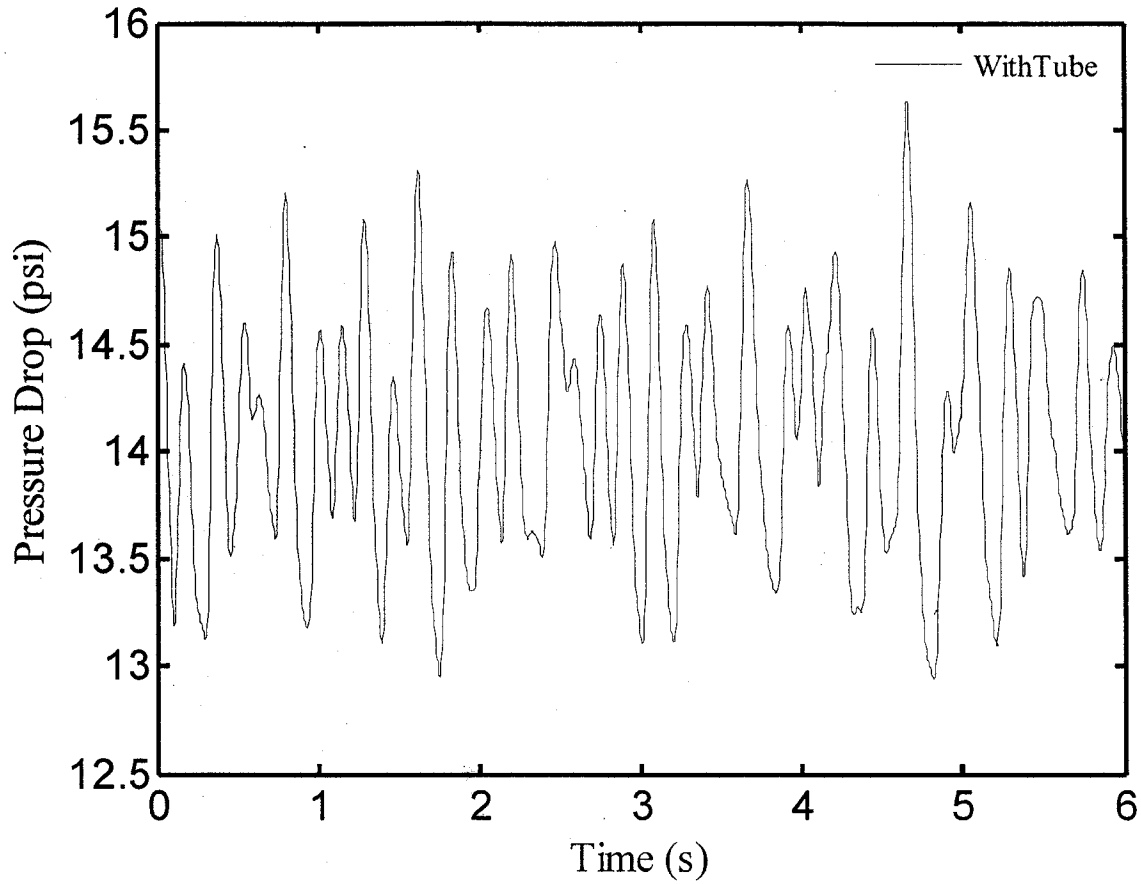

Figure 4.17. Sample of two-phase pressure drop oscillation.

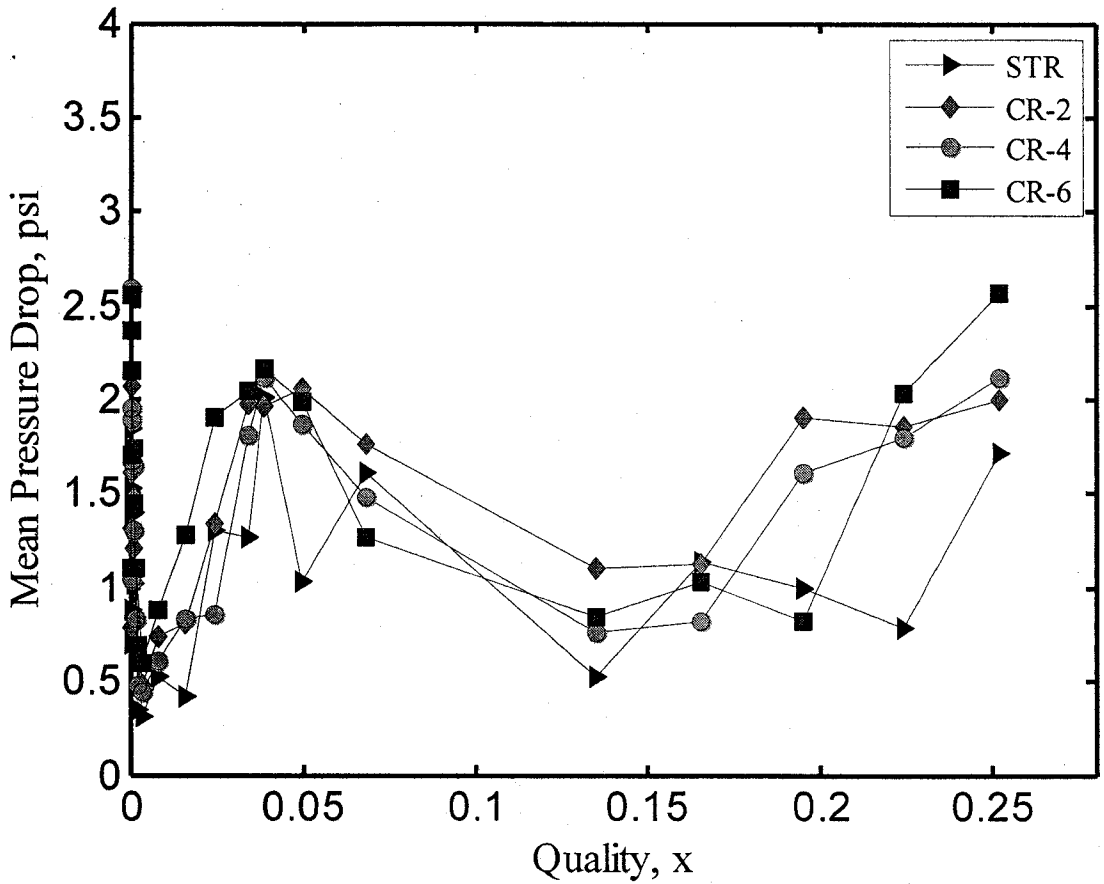

Figure 4.18. Effects of number of cross-links on pressure drop.

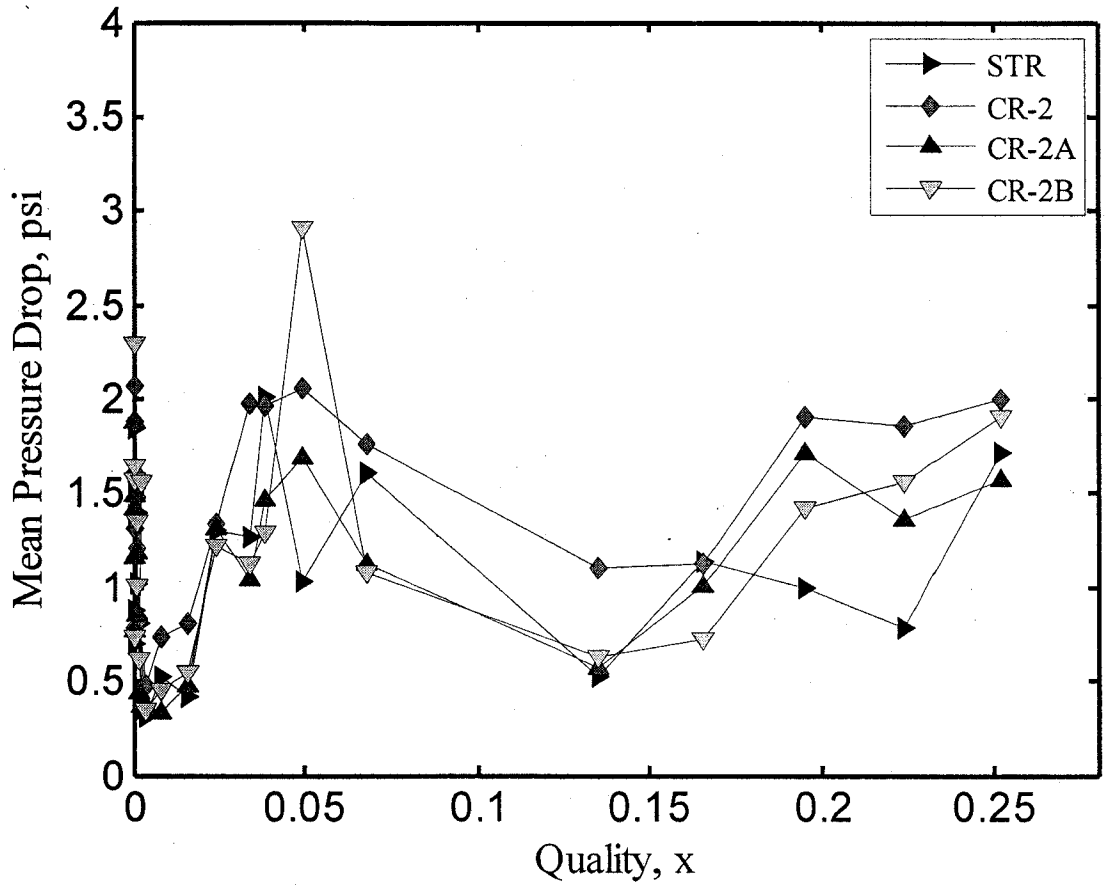

Figure 4.19. Effects of cross-link width on pressure drop.

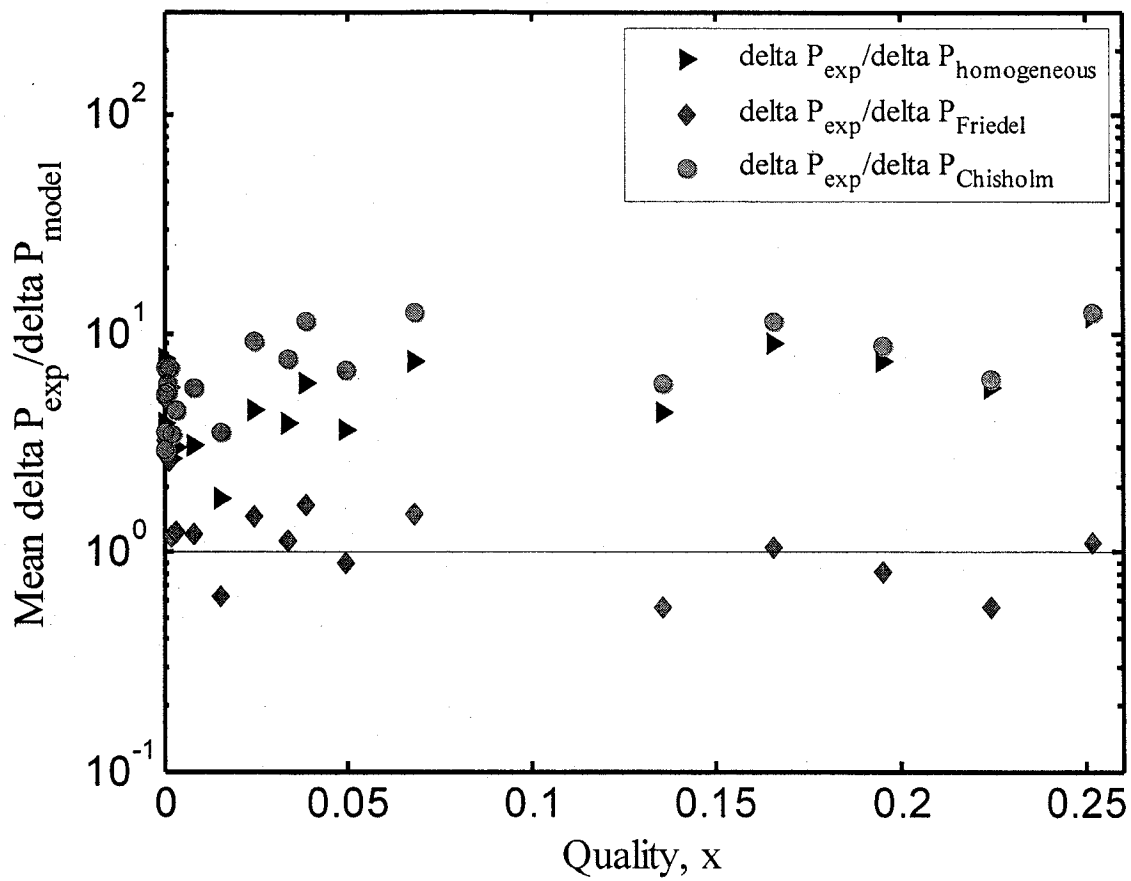

Figure 4.20. Comparisons of pressure drop from the STR test section with those obtained from models.

4.5 Summary

The results of two-phase flow distribution and visualization for six test configurations are presented in this chapter. One is a straight standard microchannel heat sink, whereas five others include cross connections between the channels. The results show that six test sections exhibited non-uniform flow distribution. However, the introduction of cross-links to the channel core significantly influences flow distribution in multiple channels.

The influence of cross-link configurations improves flow distribution compared to the standard straight channel configuration. This is due to flow sharing along the cross-links. The six cross-linked (CR-6), the two-time larger cross-linked (CR-2A), and the three-time larger cross-linked (CR-2B) test sections produced better results due to more paths and larger available space for flow in communication. Moreover, the CR-2A test section is considered as an appropriate design for flow efficiently communicating through cross-links.

The dispersed, intermittent (plug, elongated bubble flows), and annular flow regimes were all observed in six test sections. More instances of intermittent flow patterns are observed in the cross-linked test sections, whereby about 90% of intermittent flow patterns were observed in the two-time and three-time larger cross-linked test sections. The dominant flow patterns in an array of parallel channels in this study can be compared with flow patterns from single channel flow pattern maps, which may be a practical guide for two phase flow in an array of parallel channels. Also, four selected channels, which are approximately 1/10 of the total channels evenly spaced, might represent the entire test

section, and so a dominant flow pattern map for a multi-channel configuration can be compiled. More data, however, should be studied to determine the limits of these assumptions.

The two-phase pressure drop for the cross-linked test sections deviate irregularly when compared with that for the straight test section. However, the lowest average deviation is observed from the two-time larger cross-linked test section (CR-2A). The pressure drop model of Friedel (1976) fairly predicts the present data from the straight test section (STR) in a range that covers plug, elongated bubble, and annular flow patterns, whereas the homogeneous and the Chisholm (1967) models under- predict for the whole studied range.

Chapter 5

Numerical Investigation

5.1 Motivation

This chapter presents a numerical study that investigates the effects of cross-links in scaled microchannel heat sinks. The results were compared with experimental data obtained from the experiments presented in the previous chapter. The experimental results showed that there was a significant impact on flow distribution due to the effect of cross-links incorporated in the channel core. However, additional investigations of the effects of cross-links should be carried out since their impact cannot overcome the mal-distribution due to the entrance effect. There are several approaches suggested, based on the experience gained from the experimental work. For example, an increased number of cross-links, with two- times larger width of channel width, should be incorporated. As well, inclined angles between cross-links and channels should be studied. These approaches are suggested based on the fact that flow could be easily shared along the cross-links from high flow channels to low flow channels. However, experimentally investigating these approaches could be an expensive endeavor, so a numerical study is a practical approach for seeking the optimal designs.

5.2 Numerical Simulation

Three dimensional simulation of two-phase flow in multiple channels is not an easy task at this time. It should be expected that some challenges would be encountered. Therefore,

computational domains, test models, and simulation methods were carefully considered in order to study the effects of cross-links in parallel multi- channel heat sinks.

5.2.1 Test Models and Proposed Design

From the experimental results, the CR-2A test section was considered as an appropriate design for flow communication between channels through the cross-links. To understand more the effects of cross-links from this design, a model, having the same geometry of the CR-2A test section, was simulated in this numerical work. In addition, models of the STR and the CR-2 test sections were also simulated for comparison. The computational domain is shown in Figure 5.1. The origin is located at the center of the bottom surface of the inlet hole. The computational results of three models are validated by comparing them with those from experimental data. Such results then lead to the proposal of a new design, which was also simulated and shown in Figure 5.2. The difference between the proposed design and the test models is the geometry of cross-links which are inclined to the channels.

5.2.2 3D Two-Phase Simulation Model

The commercial CFD code, Fluent 6.3, is used to simulate the 3D two-phase flow for the same range of experimental flow conditions (see Table 5.1), except Cases 5 and 6 due to the insufficient memory of available computer resources. For the three dimensional two-phase flow models, there are several available models in Fluent, models such as Volume of Fluid (VOF), discrete phase, mixture, and Eulerian. However, each model can be used depending on particular interest of researchers.

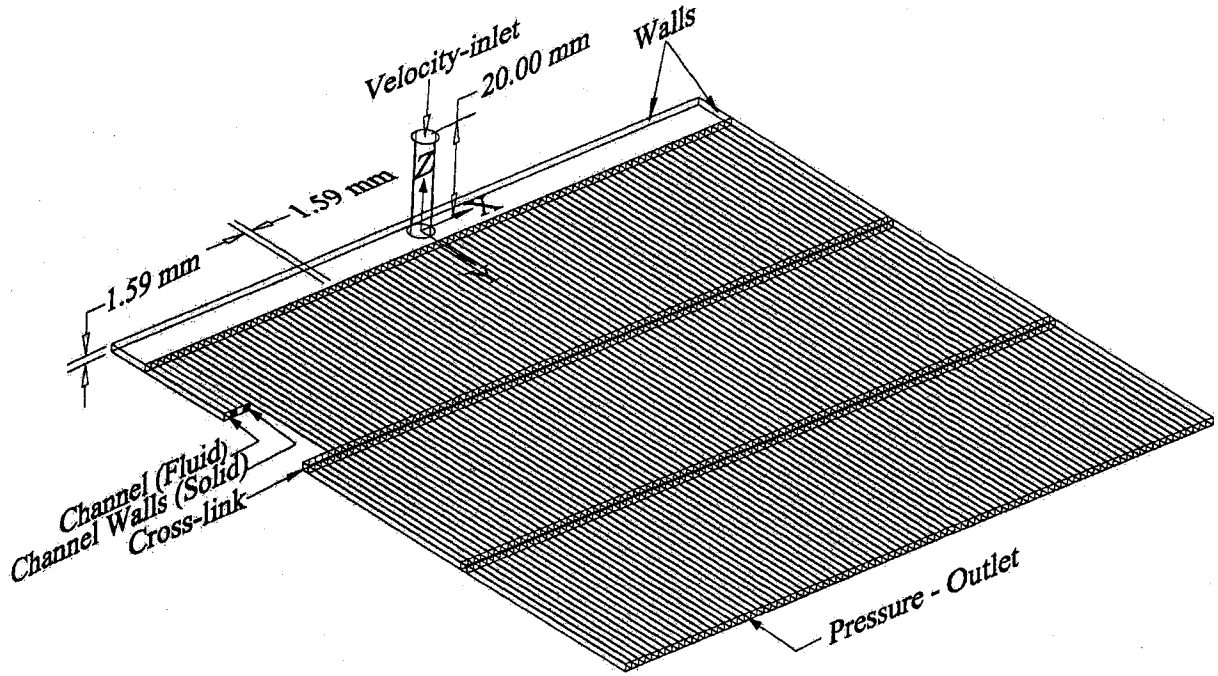

Figure 5.1. Computational domain.

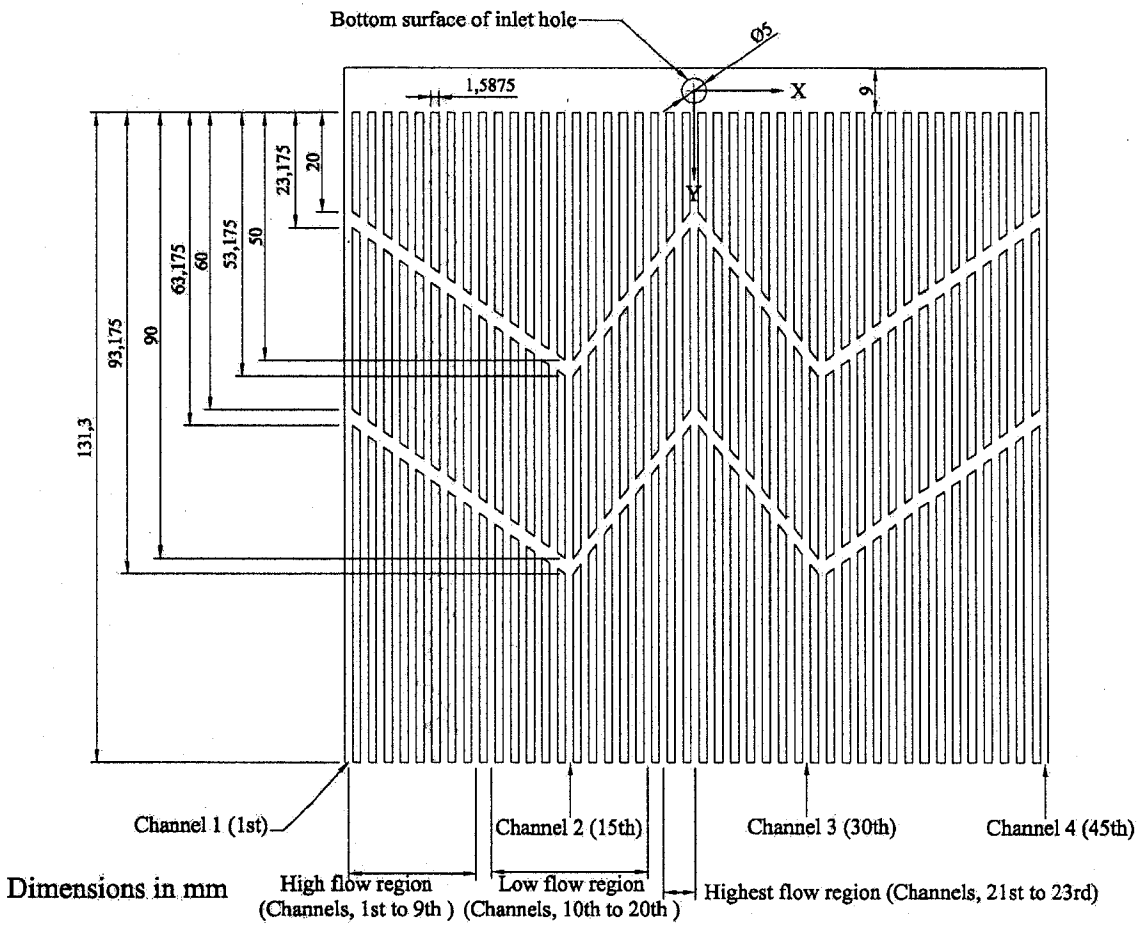

Figure 5.2. Proposed design.

Table 5.1. Flow conditions for computational work.

Case	J_G (m/s)	J_L (m/s)	J_m (m/s)	β_{air}	x
1	0.142	4.828	4.970	0.029	3E-05
2	2.186	1.581	3.766	0.580	0.002
3	2.186	0.819	3.004	0.727	0.003
4	26.642	0.819	27.461	0.970	0.037

For example, the VOF, free surface flow model, is used most often to simulate two-phase flow pattern. However, this model cannot allow two-phase flow to be interpenetrating. It is therefore used for particular flow patterns, for example, plug, bubble flow, without dispersed phases.

The mixture model is a simplified multiphase flow model, and it is less computationally expensive. It allows phases to interpenetrate and to move with different velocities. It is also used as a homogeneous two-phase model when phases move at the same velocity. The volume fractions of phases can vary from 0 to 1 for a control volume. The mixture model is therefore used as a suitable two-phase model to seek appropriate designs for microchannel heat sinks in terms of flow distribution. The governing equations of the mixture formulations on multi-phase flow can be expressed as following.

Continuity equation

$$\frac{\partial}{\partial t}(\rho_m) + \nabla \cdot (\rho_m \vec{v}_m) = \dot{M} \qquad 5.1$$

where, the mass average velocity, $\vec{v}_m$, is:

$$\vec{v}_m = \frac{\sum_{k=1}^{n} \beta_k \rho_k \vec{v}_k}{\rho_m} \text{ (m/s)} \qquad 5.1.1$$

and, $\dot{M}$ is mass transfer due to cavitation (kg/s)

and, β_k is volume fraction of phase k

Momentum equation

$$\frac{\partial}{\partial t}(\rho_m \vec{v}_m) + \nabla \cdot (\rho_m \vec{v}_m \vec{v}_m) = -\nabla P + \nabla \cdot [\mu_m (\nabla \vec{v}_m + \nabla \vec{v}_m^T)] + \rho_m \vec{g} + \vec{F} + \nabla \cdot (\sum_{k=1}^{n} \beta_k \rho_k \vec{v}_{dk,k} \vec{v}_{dk,k}) \quad 5.2$$

where, the drift velocity for secondary phase k, $\vec{v}_{dr,k}$, is:

$$\vec{v}_{dr,k} = \vec{v}_k - \vec{v}_m \quad 5.2.1$$

and, the dynamic viscosity of the mixture, μ_m, is:

$$\mu_m = \sum_{k=1}^{n} \beta_k \mu_k \ (\text{N.s/m}^2) \quad 5.2.2$$

and, the mixture density, ρ_m, is:

$$\rho_m = \sum_{k=1}^{n} \beta_k \rho_k \ (\text{kg/m}^3) \quad 5.2.3$$

Volume fraction equation

$$\frac{\partial}{\partial t}(\beta_k \rho_k) + \nabla \cdot (\beta_k \rho_k \vec{v}_m) = -\nabla \cdot (\beta_k \rho_k \vec{v}_{dk,k}) \quad 5.3$$

Assumptions

The two-phase flow is considered as incompressible for a studied flow range. The steady state is also assumed in this study, while the standard k-ε turbulent model is taken into account. The cavitation model is not considered in this study. Moreover, since the hydraulic diameter of the channel is small, the effect of gravity can be neglected. The governing equations can be rewritten as following.

Continuity equation

$$\nabla \cdot (\vec{v}_m) = 0 \tag{5.4}$$

Momentum equation

$$\nabla \cdot (\rho_m \vec{v}_m \vec{v}_m) = -\nabla \mathrm{P} + \nabla \cdot [\mu_m (\nabla \vec{v}_m + \nabla \vec{v}_m^T)] + \vec{F} + \nabla \cdot (\sum_{k=1}^{n} \beta_k \rho_k \vec{v}_{dk,k} \vec{v}_{dk,k}) \tag{5.5}$$

Volume fraction equation

$$\nabla \cdot (\vec{v}_m) = -\nabla \cdot (\vec{v}_{dk,k}) \tag{5.6}$$

Inlet and Outlet Boundary Conditions

For the inlet boundary condition, the two-phase flow mixture is assumed as homogeneous flow. Moreover, the above assumptions lead to determining the volume fraction and the mixture velocity for the inlet flow boundary condition from the Equations 5.7 and 5.8. From the Equation 5.7, the volume fraction is determined as same as the volume quality, which is the ratio of the volume flow rates of a gas and a mixture. They are therefore considered as the same based on the assumptions stated in this study. The boundary conditions at the channel outlets are set as a pressure outlet, with absolute gauge pressure.

$$\beta_G = \frac{Q_G}{Q_m} \tag{5.7}$$

$$j_m = \frac{j_G}{\beta_G} \tag{5.8}$$

5. 3 Results and Discussion

5.3.1 Mesh Independence

Mesh independence is studied for the STR model, using four mesh types, namely coarse mesh, base mesh, fine mesh and finer mesh (Table 5.2). A structured mesh is used for the header, the channels and the cross-links, while an unstructured mesh is used for the inlet tube, as illustrated in Figure 5.3. The V- velocity profiles along a line in the header and at the channel outlets are tested for mesh independence, as shown in Figure 5.4. The results, from Figures 5.4 and 5.5, show that almost the same velocity profiles are observed when using the fine and the finer mesh types. Moreover, using these mesh types, the V-velocity profiles at the corner of the header are reasonable. The flow gradually reduces near the end wall of the header and ends up at zero velocity when they reach the wall. This cannot be seen when using the coarse and the base mesh types since the grid size from these meshes is too large. It is interesting to note that the finer mesh has almost double the number of cells as the fine mesh system. To conserve computational time, the fine mesh was used. This selected mesh type was also used in the remaining cases. The results converge in a range of 3500 to 4500 iterations with 10^{-6} residuals.

5.3.2 Validation

To validate the CFD results, the mass flow rates of water in four channels, 1, 2, 3, and 4, corresponding to the 1^{st}, the 15^{th}, the 30^{th}, and the 45^{th} channels of the 45 channels (Figure 5.2), are compared with experimental data, as shown in Figures 5.6, 5.7, and 5.8.

Table 5.2. Mesh information.

Examined Mesh	Total number of cells
Coarse	419235
Base	430329
Fine	636838
Finer	1250419

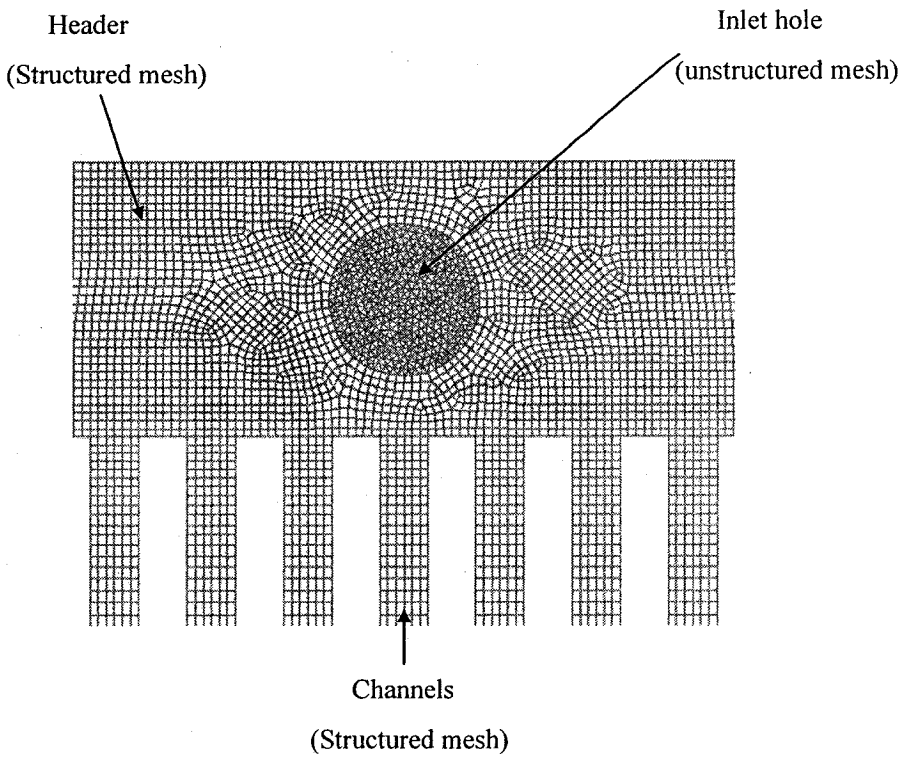

a) Mesh for header and channels

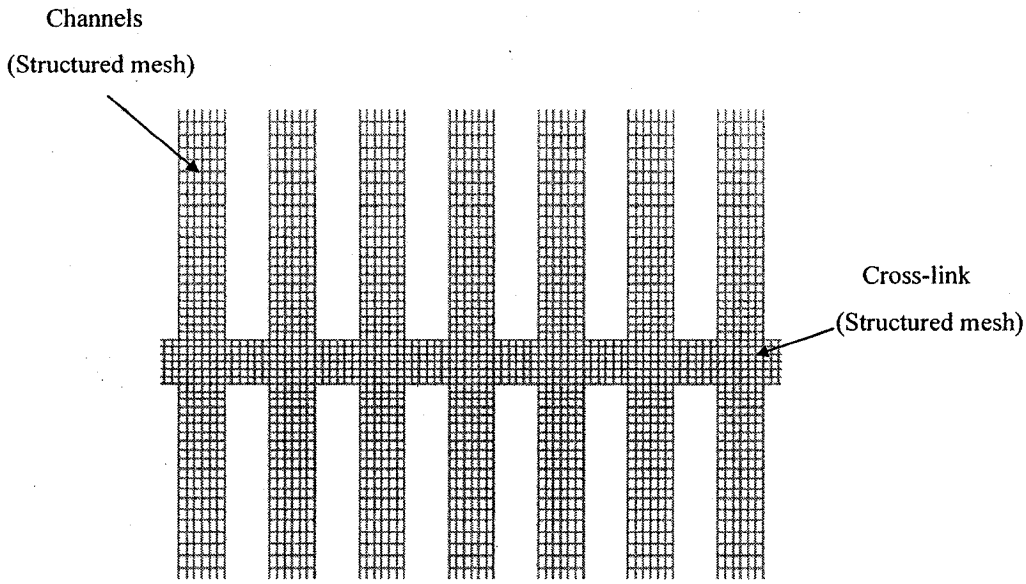

b) Mesh for channels and cross-links

Figure 5.3. Sample of chosen mesh.

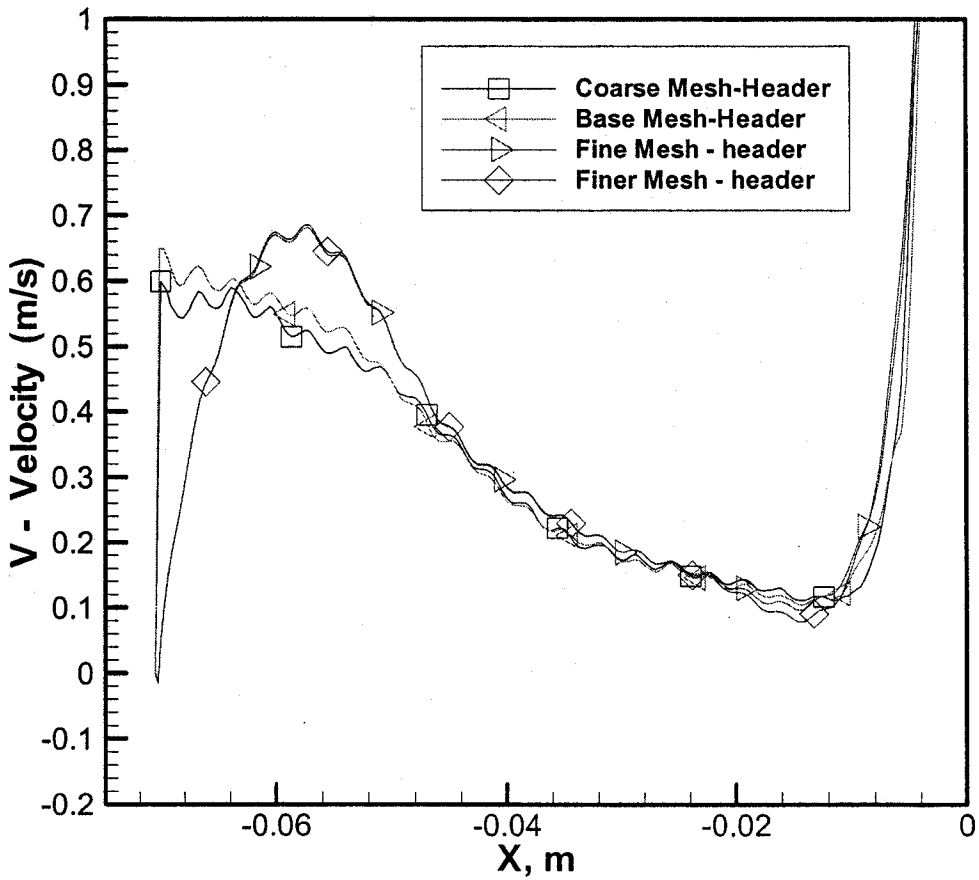

Figure 5.4. V - Velocity profile along a line in the header.

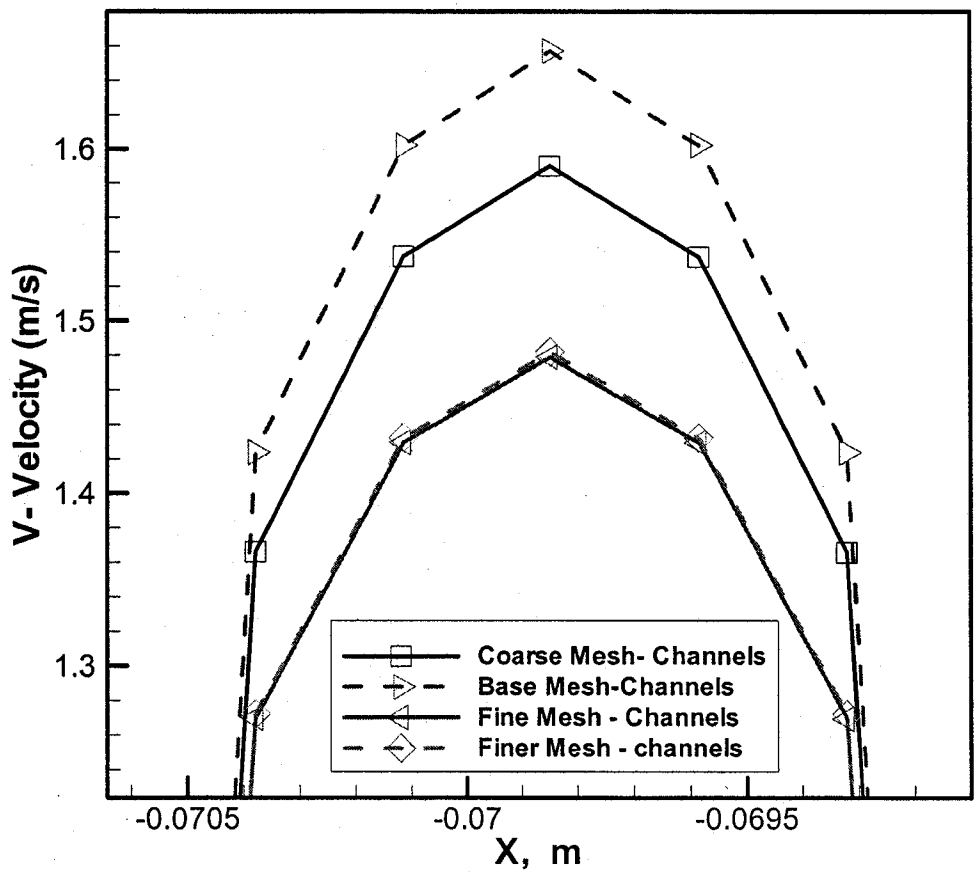

Figure 5.5. V-velocity profile along the line at the outlet of channel 1 (1^{st}).

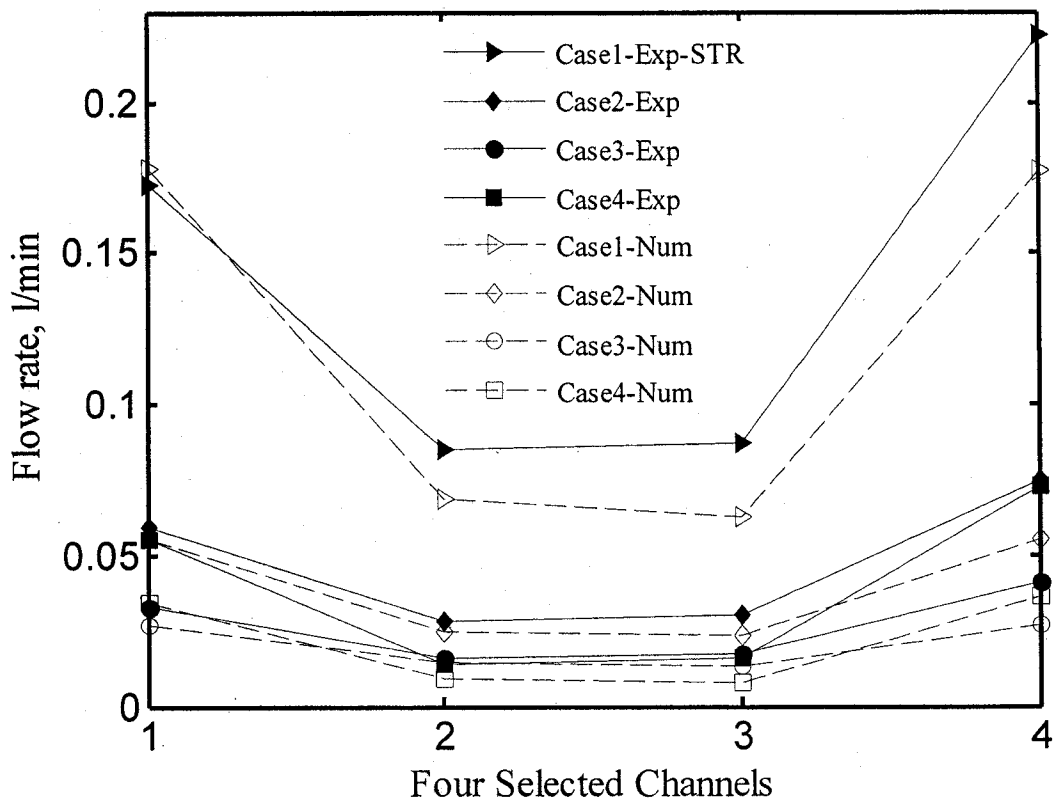

Figure 5.6. Mass flow rate comparison for the STR model.

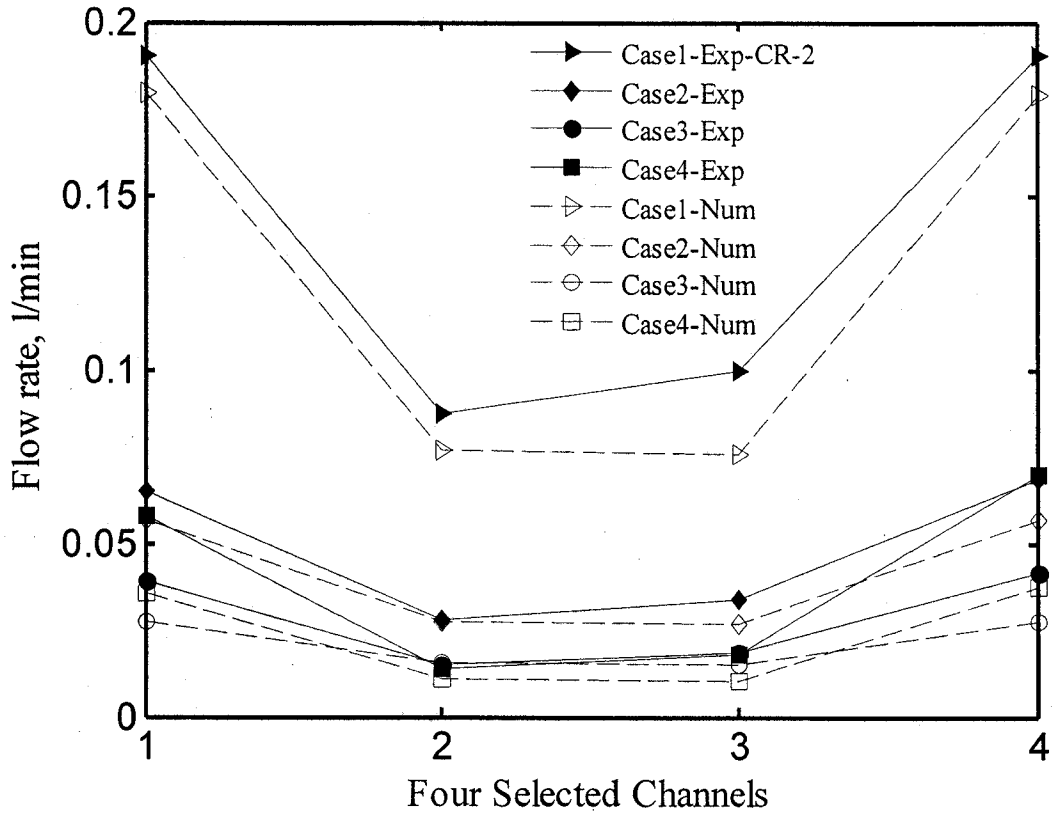

Figure 5.7. Mass flow rate comparison for the CR-2 model.

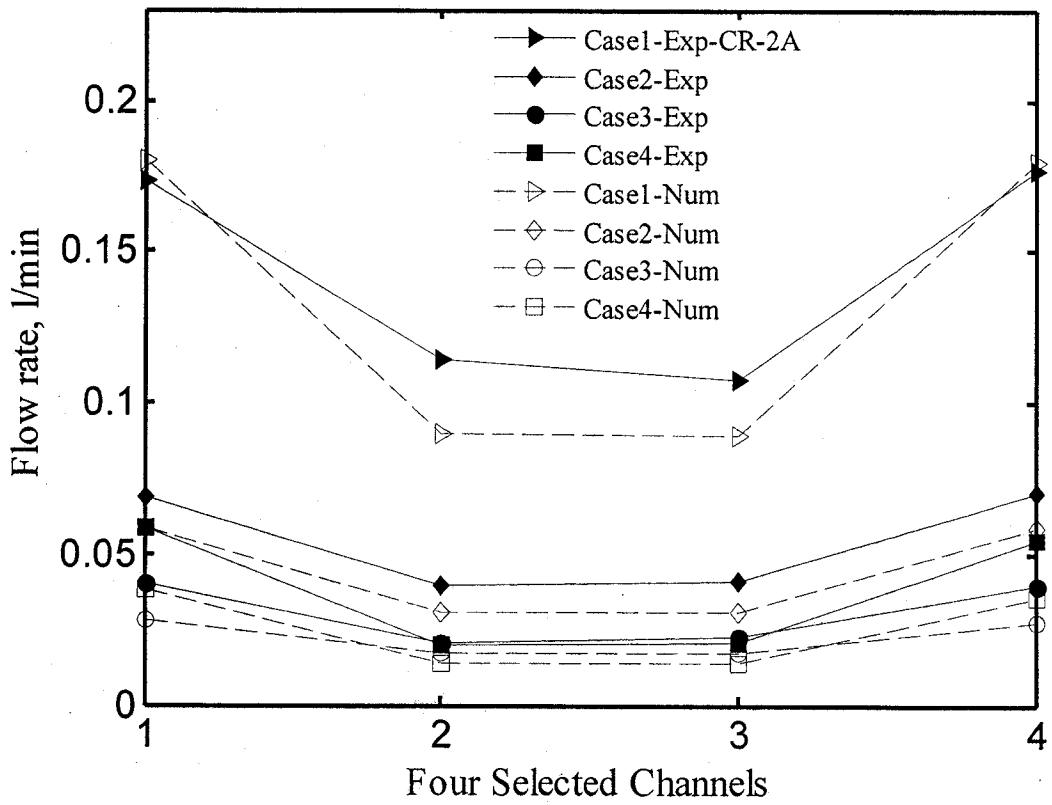

Figure 5.8. Mass flow rate comparison for the CR-2A model.

The results show that both numerical and experimental data have the same trend of flow distribution in the four selected channels. The results, however, show that the CFD models under-predict the experimental data for all cases. The flow distribution is fairly symmetrical from the CFD results, whereas it is not from the experimental results. Differences between numerical and experimental data are less for channels 1 and 2, when compared to those for channels 3 and 4. Differences exist because of the CFD assumption but also due to the experimental uncertainty.

5.3.3 Flow Distribution

The CFD study enables us to easily gain further insight into flow distribution throughout the entire 45 channels, whereas it is difficult with experimentation. Figures 5.9 to 5.12 present the flow distribution comparison between the test models at the channel outlets, from Case 1 to Case 4. The results of flow distribution show that high flow occurs at some central channels and some outermost channels for all test models. The results show almost symmetrical flow distribution throughout 45 channels for all test models. For simplification, a flow distribution profile can be divided into three regions with respect to the ideal flow distribution. The highest flow region is from the 21^{st} to 23^{rd} channels, the high flow region is from the 1^{st} to 9^{th} channels, and the low flow region is from the 10^{th} to 20^{th} channels (Figure 5.2). These flow regions are considered to be the same as flow distribution in the other side (24^{th} to 45^{th} channels), assuming symmetrical flow distribution as discussed earlier. In the low flow region, mass flow rate is observed lower than ideal mass flow rate for all test models. However, the deviation between the measured flow rate and the ideal flow rate tends to decrease close to the ideal line, when

the cross-links are incorporated. It is also observed in the same results from other flow regions. Figure 5.13 presents comparisons of flow distribution between test models in terms of the standard deviation calculated from Equation 5.6.

$$STDEV = \sqrt{\frac{1}{N-1}\sum_{i=1}^{N}(x_i - \bar{x})^2} \qquad 5.6$$

The results show that the standard deviation decreases from Case 1 to Case 3, but it starts to increase at Case 4 for all test models. The lowest standard deviation was observed at Case 3. It is good to note that intermittent flow patterns (plug and elongated bubble flow patterns) are experimentally observed as dominant flow patterns in the straight and the cross-linked models in this case. However, more data between these studied cases should be investigated to see what flow conditions will result in uniform flow distribution. Compared to the standard straight model (STR), the cross-linked and the proposed models have lower standard deviations in which the standard deviations are improved up to 25%, 40%, and 55% for the CR-2, the CR-2A, and the proposed models, respectively, in the flow range studied.

5.3.4 Velocity Flow Field

The header plays an important role in the flow distribution for an array of parallel multiple channels. To understand the physical flow behavior inside the header, Figure 5.14 presents velocity fields of two-phase flow near the inlet tube of the header (Figure 5.14a), and at the corner end of the header (Figure 5.14b).

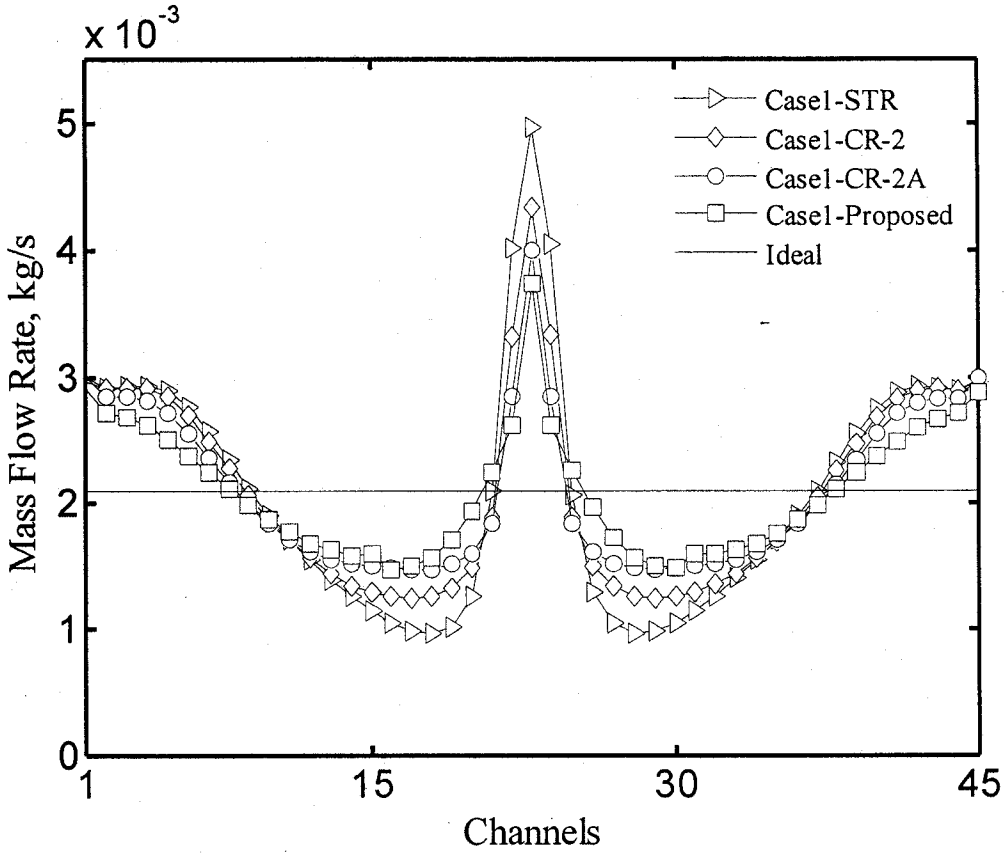

Figure 5.9. Comparison of flow distribution for all test models, at Case 1 ($\beta = 0.0286$).

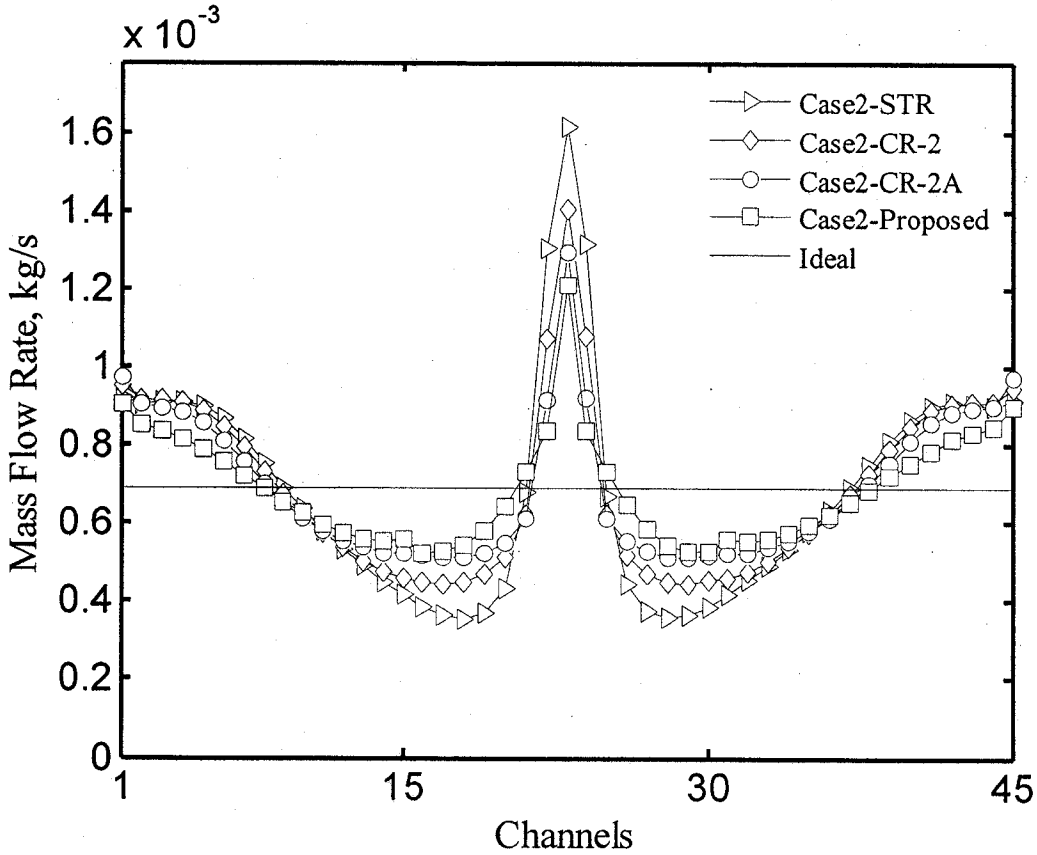

Figure 5.10. Comparison of flow distribution for all test models, at Case 2 ($\beta = 0.5803$).

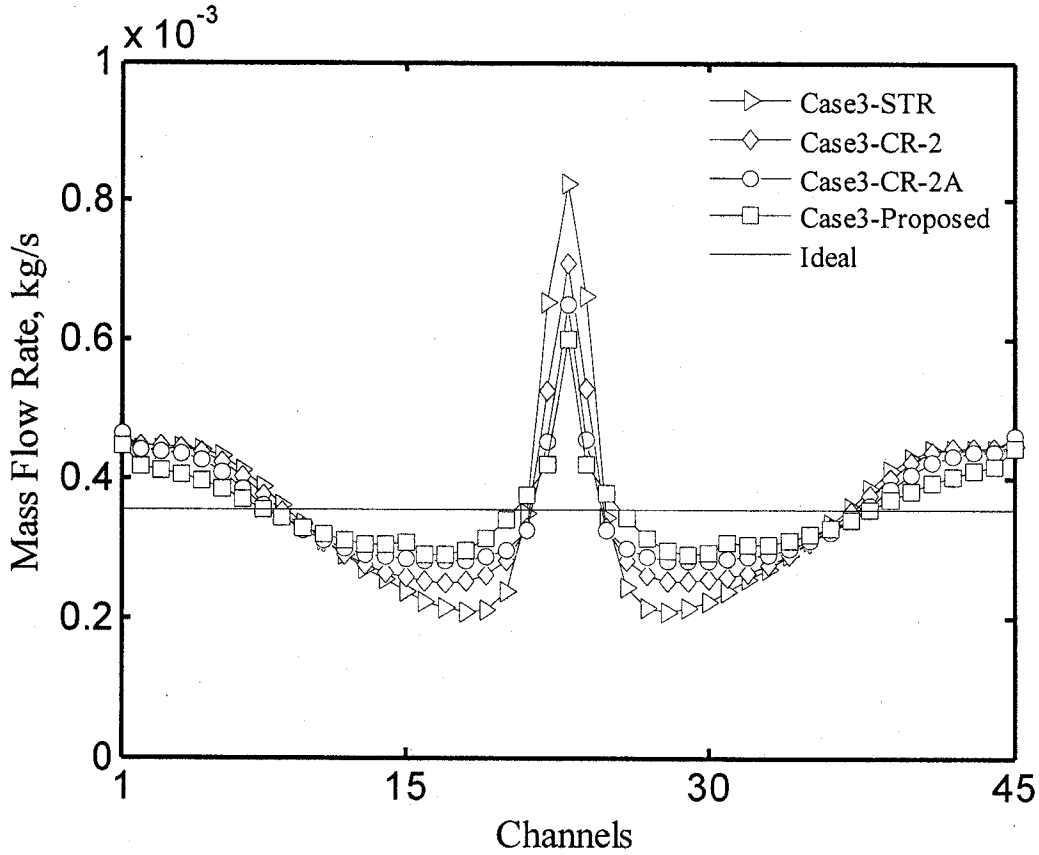

Figure 5.11. Comparison of flow distribution for all test models, at Case 3 ($\beta = 0.7274$).

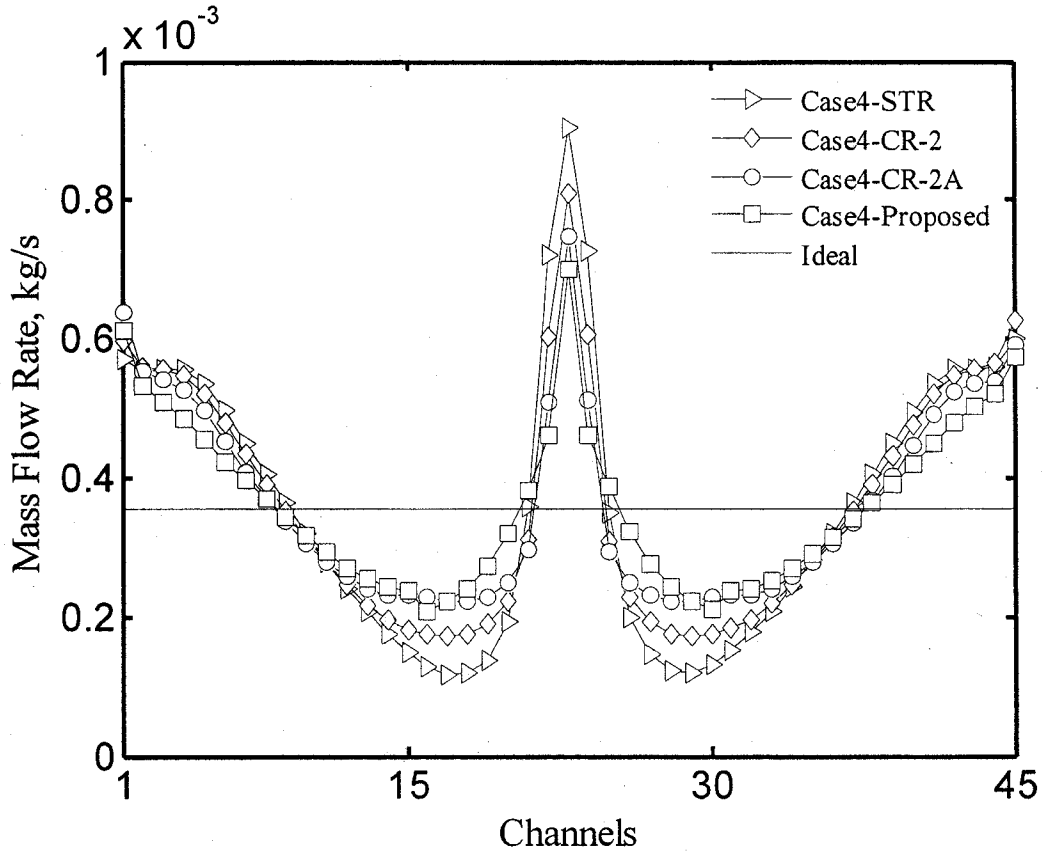

Figure 5.12. Comparison of flow distribution for all test models, at Case 4 ($\beta = 0.9702$).

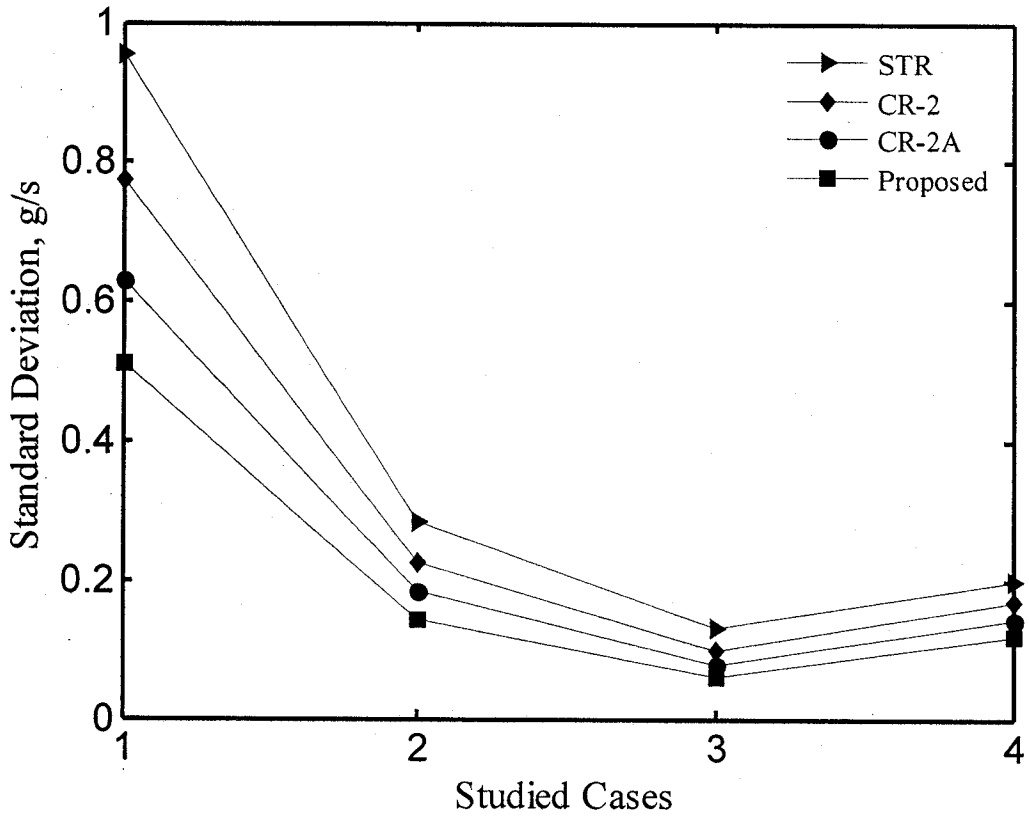

Figure 5.13. Standard deviation of flow distribution.

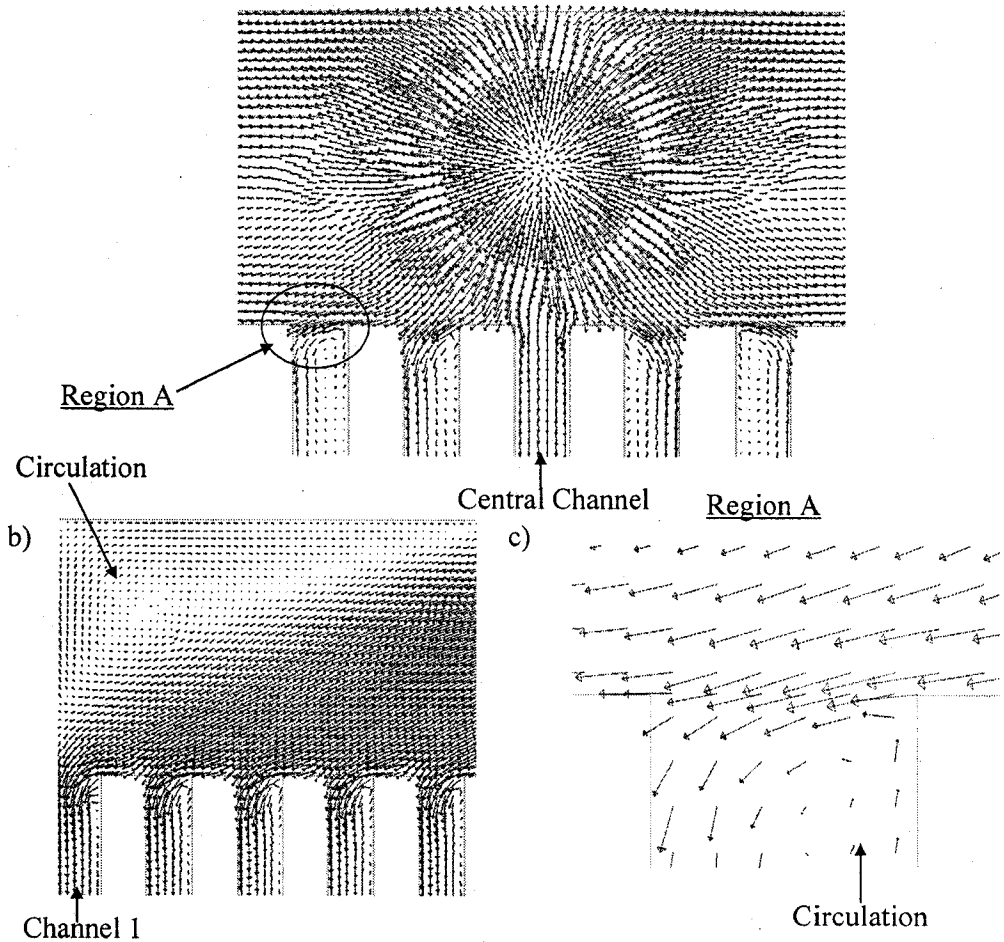

Figure 5.14. Samples of velocity flow field.

From these figures, circulation regions are observed at the corners of the header due to flow impinging on the walls of the header. It is also observed that circulation regions occurred at the inlet of channels. Small circulations are observed at the high and highest flow regions, whereas larger circulations are observed in the low flow region (Figure 5.2). Less flow will enter the channels where large circulations are present. Circulations at the channel inlet are possibly due to the cross flow effects, such as a high momentum cross flow passing by the cavity which in this case is the entrance of channels, as seen in Figure 5.14 c. No cross flow is observed at the inlet of the central channel which is in line with the flow inlet. As a result, the highest flow is observed in the central channel for all studied cases. It is suggested that rounding the inlets of channels will lessen the cross flow effect at the channel inlets.

Introducing cross-links into the channel core allows flow sharing from high flow channels to low flow channels. This can be seen in Figure 5.15, which presents the velocity field at cross-links of Case 1. The two-phase mixture velocities show that they traverse from high flow channels to low flow channels along the cross-links, as supported by the images shown in Figure 5.15a. Although the bubbles cannot be seen in the CFD results, it can be shown that the circulation is present in the cross-links and the channels. It is observed that the larger cross-links permit more flow sharing compared to smaller cross-links as seen in Figure 5.15 a and b. The cross-links are considered as additional inlets and exits along channels. Circulations are also observed in the cross-links between channels as well as in the channels, after flow goes through the cross-links. This prevents parts of flow sharing among channels through the cross-links. Figure 5.15 b also presents

the volume fraction of air in the channels. This figure shows that some regions having high volume fraction of air among the channels and the cross-links, for example a value of 0.032 can mean the possibility of bubbles. Figure 5.16 shows more two-phase flow sharing between channels due to less circulation observed in the inclined cross-links. As a result, the proposed design improves flow sharing from high flow channels to low flow channels.

5.3.5 Effects of Cross-links on Flow Profile

The effect of the cross-links on flow distribution will be more understood from flow analysis through the Figures 5.17 to 5.19, which present the V-velocity distribution along the center lines of the 1st, 15th, and 23rd channels at Case 1. From these figures, two-flow velocity is disturbed at the entrance of channels, especially from the 15th channel due to the effect of cross flow (Figure 5.14). Two-phase flow then enters the channels and develops along the channel. Fully developed flow is observed in the STR model results, whereas it is developing in the CR-2, the CR-2A, and in the proposed design results. Two-phase flow velocities are disturbed (as observed from the entrances of channels) when flow goes through the cross-links. This is due to cross flow sharing between channels along the cross-links. The velocity profiles can explain how flow distribution improves due to the effects of cross-links. Figure 5.17 shows that high velocity is observed at the exit of the 1st channel for the CR-2 and the CR-2A models, but low velocity is observed from the proposed design, when compared with the straight model. The straight cross-links cannot be effective in this channel, whereas the inclined cross-links can be. A difference of approximately 2.1% and -1.2% in velocity for the two cross-

linked model and for the proposed design respectively, compared to the straight model was found. The improvement is observed in the 15th channel. The V- velocity increases 38.4 % for the proposed model compared to that for the STR model, whereas 13.6 % and 30.8 % of that results observed for the CR-2 and the CR-2A models respectively (Figure 5.18). The improvement is also observed in the 23rd channel, where the V- velocity in this channel decreases 24.4 % for the proposed model and 12.6 % and 19.3 % for the CR-2 and the CR-2A models respectively (Figure 5.19). The pressure distribution along the center of the 23rd channel is also presented in Figure 5.20. This figure shows that pressure jumps up and down when the flow traverses the cross-links. This result is due to flow sharing along cross-links, as discussed earlier. However, the pressure drop along this channel with respect to the outlet is lower for the cross-linked models compared to the straight model, whereas the proposed model produces the lowest pressure drop. The results overall show how flow distribution can be improved due to the effects of cross-links and the inclined cross-link geometry is most effective to allow flow sharing easily among channels.

5.3.3 Two-Phase Pressure Drop

The two-phase pressure drop is calculated using the surface weight average from the bottom surface of the inlet hole (Figure 5.2). The results are compared for all test models as shown in Figure 5.21. The results show that no significant differences are observed between the test models. The average deviation percentage is presented to compare the two-phase pressure drop results. It is defined as the average of the two-phase pressure drop deviations, accounted for in all cases studied. The deviation is the difference of the

two-phase pressure drop between two test models. The pressure drop average deviation for the CR-2 and the CR-2A are 0.5% and 1.2% higher when compared with the STR models respectively. Whereas, the proposed design has a 0.48% lower pressure drop average deviation than the STR.

Figure 5.22 presents a comparison with the experimental pressure drop results. CFD results over-predict the experimental pressure drop at Case 1, and under-predict Cases 2 - 4 for all three test model. The average deviations are 65.3%, 60.9%, and 42.3% compared to the experimental results for the STR, the CR-2, and the CR-2A models, respectively. There is a low deviation from Case 2 to Case 4, of 39.9%, 46 %, and 19.5% as average deviation for the STR, CR-2, and CR-2A, respectively. As a result, the numerical results can fairly predict the experimental pressure drop for the CR-2A model from Cases 2 to Case4.

The pressure drop of the STR model is compared to those obtained from three widely used two-phase pressure drop models. Figure 5.23 presents the comparison of the present data to the two-phase pressure drop models, the homogeneous model, the Friedel (1979) model and the Chisholm (1967) model. The results show that the average deviation percentages from the present data to the three models are 317.74%, 166.67 %, and 441.58%, respectively. Similar to the results compared with experimental results, the present data over-predicts two-phase pressure drop from the three above models in Case 1. It is interesting to note that the present data fairly predicts the Friedel model from Case 2 to Case 4. In these cases, the average deviations from the present data are

observed as 28.7%, 198.6%, and 350.5% compared to the Friedel, the homogeneous and the Chisholm models, respectively. In this flow range, the Friedel model fairly predicts the experimental data. However, more data should be numerically investigated to verify this agreement.

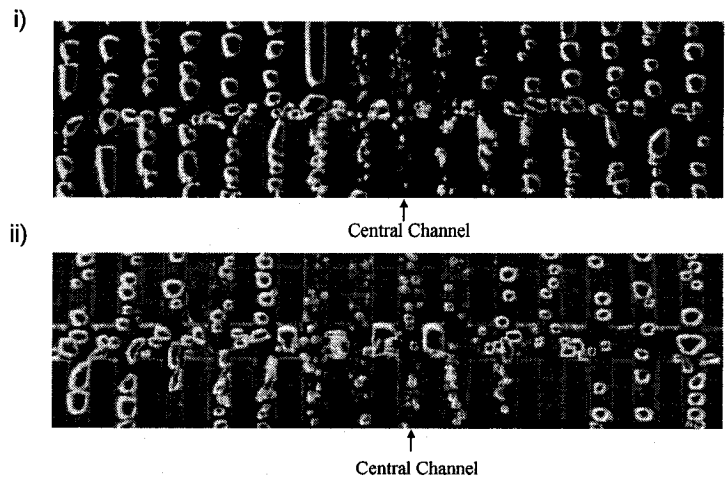

a) Samples of flow interaction- i) CR-2; ii) CR-2A, from experiment

(Direction of flow is from top to bottom)

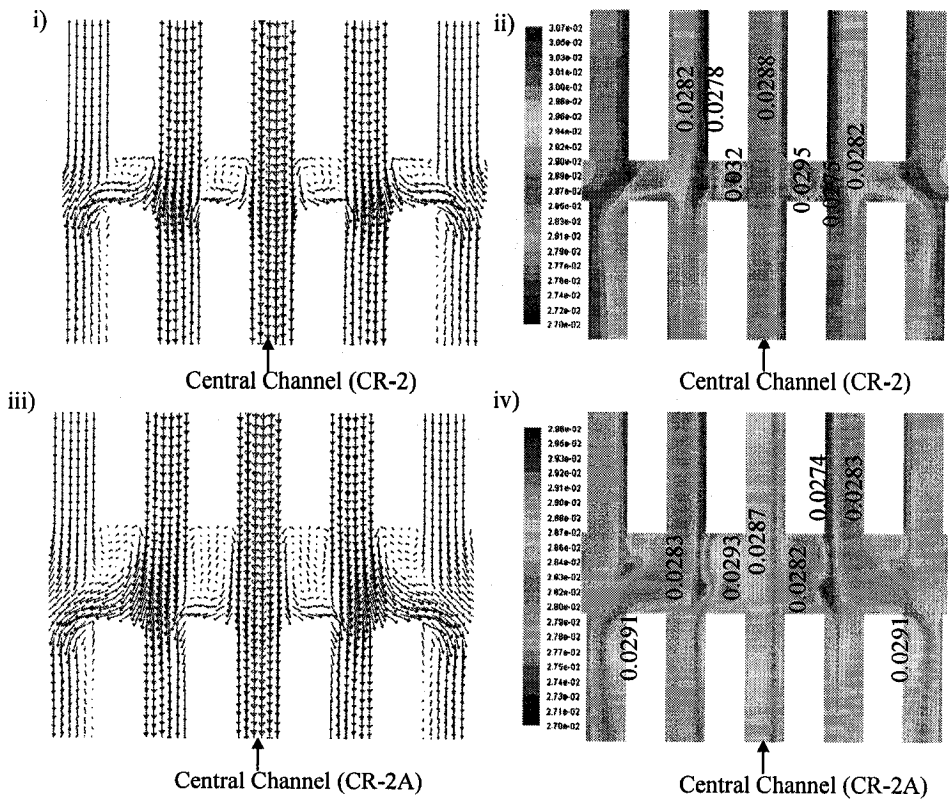

b) Samples of mixture velocity along the cross-links,

for Case 1 ($\beta = 0.0286$).

Figure 5.15. Sample of flow sharing along cross-links.

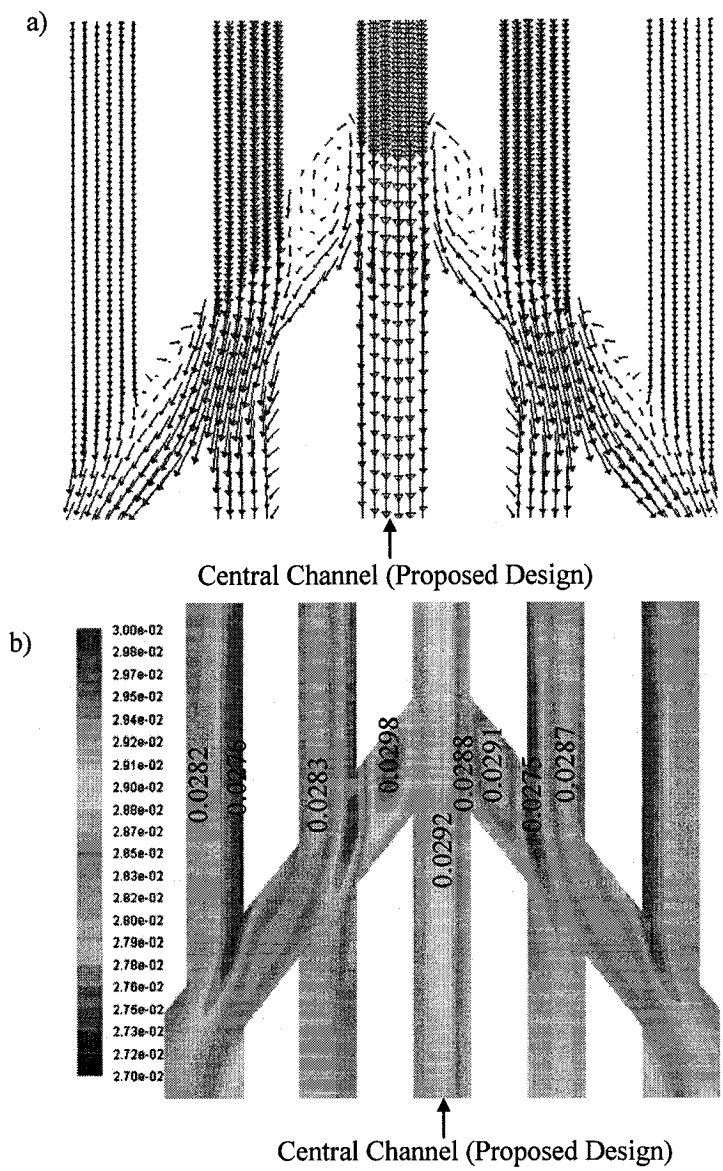

Figure 5.16. Samples of flow sharing along cross-links for the proposed design, images taken from Case 1 ($\beta = 0.0286$).

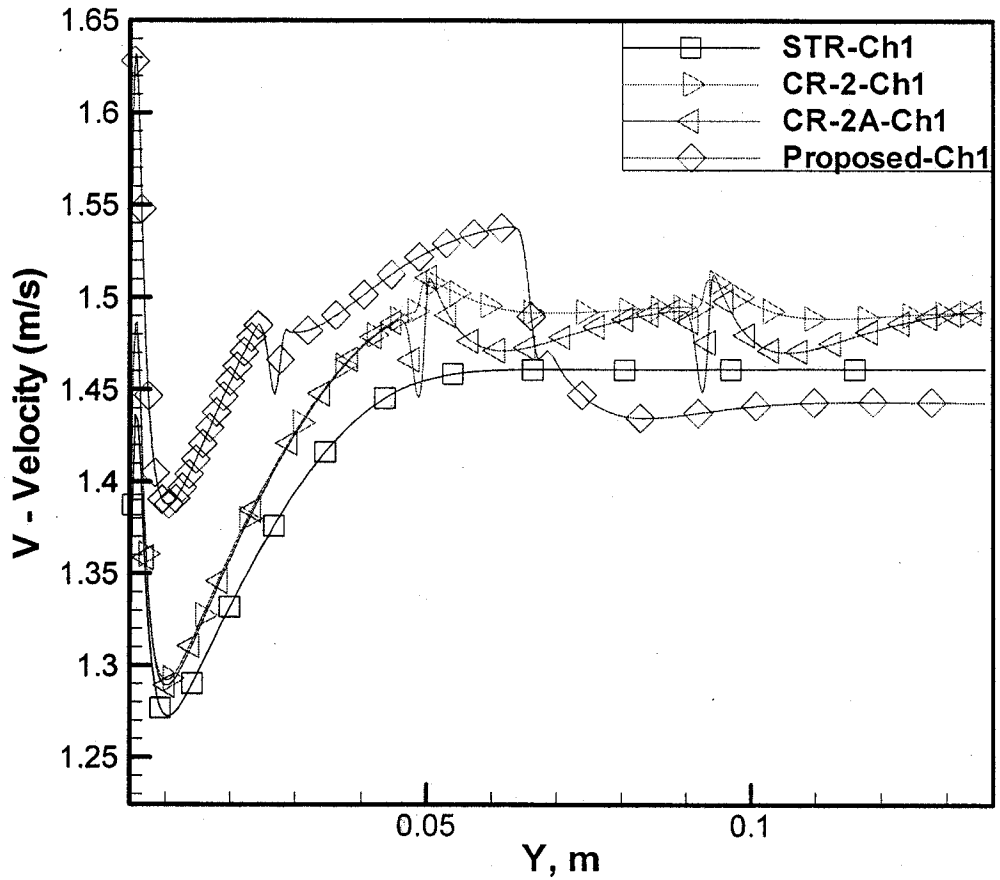

Figure 5.17. V-velocity profile of the center line in the 1st channel.

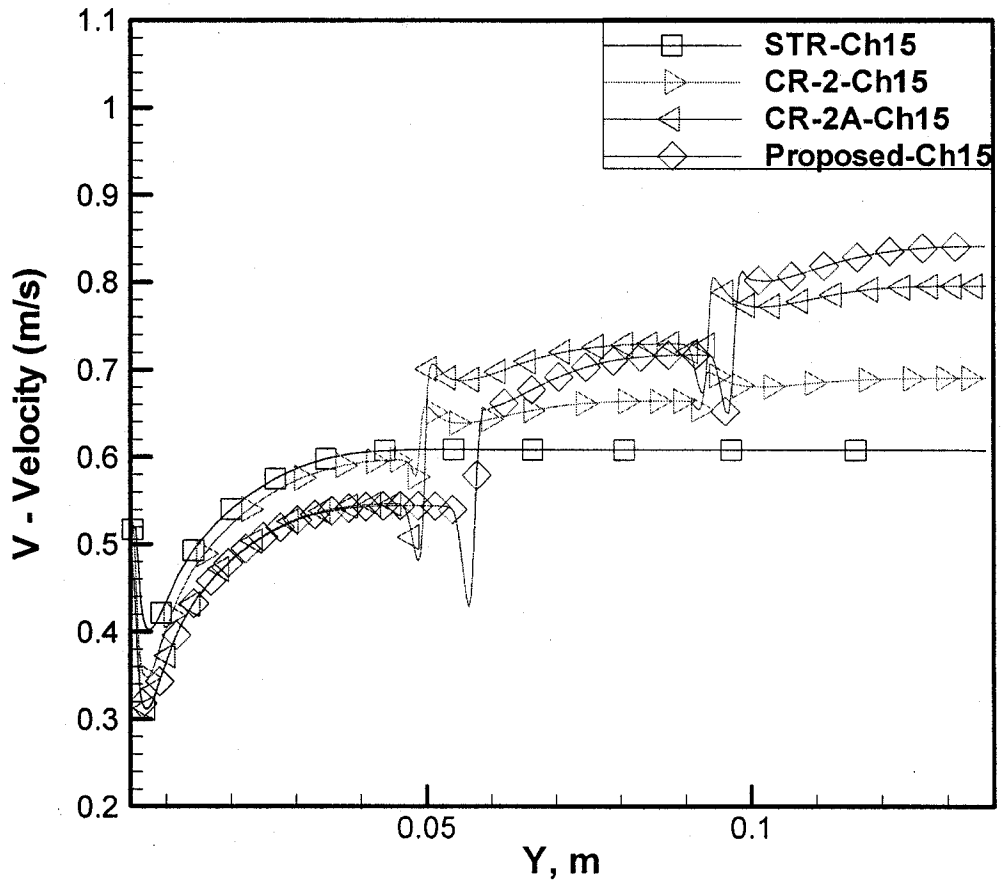

Figure 5.18. V-velocity profile of the center line in the 15th channel.

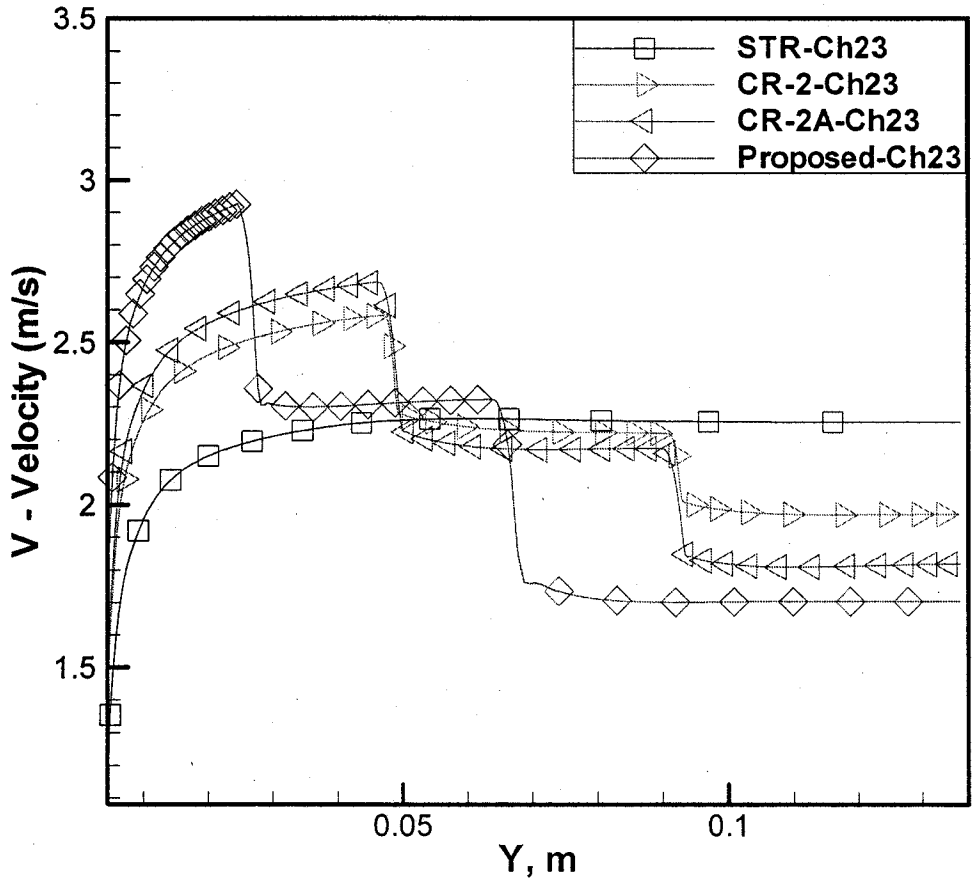

Figure 5.19. V-velocity profile of the center line in the 23rd channel.

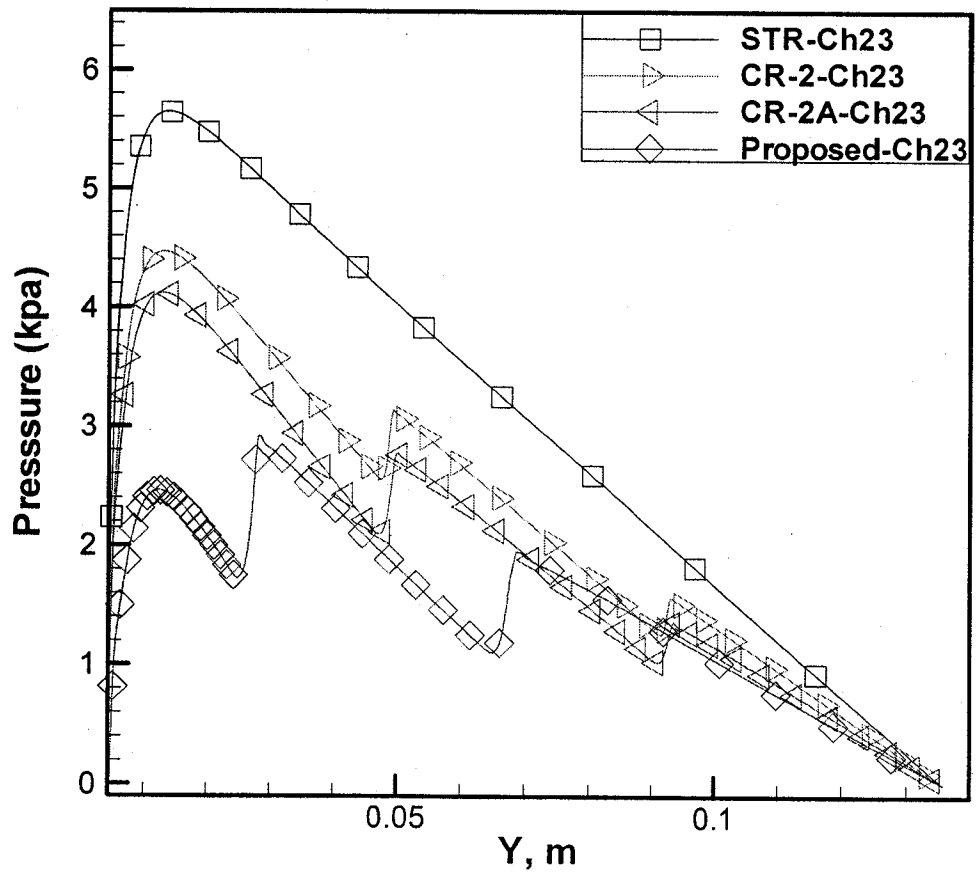

Figure 5.20. Pressure profiles along a center line of the 23rd channel, at Case 1 ($\beta = 0.0286$).

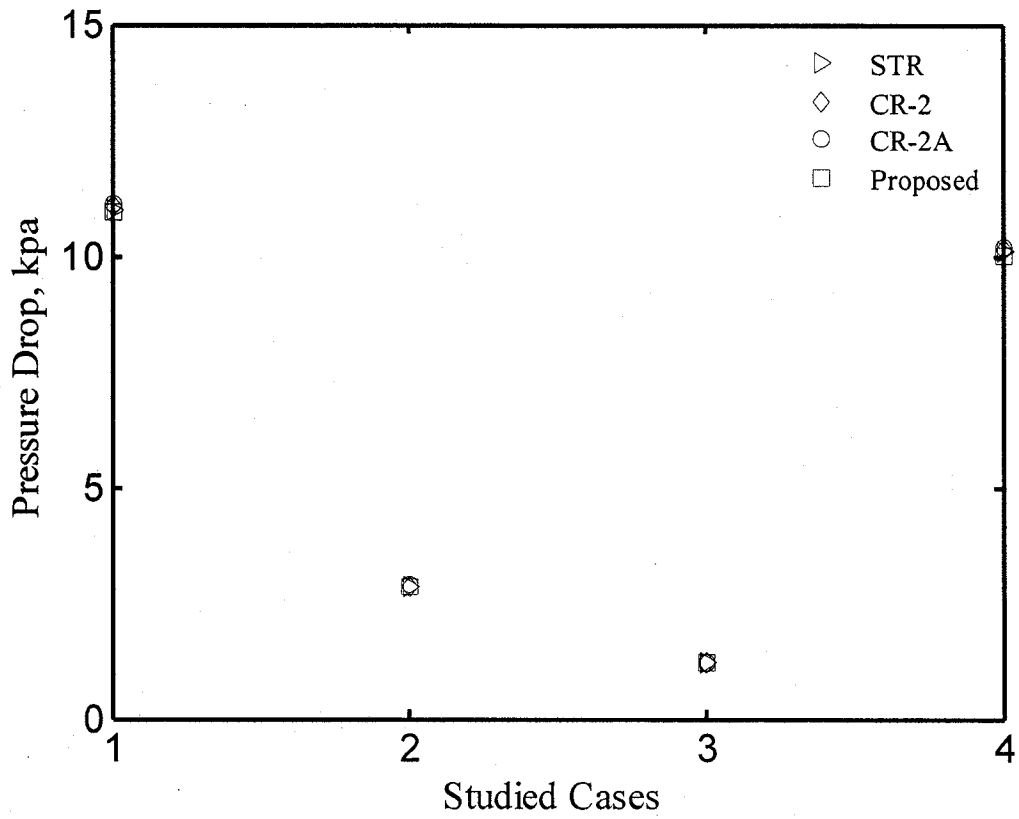

Figure 5.21. Pressure drop comparison for all test model.

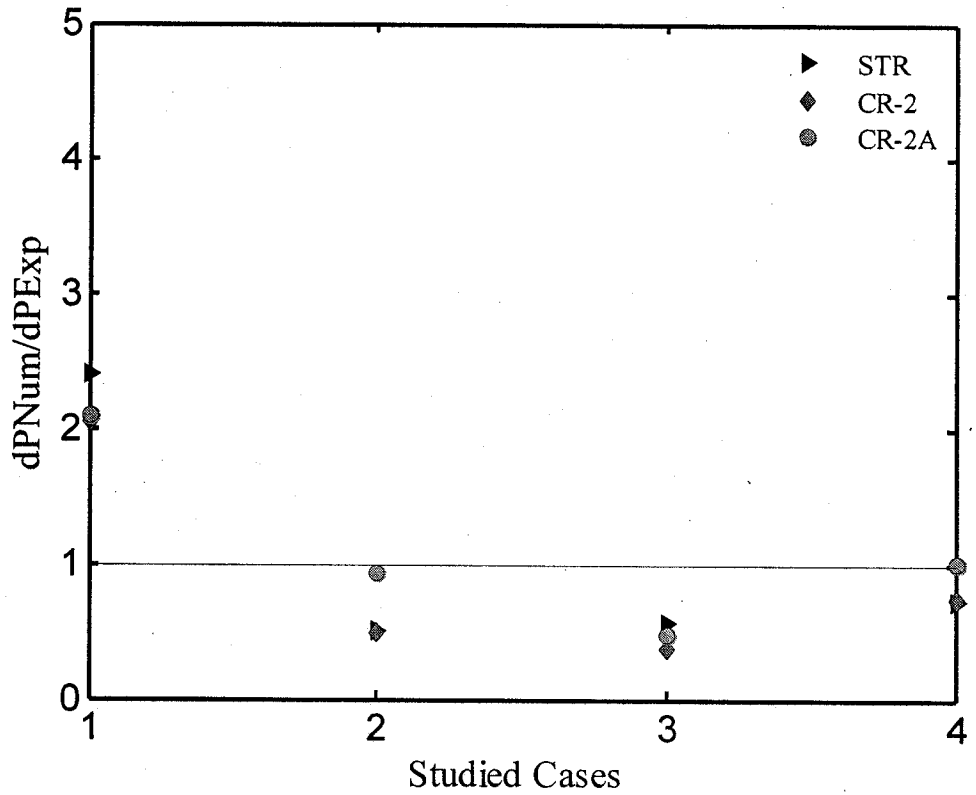

Figure 5.22. Pressure drop comparison with experimental data.

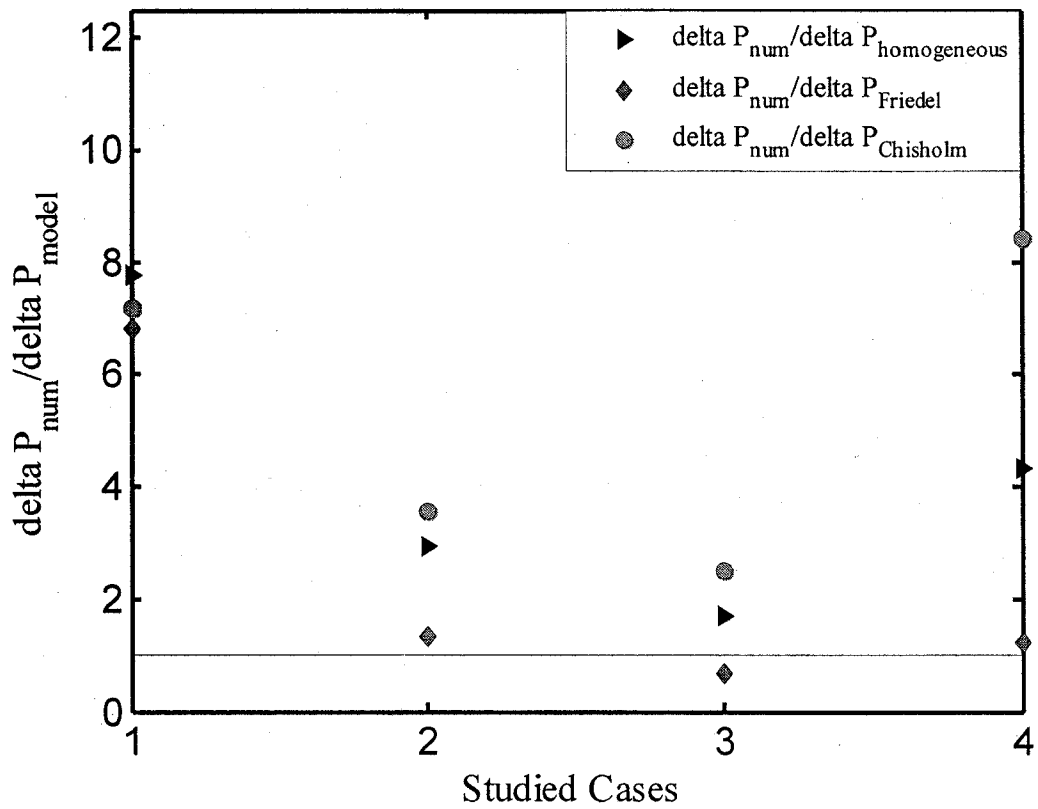

Figure 5.23. Pressure drop comparison with models, from the STR model.

5.3 Summary

Two-phase flow in the cross-linked microchannel heat sinks was numerically studied under adiabatic flow conditions. The mixture and the standard k-ε turbulent flow models were used to simulate the three dimensional two-phase flow in three test geometries, namely the STR, the CR-2, and the CR-2A. Mesh independence was accounted for, and the fine structure mesh was chosen for the two-phase simulation. The results of flow distribution were validated with experimental results, and the same trend of flow distribution was observed between experimental and numerical results.

A new design was proposed and simulated with the three test models in this numerical study. The results showed that the proposed design improves two-phase flow distribution, up to 55% compared to the standard straight channel model. There are no significant differences between the test models when they were compared for two-phase pressure drop. The CR-2 and the CR-2A test models produced slightly higher pressure drop compared to the STR test model, whereas the lowest case is from the proposed design.

The numerical two-phase pressure drop over-predicts the experimental results for Case 1. However, the results from the CR-2A test model fairly predict the experimental results of Case 2 and Case 4. Compared to two-phase pressure drop models, the Friedel model fairly predicts the numerical pressure drop for the STR test model from Case 2 to Case 4, while the homogeneous model and the Chisholm model, under-predict the present data for all studied cases.

Chapter 6

Conclusions and Future Work

6.1 Conclusion

In this study, the effects of cross-links in scaled microchannel heat sinks were experimentally and numerically investigated under adiabatic two-phase flow. The results provide new data for the research of two-phase flow characteristics in multiple parallel channels. Six different configurations were investigated experimentally. One is the standard straight configuration, whereas the remaining five test sections incorporate the cross-links into the channel core. Three of these were modeled and simulated through CFD, using Fluent 6.3. The numerical results were validated by comparing them with experimental data, and a new cross-linked configuration was proposed.

The experimental results show that six test sections exhibited non-uniform flow distribution. However, the introduction of cross-links to the channel core significantly influences flow distribution in multiple channels due to flow sharing through the cross-links. It is proposed that a higher number of cross-links and a larger width of cross-link will provide more paths and a larger space for fluid sharing between channels. Moreover, a cross-link whose width is two-times larger than the channel width is preferable for flow efficiently sharing through the cross-links.

The dispersed, intermittent (plug, elongated bubble flows), and annular flow regimes were all observed in six test sections. More instances of intermittent flow patterns are observed in the cross-linked test sections. Such observations in the cross-linked test sections occur from 70% to 90 %, compared to 65% to 80% in the straight design. Intermittent flow patterns were observed to occur about 90% in the two-time and three-time larger cross-linked test sections. The dominant flow patterns in the present study are comparable with flow patterns from single channel flow pattern maps. Hence, dominant flow patterns in four selected channels, which are approximately 1/10 of the total channels evenly spaced, might represent the entire test section. This allows a dominant flow pattern map for multi-channel configuration to be compiled. More data, however, should be studied to determine the limits of these assumptions.

The single-phase pressure drop was measured to calibrate the system. The frictional pressure drop results in the standard straight test section show good agreement with the theoretical results. The results for the cross-linked test section increased with increasing flow rate due to re-developed flow caused by the cross-links. Unlike single-phase pressure drop, the two-phase pressure drop from the cross-linked test sections deviates irregularly from the straight test section. The lowest average deviation is from the two-time larger cross-linked test section (CR-2A). The pressure drop model of Friedel (1976) fairly predicts the present data from the straight test section (STR) in a range that covers plug, elongated bubble, and annular flow patterns, whereas the homogeneous and the Chisholm models under- predict the pressure drop for the whole studied range.

The numerical work attempts, in this study, to gain further insight into the effects of cross-links in scaled microchannel heat sinks. The results are validated with experimental data and they both show the same trend of two-phase flow distribution. A new configuration of cross-linked design was proposed, and the results of flow distribution from this new design shows significant improvement, up to 55%, compared to the standard straight channel model.

Numerical results of two-phase pressure drop show no significant differences between the test models. The CR-2 and the CR-2A test models produce a slightly higher pressure drop compared to the STR test model, and the lowest is from the proposed design. Compared to experimental data, it over-predicts at Case 1 for all test models. However, the results from the CR-2A fairly predict the experimental data from Case 2 to Case 4. The results from the straight test models were compared to two-phase pressure drop models. The Friedel model fairly predicts from Case 2 to Case 4, while the homogeneous model and the Chisholm model under-predict the pressure drop for all studied cases.

Although the accuracy of the simulation of 3D two-phase flow using the CFD code, Fluent 6.3, requires further investigations, the results from the present work provide significant data for seeking appropriate designs of parallel multi-channel heat sinks in terms of flow distribution.

6.2 Future Work

The results from the study on two-phase flow in the cross-liked microchannel heat sinks provide new data in the research field of two-phase flow characteristics in multiple channels. However, more studies should be further investigated to seek appropriate designs for microchannel heat sinks, to construct a flow pattern map for multiple channels, and to correlate two-phase pressure drop, based on flow patterns.

In terms of multiple channel flow pattern maps and two-phase pressure drop models, further experimental investigations in the existing test sections should be carried out for a wide range of flow conditions. Pressure drop measurements should be recorded from inside the test section, using pressure taps to avoid high oscillations occurring from the inlet tube which connects a two-phase flow mixer with the test section. More pressure drop models, such as models based flow patterns, if available, should be studied, and the effects of acceleration and wall friction should also be taken into account.

In terms of flow distribution, numerical studies are recommended before proceeding with any further experimental investigations. This is suggested because of the cost effectiveness of numerical studies. This study should focus on the same geometry of the proposed design, with more cross-links incorporated into the channel core, while rounding all sharp corners at the channel inlets to avoid stagnation points. Moreover, various angles of the cross-links related to the channels should be taken into account as well as locations of cross-links along the channels. An experimental investigation should be followed with an appropriate design obtained from numerical work for validation.

Such research will lead to investigation of two-phase flow characteristics in to-scale microchannel heat sinks under heat transfer conditions.

References

Amornkul, S. S., Steward, F. R., Lister, D. H., "Modeling two-phase flow in pipe bends", Journal of Pressure Vessel Technology, 127, 204-209, 2005.

Aliabadi, S., Johnson, A., Zellars, B., Abatan, A., and Berger, C., "Parallel simulation of flows in open channels", Future Generation Computer System 18, 627-637, 2002.

Bretherton, F.P., "The motion of long bubbles in tubes", Journal of Fluid Mechanics 10, 166-188, 1961.

Chen, I. Y., Yang, K. S., Chang, Y. J., & Wang, C. C., "Two-phase pressure drop of air-water and R-410A in small horizontal tubes" International Journal of Multiphase Flow, 27, 1293-1299, 2001.

Chisholm, D., "A theoretical basis for the Lockhart Martinelli Correlation for two-phase flow", Int. J. Heat Mass Transfer 10, 1767–1778, 1967.

Cho, E. S., Koo, J., Jiang, L., Prasher, R. S., Kim, M. S., Santiago, J. G., Kenny, T. W., & Goodson, K. E., " Experimental study on two-phase heat transfer in microchannel heat sinks with hotspots," Annual IEEE Semiconductor Thermal Measurement and Management Symposium, 242-246, 2003.

Chung, P. M.-Y., Kawaji, M., Kawahara, A., & Shibata, Y., "Two-phase flow through square and circular microchannels—effects of channel geometry" Transactions of the ASME, 126, 546-552, 2004.

Coleman. J. W., & Garimella. S., "Characterization of two-phase flow patterns in small diameter and rectangular tubes" International Journal of Heat and Mass Transfer, 42, 2869-2881, 1999.

Collier, J.G., and Thome, J.R., "Convective boiling and condensation" Third ed., Oxford University Press, Oxford, 1994.

Conde, R., Parra, M. T., Castro, F., Villafruela, J. M., Rodriguez, M. A., and Méndez, C., "Numerical model for two-phase solidification problem in a pipe", Applied Thermal Engineering 24, 2501-2509, 2004.

Friedel, L., "Improved friction pressure drop correlations for horizontal and vertical two-phase pipe flow", Paper E2, European Two-Phase Group Meeting, Ispra, Italy, 1979.

Hassan, I., Vaillancourt, M., & Pehlivan, K., "Two-phase flow regime transition in microchannels: a comparative experimental study" Microscale Thermophysical Engineering, 9, 165-182, 2005.

Hibiki, T., & Mishima, K., "Flow regime transition criteria for upward two-phase flow in vertical narrow rectangular channels" Nuclear Engineering and Design", 203 , 117-131, 2001.

Hrnjak, P., "Developing adiabatic two-phase flow in headers- distribution issue in parallel flow microchannels heat exchangers" Heat Transfer Engineering, 25(3), 63-68, 2004.

Jiang, L., Koo, J. M., Wang, E., Bari, A., Cho, E. S., Ong, W., Prasher, R. S., Maveety, J., Kim, M. S., Kenny, T. W., Santiago, J. G., & Goodson, K. E., "Cross-linked microchannels for VLSI hotspot cooling. Proc" ASME International Mechanical Engineering Congress & Exposition, 13-17, 2002.

Kandlikar, S. G., "Effect of liquid-vapor phase distribution on the heat transfer mechanisms during flow boiling in minichannels and microchannels" Heat Transfer Engineering, 27(1), 4-13, 2006.

Lockhart, R.W. and Martinelli, R.G., "Proposed correlations for isothermal two-phase two-component flow in pipes" Chem. Eng. Prog, 45, 39–48, 1949.

Lu, M. C. and Wang, C. C., "Effect of the inlet location on the performance of parallel-channel cold – plate", IEEE Transactions on Components and Packing Technologies, 29, 30-38, 2006.

Lun, I., Calay, R. K., and Holdo, A. E., "Modelling two-phase flows using CFD", Applied Energy, 53, 299-314, 1996.

Maharudrayya, S., Jayanti, and S., Deshpande, A. P., "Pressure drop and flow distribution in multiple parallel-channel configurations used in proton-exchange membrane fuel cell stacks", Journal of Power Sources, 157, 358-367, 2006.

Muwanga, R., & Hassan, I., "Flow boiling oscillations in microchannel heat sinks" 9th AIAA/ASME Joint Thermoophysics and Heat Transfer Conference, 11p, 2006.

Nino, V. G., Hrnjak, P. S., & Newell, TY. A., "Two-phase flow visualization of R134A in A multiport microchannel tube" Heat Transfer Engineering, 24(1), 41-52, 2003.

Oberg, E.; Jones, F.D.; Horton, H.L.; Ryffell, H.H., "Machinery's Hand Book" Industry Press, 26th edition, 2000.

Osakabe, M., Hanada, T., & Horiki, S., "Water flow distribution in horizontal header contaminated with bubbles" International Journal of Mutiphase Flow, 25, 827-840, 1999.

Pehlivan, K. K., "Experimental study on two-phase flow regimes and frisctional pressure drop in mini- and micro-channels", Master Thesis, Concordia University, 2003.

Qian, D. and Lawal A., "Numerical study on gas and liquid slugs for Taylor flow in a T-junction microchannel", Chemical Engineering Science, 61, 7609-7625, 2006.

Qu, W., Yoon, S. M., and Mudawar, I., "Two-phase flow and heat transfer in rectangular micro-channels" Transactions of the ASME, 126, 288-300, 2004.

Rohsenow, W. M., Hartnett, J. P., Cho, Y. I, "Handbook of heat transfer" McGraw-Hill Handbooks, 3rd edition.

Samson, E., B., Stark, J., A., and Grote, M. G., "Two-phase flow header tests" 17th Intersociety Conference on Environmental Systems, SAE Technical Paper Serie, 17p, 1987.

Shepel, S. V. and Smith, B. L., "New finite-element/finite-volume level set formulation for modeling two-phase incompressible flows", Journal of Computational Physics, 218, 497-494, 2006.

Steinke, M. E., and Kandlikar, S. G., "An experimental investigation of flow boiling characteristics of water in parallel microchannels" Transactions of the ASME, 126, 518-526, 2004.

Tonomura, O., Tanaka, S., Noda, M., Kano, M., Hasebe, S., and Hashimoto, I., "CFD-based optimal design of manifold in plate-fin microdevices", Chemical Engineering Journal, 101, 397-402, 2004.

Triplett, K. A., Ghiaasiaan, S. M., Abdel-Khalik, S. I., and Sadowski, D. L., "Gas-liquid two-phase flow in microchannels- part I: two-phase flow patterns" International Journal of Multiphase Flow, 25, 377-394, 1999.

Tuckerman, D. B., and Pease, R. F. W., "High-performance heat sinking for VLSI" IEEE Electron Device Letters, EDL-2, 126-129, 1981.

Whalley, P.B., "Boiling, Condensation and Gas–Liquid Flow", Oxford University Press, New York, 1987.

Xu, J. L., Cheng, P., and Zhao, T. S., "Gas - liquid two-phase flow regimes in rectangular channels with mini/micro gaps" International Journal of Multiphase Flow, 25, 441-432, 1999.

Yang, Z. L., Palm, B., and Sehgal, B. R., "Numerical simulation of bubbly two-phase flow in a narrow channel", International Journal of Heat Mass Transfer, 45, 631-639, 2002.

Appendix A

Experimental Data

The experimental study on two-phase flow characteristics in the cross-linked microchannel heat sinks investigates the effects of cross-links on two-phase flow distribution, visualization, and pressure drop. The results of two-phase flow distribution in the four selected channels of the six test sections are tabulated in the Table A.1 for six studied cases (Table 4.1). The data is tabulated in terms of volume flow rate (l/min). Tabulated in Table A.2 is the number of flow pattern observations in terms of fractional time function for six test section, assuming the four selected channels represent the entire channels. The fractional time function is determined by dividing the number of observations of flow configurations by 120 (30 images x 4 channels). The sum of fractional time for all flow patterns should be one in a particular case. The single-phase flow conditions and pressure drop results and are tabulated in the Table A.3 and Table A.4, respectively. Whereas, the two-phase flow conditions and pressure drop results are tabulated in the Table A.5 and Table A.6, respectively. This section also provide the Matlab code for the comparison of two-phase pressure drop for the STR test section with those obtained from three two-phase pressure drop models, namely, the homogeneous model, the Chisholm (1967) model, and the Friedel (1979) model.

Table A.1 Flow measurements in the four selected channels for 6 test section.

Studied Cases	Test Sections	Volume Flow Rates in the Four Selected Channels (l/min)			
		Channel 1	Channel 2	Channel 3	Channel 4
1	STR	0.173	0.085	0.088	0.222
	CR-2	0.190	0.088	0.100	0.190
	CR-4	0.185	0.110	0.103	0.182
	CR-6	0.178	0.114	0.116	0.200
	CR-2A	0.174	0.115	0.108	0.177
	CR-2B	0.179	0.110	0.120	0.200
2	STR	0.060	0.028	0.030	0.075
	CR-2	0.065	0.028	0.034	0.069
	CR-4	0.078	0.036	0.033	0.075
	CR-6	0.079	0.034	0.039	0.082
	CR-2A	0.069	0.040	0.041	0.070
	CR-2B	0.067	0.033	0.037	0.076
3	STR	0.033	0.016	0.017	0.041
	CR-2	0.039	0.015	0.018	0.042
	CR-4	0.044	0.019	0.018	0.042
	CR-6	0.048	0.019	0.021	0.049
	CR-2A	0.040	0.021	0.023	0.040
	CR-2B	0.040	0.018	0.020	0.043
4	STR	0.055	0.014	0.016	0.073
	CR-2	0.058	0.014	0.018	0.070
	CR-4	0.058	0.019	0.021	0.053
	CR-6	0.055	0.020	0.023	0.059
	CR-2A	0.059	0.020	0.021	0.054
	CR-2B	0.061	0.017	0.021	0.059
5	STR	0.010	0.005	0.006	0.010
	CR-2	0.007	0.004	0.006	0.014
	CR-4	0.012	0.008	0.007	0.007
	CR-6	0.006	0.007	0.008	0.008
	CR-2A	0.007	0.007	0.008	0.008
	CR-2B	0.006	0.006	0.008	0.007
6	STR	0.003	0.004	0.004	0.002
	CR-2	0.002	0.004	0.007	0.004
	CR-4	0.006	0.008	0.008	0.002
	CR-6	0.003	0.007	0.009	0.002
	CR-2A	0.003	0.008	0.008	0.003
	CR-2B	0.003	0.008	0.010	0.003

Table A.2. Flow Patterns in terms of fractional time function, assuming four selected channel represent the entire channels.

Studied Cases	Test Section	Fractional Time Flow Patterns			
		Bubbly	Plug	Elongated	Annular
1	STR	0.36	0.59	0.05	0
	CR-2	0.35	0.64	0.01	0
	CR-4	0.45	0.55	0	0
	CR-6	0.45	0.55	0	0
	CR-2A	0.43	0.57	0	0
	CR-2B	0.46	0.54	0	0
2	STR	0	0.51	0.27	0.22
	CR-2	0	0.54	0.31	0.15
	CR-4	0	0.63	0.2	0.17
	CR-6	0	0.58	0.27	0.15
	CR-2A	0	0.53	0.37	0.10
	CR-2B	0	0.52	0.39	0.09
3	STR	0	0.46	0.22	0.32
	CR-2	0	0.47	0.24	0.29
	CR-4	0.02	0.50	0.28	0.20
	CR-6	0	0.57	0.26	0.17
	CR-2A	0	0.51	0.33	0.16
	CR-2B	0	0.49	0.35	0.16
4	STR	0	0.23	0.13	0.64
	CR-2	0	0.23	0.19	0.58
	CR-4	0	0.11	0.17	0.72
	CR-6	0	0.17	0.07	0.76
	CR-2A	0	0.07	0.24	0.69
	CR-2B	0	0.16	0.23	0.61

Table A.3. Studied cases for single-phase pressure drop measurements.

Data Points	Volume Flow Rate (l/min)	Re
1	1.641	341
2	1.859	386
3	1.892	393
4	2.271	472
5	2.650	550
6	3.028	630
7	3.785	787
8	4.164	866
9	4.542	944
10	4.921	1023
11	5.299	1102
12	5.678	1180
13	6.056	1259
14	6.435	1338

Table A.4. Single Phase Pressure Drop Measurements

Test Sections	Single Phase Pressure Drop (psi)													
	Point 1	Point 2	Point 3	Point 4	Point 5	Point 6	Point 7	Point 8	Point 9	Point 10	Point 11	Point 12	Point 13	Point 14
STR	0.079	0.075	0.080	0.092	0.088	0.082	0.108	0.107	0.159	0.138	0.276	0.215	0.229	0.176
CR-2	0.097	0.104	0.124	0.107	0.088	0.191	0.171	0.245	0.264	0.261	0.404	0.377	0.408	0.440
CR-4	0.136	0.157	0.189	0.192	0.226	0.235	0.258	0.381	0.428	0.453	0.591	0.546	0.749	0.689
CR-6	0.161	0.187	0.181	0.211	0.188	0.262	0.415	0.517	0.581	0.622	0.771	0.864	0.937	1.008
CR-2A	0.156	0.160	0.182	0.209	0.197	0.238	0.308	0.368	0.431	0.401	0.539	0.658	0.692	0.664
CR-2B	0.171	0.177	0.191	0.245	0.260	0.332	0.385	0.472	0.550	0.544	0.756	0.679	0.965	0.766

Table A.5. Studied cases for two-phase pressure drop measurements

Data Points	j_G	j_L	Quality (x)
1 (Case 1)	0.025	0.835	3.61E-05
2	0.102	0.835	1.5E-04
3	0.189	0.835	2.8E-04
4	0.378	0.835	5.5E-04
5	0.378	0.723	6.4E-04
6	0.378	0.556	8.3E-04
7	0.378	0.445	0.001
8	0.378	0.223	0.002
9 (Case 2)	0.378	0.273	0.002
10 (Case 3)	0.378	0.142	0.003
11	0.917	0.142	0.008
12	1.827	0.142	0.016
13	2.863	0.142	0.024
14	4.011	0.142	0.034
15 (Case 4)	4.604	0.142	0.038
16	4.604	0.109	0.049
17	4.604	0.078	0.068
18 (Case 5)	4.604	0.036	0.135
19	5.837	0.036	0.165
20	7.137	0.036	0.195
21	8.500	0.036	0.224
22 (Case 6)	9.926	0.036	0.245

Table A.6. Two-Phase Pressure drop measurements from point 1 to point 11.

Test Sections	Two-Phase Pressure Drop (psi)										
	Point 1	Point 2	Point 3	Point 4	Point 5	Point 6	Point 7	Point 8	Point 9	Point 10	Point 11
STR	0.662	0.876	1.004	1.530	1.383	1.404	1.016	0.344	0.810	0.313	0.524
CR-2	0.781	1.310	1.232	1.882	1.607	1.485	1.205	0.460	0.836	0.479	0.738
CR-4	1.041	1.674	1.752	1.948	1.888	1.645	1.299	0.481	0.830	0.445	0.608
CR-6	1.098	1.699	1.713	2.360	2.154	1.741	1.444	0.692	1.103	0.593	0.885
CR-2A	0.767	1.160	1.047	1.494	1.422	1.187	0.860	0.374	0.447	0.369	0.336
CR-2B	0.734	1.575	1.459	1.579	1.645	1.352	1.005	1.563	0.618	0.353	0.450

Table A.7. Two-Phase Pressure drop measurements from point 12 to point 22.

Test Sections	Two-Phase Pressure Drop Measurements (psi)										
	Point 12	Point 13	Point 14	Point 15	Point 16	Point 17	Point 18	Point 19	Point 20	Point 21	Point 22
STR	0.422	1.300	1.264	2.010	1.029	1.611	0.524	1.142	0.997	0.781	1.716
CR-2	0.805	1.341	1.972	1.959	2.059	1.768	1.100	1.126	1.907	1.860	2.002
CR-4	0.833	0.857	1.814	2.112	1.873	1.478	0.764	0.824	1.616	1.799	2.120
CR-6	1.285	1.904	2.046	2.168	1.990	1.266	0.839	1.030	0.822	2.030	2.571
CR-2A	0.477	1.321	1.047	1.468	1.697	1.132	0.575	1.008	1.713	1.357	1.572
CR-2B	0.548	1.227	1.131	1.295	2.905	1.075	0.626	0.731	1.421	1.560	1.907

```
%%%%%%%%%%%%%%%%%%%%%%%%%%%%%%%%%%%%%%%%%%%%%%%%%%%%%%%%%%%%%%%%%%%%%%%
%Comparison of pressure Drop for the STR with those obtained
%from the homogeneous model, Chisholm (1967) model, and the
%the Friedel (1979) model.
%Author: Minh Nhat Dang
%Date: May, 2007
%%%%%%%%%%%%%%%%%%%%%%%%%%%%%%%%%%%%%%%%%%%%%%%%%%%%%%%%%%%%%%%%%%%%%%%

clear all
close all

// Reynold's number

Re_L1=[1500 1182.678414 1182.678414 1182.678414 1024.987958 788.4522758
630.7618206     387.077387 315.3809103 200.5139987  201 201 200.5139987
200.5139987 200.5139987 154.706024  109.9391395 51.22164454 51.22164454
51.22164454 51.22164454 0];

Re_L=[1182.678414   1182.678414 1182.678414 1182.678414 1024.987958
788.4522758 630.7618206     387.077387 315.3809103  200.5139987 201 201
200.5139987 200.5139987 200.5139987 154.706024  109.9391395 51.22164454
51.22164454 51.22164454 51.22164454 51.22164454];

% Flow quality

x1= [0   0.000149304 0.000277181 0.000555072 0.000640413 0.000832377
0.001040255 0.001694037 0.002078347 0.003265067 0.007889587 0.015596372
0.024227946 0.03361499  0.038400245 0.049210902 0.067889035 0.135191876
0.165407169 0.195039902 0.223964952 0.26];

x= [3.60876E-05 0.000149304 0.000277181 0.000555072 0.000640413
0.000832377 0.001040255 0.001694037 0.002078347 0.003265067 0.007889587
0.015596372 0.024227946 0.03361499 0.038400245 0.049210902 0.067889035
0.135191876 0.165407169 0.195039902 0.223964952 0.252057536];

% Experimental Two-phase pressure drop for the STR test section

Dp_exp= [0.661589436 0.875674573 1.843297274 1.52957892 1.383383896
1.403839462 1.016434302     0.809706128 0.344477161 0.313350341
0.523565498 0.422099269 1.300334348 1.26373803  2.009469908 1.028689458
1.611474723 0.524205923 1.142316198 0.997173578 0.780782562
1.71648624];

% Flow conditions

Gflux = [833.1117149    833.2060506 833.3126283 833.5443269 722.4667736
555.8504436 444.7728903 273.1209622 222.6177837 141.7052422 142.3657723
143.4803379 144.7495494 146.1555836 146.8829047 114.615652 83.08174602
41.72099485 43.23144646 44.82291157 46.49358988 48.23988078];

Dh=0.0015875; // hydraulic diameter
sigma = 0.0728; // surface tension
gravity = 9.81;
rho_f = 999;       // density of water
rho_g = 1.23;      // density of air
miu_g=1.79E-05;    // dynamic viscosity of air
```

```
miu_f=1.12E-03;    // dynamic viscosity of water
l=.131;            // channel length
N=22;              // number of data points

% Homogeneous correlation

for i=1:N
    rho_tp(i)= (x(i)/rho_g + (1-x(i))/rho_f)^-1;
    miu_tp(i)= (x(i)/miu_g + (1-x(i))/miu_f)^-1;

Re_tp(i) = Gflux(i)*Dh/miu_tp(i);
end
for i=1:22
if Re_tp(i)<2000
        f_tp(i)=57/Re_tp(i);
        else
        f_tp(i)=0.316*(Re_tp(i)^-.25);
        %f_tp=(1.82.*log(Re_tp)).^-2;
end
end

for i=1:N

DP_hom(i) = f_tp(i)*l*Gflux(i)^2/(2*Dh* rho_tp(i));

% Friedel Correlation

We(i) = Gflux(i)^2*Dh/(rho_tp(i)*sigma);

Fr(i) = Gflux(i)^2/(gravity*Dh*rho_tp(i)^2);

A3= ((rho_f/rho_g)^0.91)*((miu_g/miu_f)^0.19)*((1-miu_g/miu_f)^0.7);

A2(i)= (x(i)^0.78)*((1-x(i))^0.224);

Re_fo(i) = Gflux(i)*Dh/miu_f;
end
for i=1:N
if Re_fo(i)< 2000
        f_fo(i)=57/Re_fo(i);
        else
       f_fo(i)=0.316*Re_fo(i)^-.25;
       % f_fo=(1.82.*log(Re_fo)).^-2;
end
end

for i=1:22
Re_go(i)= Gflux(i)*Dh/miu_g;
end

for i=1:N
if Re_go (i)< 2000
        f_go(i)=57/Re_go(i);
        else
      f_go(i)=0.316*Re_go(i)^-.25;
```

```
        %f_go=(1.82.*log(Re_go)).^-2;
    end
end
for i=1:N;
A1(i) = (1-x(i))^2 + x(i)^2*((f_go(i)* rho_f)/(f_fo(i)*rho_g));

phi2_fo(i) = A1(i)+((3.24*A2(i)*A3)/((Fr(i)^0.045)*(We(i)^0.035)));

DP_fo(i) = f_fo(i)*l*(Gflux(i)^2)/(2*Dh*rho_f);
end

% Chisholm Correlation

for i=1:N
Re_f(i) = Gflux(i)*(1-x(i))*Dh/miu_f;
end
for i=1:N
    if Re_f(i)<2000
        f_f(i)=57/Re_f(i);
        else
        f_f(i)=0.316*(Re_f(i)^-0.25);
       % f_f=(1.82.*log(Re_f)).^-2;
end
end
for i=1:N
Re_g= Gflux.*x.*Dh./miu_g;
end
for i=1:N
if Re_g(i)<2000
        f_g(i)=57/Re_g(i);
        else
        f_g(i)=0.316*(Re_g(i)^-.25);
       % f_g=(1.82.*log(Re_g)).^-2;
end
end
for i=1:N
DP_f(i) = f_f(i)*l*Gflux(i)^2*(1-x(i))^2/(2*Dh* rho_f);

DP_g(i) = f_g(i)*l*Gflux(i)^2*x(i)^2/(2*Dh* rho_g);

X2(i) = DP_f(i)/DP_g(i);
end

for i=1:N
if ((Re_f(i) > 2000) & (Re_g(i) > 2000))
        PHI2_tt(i)= 1 + 1/X2(i) + 20/(X2(i)^0.5);
       DP_Chisholm(i) = PHI2_tt(i)*DP_f(i);
elseif ((Re_f(i) > 2000) & (Re_g(i) < 2000))
        PHI2_tl(i)= 1 + 1/X2(i) + 10/(X2(i)^0.5);
       DP_Chisholm(i) = PHI2_tl(i)*DP_f(i);
elseif ((Re_f(i) < 2000) & (Re_g(i) > 2000))
        PHI2_lt(i)= 1 + 1/X2(i) + 12/(X2(i)^0.5);
       DP_Chisholm(i) = PHI2_lt(i)*DP_f(i);
elseif ((Re_f(i) < 2000) & (Re_g(i) < 2000))
        PHI2_ll(i)= 1 + 1/X2(i) + 5/(X2(i)^0.5);
       DP_Chisholm (i)= PHI2_ll(i)*DP_f(i);
```

```
end
end
for i=1:N
DP_Chisholm(i);

Dp_Friedel(i) = DP_fo(i)*phi2_fo(i)*0.000145;

Dp_hom(i)= DP_hom(i)*0.000145;
Dp_Chis(i) = DP_Chisholm(i)*0.000145;

Comp_Frie(i) = Dp_exp(i)/Dp_Friedel(i);
Comp_Hom (i)= Dp_exp(i)/Dp_hom(i);
Comp_Chis(i) = Dp_exp(i)/Dp_Chis(i);
end
for i=1:N-8

% Error

Error_Fr(i) = abs(Dp_exp(i+8)-Dp_Friedel(i+8))/Dp_Friedel(i+8);
Error_Hom (i)= abs(Dp_exp(i+8)-Dp_hom(i+8))/Dp_hom(i+8);
Error_Chis(i) = abs(Dp_exp(i+8)-Dp_Chis(i+8))/Dp_Chis(i+8);


One=[1  1   1   1   1   1   1   1   1   1   1   1   1   1   1   1   1
1   1   1   1   1];

end
AVR= mean(Error_Fr)
AVR= mean(Error_Hom )
AVR= mean(Error_Chis)
symb = ['>';'d';'o';'s';'^';'v';'p';'<';'h';
'*';'x';'>';'d';'.';'o';'+';'^';'x'];

figure(1); hold on;

plot(x,Comp_Hom,[ symb(1)],'MarkerFaceColor','k');
plot(x,Comp_Frie,[ symb(2)],'MarkerFaceColor','m')


plot(x,Comp_Chis,[symb(3)],'MarkerFaceColor','g')


plot(x1,One,['-']);
legend('delta P_e_x_p/delta P_h_o_m_o_g_e_n_e_o_u_s','delta
P_e_x_p/delta P_F_r_i_e_d_e_l','delta P_e_x_p/delta P_C_h_i_s_h_o_l_m')
set(gca,'LineWidth',2,'Box','on','FontSize',14);
set(findobj('Type','line'),'LineWidth',1,'Color','k');
xlabel('Quality, x'); ylabel('Mean delta P_e_x_p/delta P_m_o_d_e_l');

hold off;
```

Appendix B

Test Sections Geometry

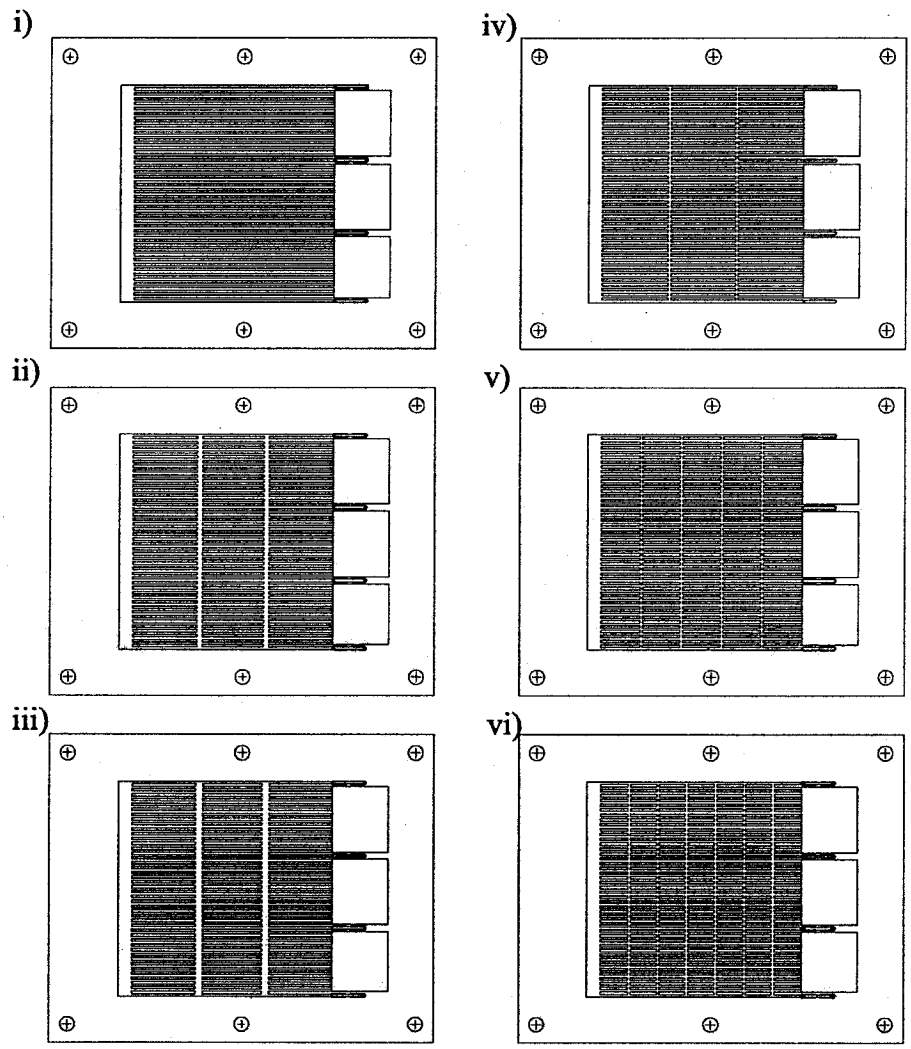

Figure B.1. Six configurations for channel plate,
i) STR, ii) CR-2, iii) CR-2A, iv) CR-2B, v) CR-4, vi) CR-6.

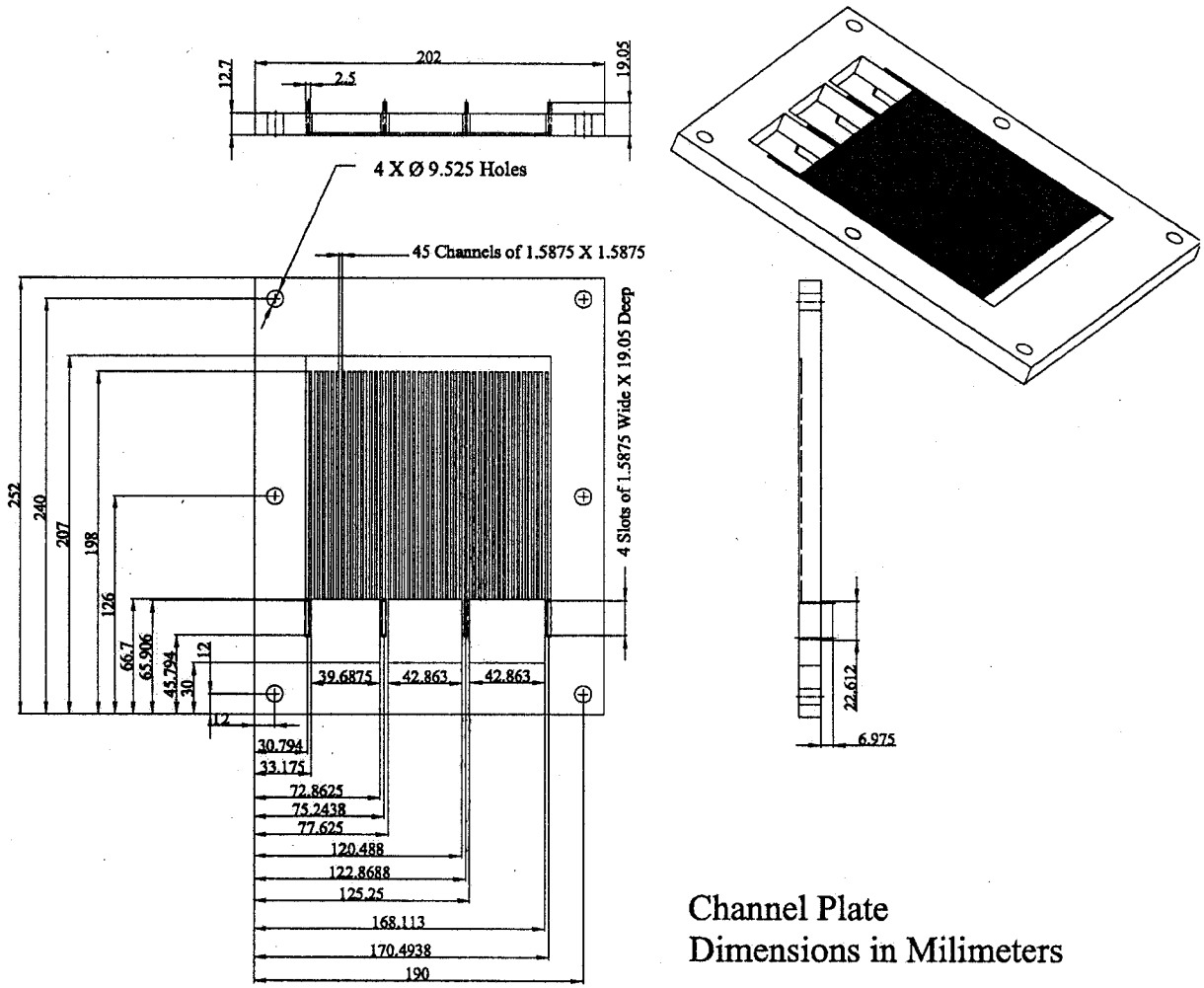

Figure B.2. The channel plate geometry.

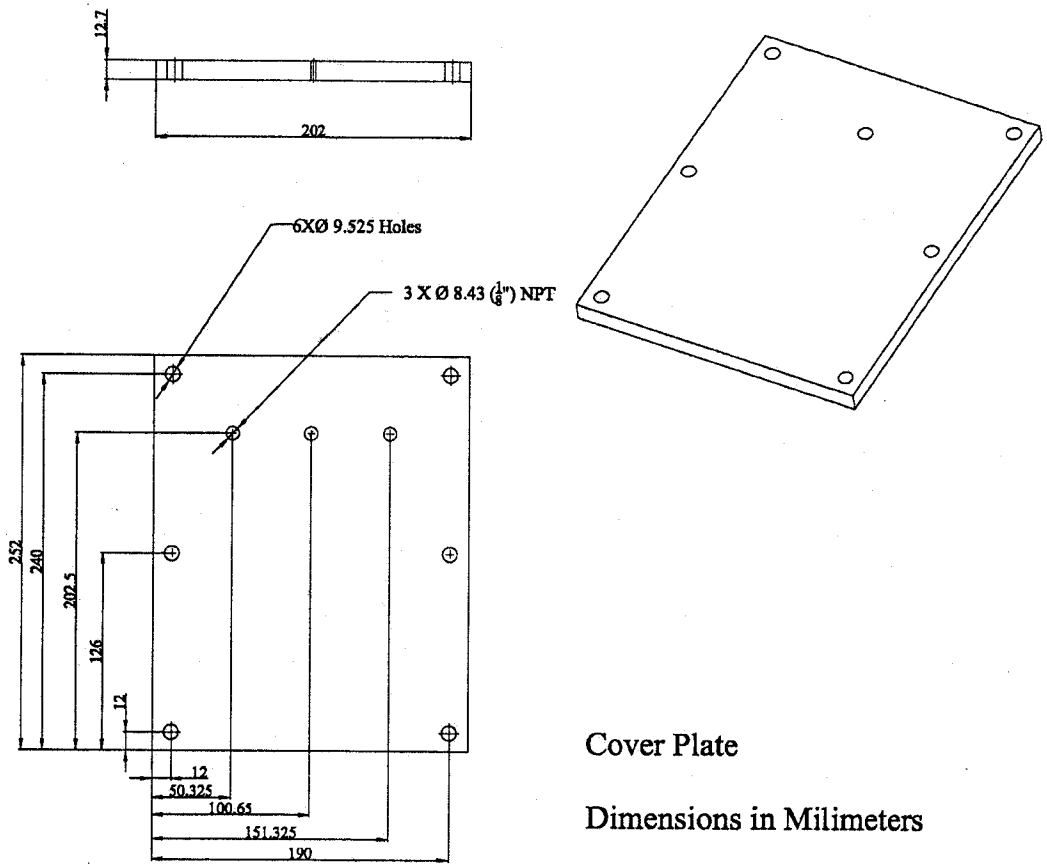

Figure B.3. The cover plate geometry.

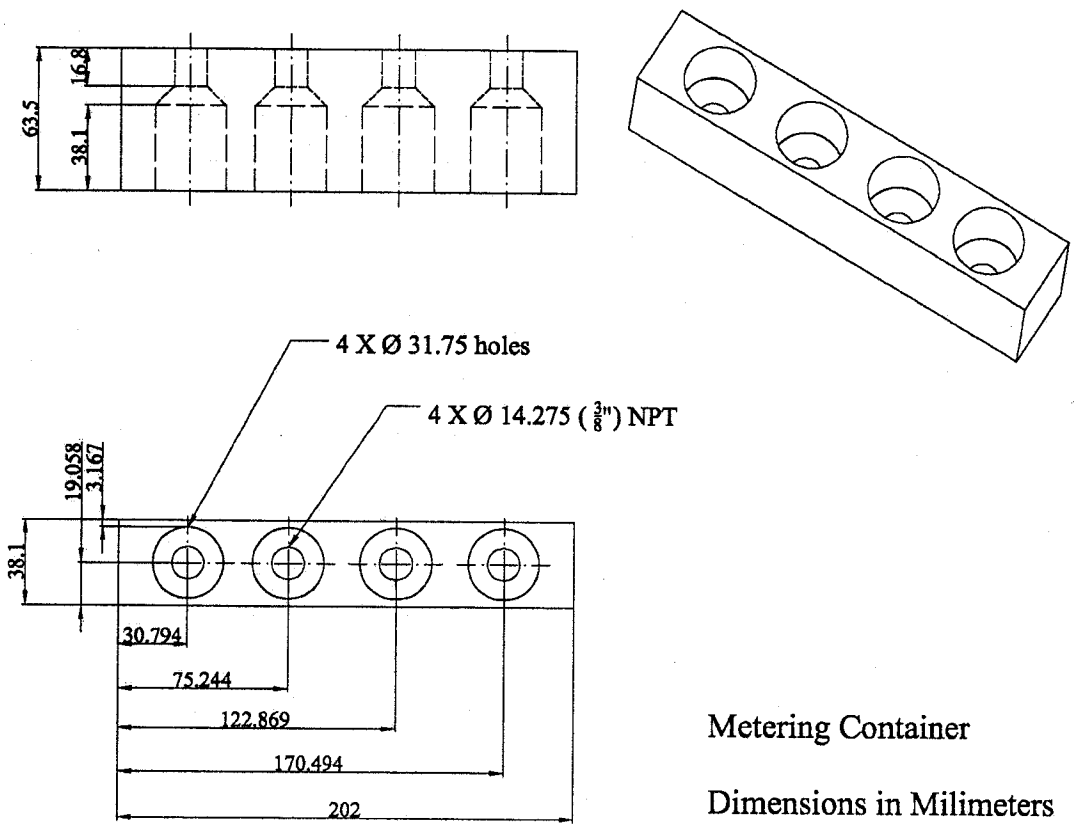

Figure B.4. The Metering container geometry.

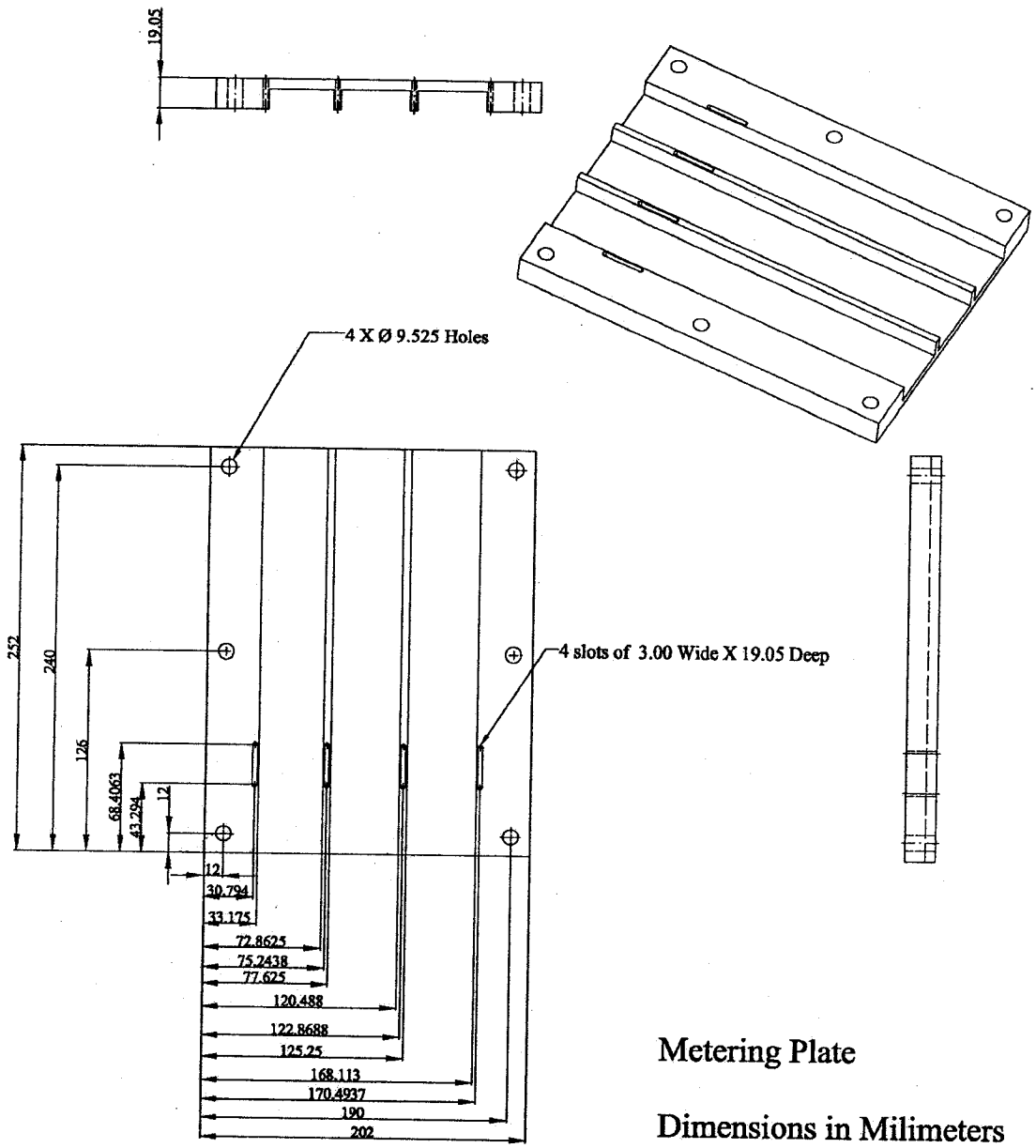

Figure B.5. The metering plate geometry.